FEDERAL UNIVERSITY OF CEARÁ

TECHNOLOGY CENTER

DEPARTMENT OF STRUCTURAL ENGINEERING AND CIVIL CONSTRUCTION

POST-GRADUATION PROGRAM IN CIVIL ENGINEERING: STRUCTURES AND CIVIL CONSTRUCTION

MASTER DEGREE IN CIVIL ENGINEERING

LUANA ANDREZA GOMES MOURA

EXPERIMENTAL AND NUMERICAL ANALYSIS OF COMPOSITES REINFORCED WITH NATURAL FIBERS

FORTALEZA

2023

LUANA ANDREZA GOMES MOURA

EXPERIMENTAL AND NUMERICAL ANALYSIS OF COMPOSITES REINFORCED WITH NATURAL FIBERS

Dissertation submitted to the Post-Graduation Program in Civil Engineering: Structures and Civil Construction of the Technology Center of the Federal University of Ceará, as a partial requirement for obtaining the title of Master in Civil Engineering. Concentration Area: Civil Engineering

Advisor: Prof. Dr. Sc. Marcelo Silva Medeiros Junior

Co-advisor: Prof. Dr. Sc. Evandro Parente Junior

FORTALEZA

2023

Dados Internacionais de Catalogação na Publicação
Universidade Federal do Ceará
Sistema de Bibliotecas
Gerada automaticamente pelo módulo Catalog, mediante os dados fornecidos pelo(a) autor(a)

M887e Moura, Luana Andreza Gomes.
Experimental and numerical analysis of composites reinforced with natural fibers. / Luana Andreza Gomes Moura. – 2023.
110 f. : il. color.

Dissertação (mestrado) – Universidade Federal do Ceará, Centro de Tecnologia, Programa de Pós-Graduação em Engenharia Civil: Estruturas e Construção Civil, Fortaleza, 2023.
Orientação: Prof. Dr. Marcelo Silva Medeiros Junior.
Coorientação: Prof. Dr. Evandro Parente Junior.

1. Natural Fibers. 2. Hybrid Composites. 3. Fiber-reiforced Composites. 4. Progressive Failure. 5. Jute. I. Título.

CDD 624.1

LUANA ANDREZA GOMES MOURA

EXPERIMENTAL AND NUMERICAL ANALYSIS OF COMPOSITES REINFORCED WITH NATURAL FIBERS

Dissertation submitted to the Post-Graduation Program in Civil Engineering: Structures and Civil Construction of the Technology Center of the Federal University of Ceará, as a partial requirement for obtaining the title of Master in Civil Engineering. Concentration Area: Civil Engineering

Approved on:

EXAMINATION BOARD

Prof. Dr. Sc. Marcelo Silva Medeiros Junior (Advisor)
Federal University of Ceará (UFC)

Prof. Dr. Sc. Evandro Parente Junior (Co-advisor)
Federal University of Ceará (UFC)

Prof. Dr. Sc. João Batista Marques de Sousa Junior
Federal University of Ceará (UFC)

Prof. Dr. Sc. Luiz Antônio Taumaturgo Mororó
Federal Institute of Ceará (IFCE)

ACKNOWLEDGEMENTS

Agradeço a Deus por Sua infinita bondade e misericórdia, por ter me proporcionado a oportunidade de concluir este mestrado em meio a tantos desafios, um sonho acalentado por muito tempo.

Agradeço aos meus pais, que não estão aqui fisicamente, mas permanecem sempre presentes em meu coração. Eles ainda hoje me provêm tudo o que necessito. Sinto a intercessão deles daqui, e sei que estão comigo, orientando-me e auxiliando-me conforme sua capacidade.

Em especial, agradeço à minha irmãzinha, Kaylanni. Você é meu guia, minha luz. Nos momentos difíceis, lembrar que tenho você ao meu lado é o que me dá coragem para buscar meus objetivos. Não apenas por mim, mas por nós duas. Obrigada por todo o amor e por cuidar tão bem de mim.

Professor Marcelo, a minha profunda gratidão a você. Além de orientador, você se tornou um amigo, demonstrando carinho e preocupação por mim. Além da orientação acadêmica, você me proporcionou conselhos e exemplos de profissionalismo e vida. Sua influência em minha jornada será eternamente apreciada.

Co-orientador Evandro, agradeço pela dedicação e tempo investidos. Desde a graduação, você desempenhou um papel crucial em minha formação.

Thamires e Leonardo, meus colegas de mestrado que me ofereceram um apoio inestimável. Especialmente a você, Thamires, que se transformou em uma amiga que muito admiro e prezo.

Lucas Brock, sua presença foi fundamental. Obrigada por todo o incentivo ao longo desta jornada, e por sempre acreditar tanto em mim.

A todos das minhas famílias: Moura, Monteiro Rebouças e Brock. Obrigada pelo amor e por acreditarem sempre em mim. Vocês são muito amados.

Aos membros da banca, agradeço pelas correções e ensinamentos que me permitiram aprimorar minha formação profissional.

E à Fundação Cearense de Apoio ao Desenvolvimento (Funcap), por financiar minha pesquisa de mestrado por meio da bolsa de estudos.

"Wait on the LORD: Be of good courage, and He shall strengthen thine heart."

(Psalm 27:14)

ABSTRACT

Composites reinforced with natural fibers are a relatively new class of engineering material that can be used in different industrial applications. While synthetic fiber-reinforced polymer composites have traditionally been employed in high-performance structures, the interest in natural fiber-reinforced composites is growing due to their ecological advantages, renewability, and cost-effectiveness. Jute is a natural fiber easily found in Brazil, its use is environment friendly and improves local economies. Natural fibers also present some drawbacks compared to synthetic fibers, such as poor resistance to moisture absorption, random properties, and a hydrophilic behavior, which can be prevented by fiber treatment. This research aims to explore the mechanical behavior of jute-glass hybrid-reinforced epoxy composites through both experimental and numerical analyses. The primary objectives include the production of hybrid composites using manual lamination, the characterization of fundamental mechanical properties of the composites and their constituents, and the development of a numerical model using Hashin's failure initiation criteria and a damage evolution law based on fracture energy. Experimental tests were conducted on treated and untreated jute fibers, as well as on different jute-glass hybrid composites. Tensile tests and fracture toughness analysis were performed to obtain critical mechanical properties for numerical modeling. The numerical study was carried out using Abaqus software, simulating the behavior of the hybrid composites. The results of the experimental tests demonstrated the feasibility and mechanical properties of the jute-glass hybrid composites. The numerical simulations using the properties from the experimental tests showed good agreement with the experimental findings. Additionally, the numerical model utilizing separate properties for jute and glass exhibited promising results, representing the mechanical behavior of the hybrid composites effectively. Overall, this research provides valuable insights into the mechanical properties and behavior of jute-glass hybrid-reinforced composites. The combination of experimental and numerical analyses offers a comprehensive understanding of the material, facilitating its potential applications. The findings contribute to the ongoing research on natural fiber composites and provide a basis for further optimization and development of hybrid materials with enhanced mechanical performance and eco-friendly attributes.

Keywords: natural fibers; hybrid composites; fiber-reinforced composites; progressive failure; jute; fiber treatment.

RESUMO

Compósitos reforçados com fibras naturais são uma nova classe de materiais de engenharia que podem ser utilizados em diferentes aplicações industriais. Enquanto os compósitos poliméricos reforçados com fibras sintéticas têm sido tradicionalmente empregados em estruturas de alto desempenho, o interesse em compósitos reforçados com fibras naturais está crescendo devido às suas vantagens ecológicas, renováveis e custo-benefício. A juta é uma fibra natural facilmente encontrada no Brasil, seu uso é ecológico e ajuda economias locais. As fibras naturais também apresentam algumas desvantagens em comparação com as sintéticas, como baixa resistência à absorção de umidade, propriedades variáveis e comportamento hidrofílico, que podem ser evitados através de tratamentos. Esta pesquisa tem como objetivo explorar o comportamento mecânico de compósitos híbridos reforçados com juta e vidro, através de análises experimentais e numéricas. Os principais objetivos incluem a produção de compósitos híbridos através de laminação manual, a caracterização das propriedades mecânicas fundamentais dos compósitos e seus constituintes, e o desenvolvimento de um modelo numérico utilizando os critérios de iniciação de falha de Hashin e uma lei de evolução de danos baseada na energia de fratura. Ensaios experimentais foram realizados em fibras de juta tratadas e não tratadas, assim como em diferentes compósitos híbridos de juta e vidro. Ensaios de tração e de energia de fratura foram realizados para obter importantes propriedades mecânicas para a modelagem, que foi realizada utilizando o software Abaqus, simulando o comportamento dos compósitos híbridos. Os resultados dos ensaios experimentais demonstraram a viabilidade e as propriedades mecânicas dos compósitos híbridos de juta e vidro. As simulações numéricas utilizando as propriedades obtidas dos ensaios experimentais apresentaram boa concordância com os resultados experimentais. Além disso, o modelo numérico utilizando propriedades separadas para a juta e o vidro apresentou resultados promissores, representando efetivamente o comportamento mecânico dos compósitos híbridos. No geral, esta pesquisa fornece insights sobre as propriedades mecânicas e comportamento dos compósitos híbridos de juta e vidro. A combinação de análises experimentais e numéricas oferece uma compreensão abrangente do material, facilitando suas potenciais aplicações. Os resultados contribuem para a pesquisa contínua sobre compósitos de fibras naturais e fornecem uma base para a otimização e desenvolvimento de materiais híbridos com melhor desempenho mecânico e atributos ecologicamente amigáveis.

Palavras-chave: fibras naturais; compósitos híbridos; compósitos reforçados com fibras; falha progressiva; juta; tratamento de fibras.

LIST OF FIGURES

LIST OF TABLES

CONTENTS

1 INTRODUCTION

Fiber-reinforced composites consist of different lamina of fibers embedded in a matrix material. Usual composites with synthetic fibers are employed in high-performance structures, usually with polymeric matrices (Fiber Reinforced Polymer - FRP). Over the past years, there has been a rapid increase in the demand for FRP composites due to their interesting properties and high performance (MISHRA; BISWAS, 2013; BARBERO, 2010). Composites with natural fibers are not the primary choice for structural applications, but they have started to gain recognition as potential materials in the automotive industry (SAFRI *et al.*, 2018).

Inorganic (or synthetic) fibers are the most common, such as glass and carbon fibers, which are classical engineering materials. However, natural fibers present several ecological advantages, such as being renewable, biodegradable, and inexpensive, in addition to being completely or partially recyclable (MONTEIRO *et al.*, 2009; MAJUMDAR, 2016; SANJAY; YOGESHA, 2016; MISHRA; BISWAS, 2013; GUJJALA *et al.*, 2014; FARUK *et al.*, 2012). Their use in composites is becoming attractive because the interest in the use of renewable resources is increasing among the present generation of researchers (SABA *et al.*, 2016; GUJJALA *et al.*, 2014). Moreover, natural fibers are light-weight, low density, high-specific strength, and present low abrasivity and toxicity (GUJJALA *et al.*, 2014). Due to their outstanding properties, natural fiber-reinforced polymer composites are mostly used in aircraft and automotive industries, and also in the manufacturing of spaceships and sea vehicles (KHALIL *et al.*, 2010; GUJJALA *et al.*, 2014).

The search for the use of natural fibers instead of synthetic ones is explained by their advantages and the large availability of these materials worldwide. The most common fibers used as a reinforcing material in polymer composite are: sisal, jute (SMAIL *et al.*, 2021; GUJJALA *et al.*, 2014), oil palm fiber (KHALIL *et al.*, 2010), pineapple leaf (AJI *et al.*, 2013; SHIH *et al.*, 2014; NOPPARUT; AMORNSAKCHAI, 2016), hemp (SAWPAN *et al.*, 2012), bamboo (KHALIL *et al.*, 2010), wood, flax, and kenaf (AJI *et al.*, 2013). In Brazil, a variety of fibers, including sisal, jute, coir, and curauá, are readily available, all of which are already being utilized in commercial applications. Brazil holds the potential to yield approximately 10,000 tons per year of vegetable fibers, sourced either from native reserves or cultivation, thereby presenting an income-generating opportunity for numerous local communities (ALVES *et al.*, 2010).

Among those, jute is a natural fiber easily found in Brazil, especially in the northeast region of the country. Jute is produced from the genus Corchorus plants, which includes about

100 species (FARUK *et al.*, 2012). Its use, besides being environmentally friendly, can boost local economies, since its fabrication and production are made by local artisans.

Jute fibers have interesting mechanical properties such as high tensile strength and stiffness for an organic fiber, making it suitable for reinforcing composite materials. Another advantage of jute is its low cost compared to other synthetic fibers such as carbon and glass (SMAIL *et al.*, 2021; GUJJALA *et al.*, 2014). This makes it a viable option for applications that demand both strength and resistance while remaining accessible. Jute is also available in very large amounts (GANGIL *et al.*, 2020), presenting in 2001 a high world annual production at about 2300 (103 ton.) (ALVES *et al.*, 2010).

Moreover, jute has low density, which means it can be used to manufacture lightweight composite materials, which are important in applications such as the aerospace and automotive industry (RAMASUBBU; MADASAMY, 2022; MARICHELVAM *et al.*, 2021), where weight reduction can lead to significant performance improvements. Another advantage is its biodegradability, which means that at the end of the product's life, the material can be easily decomposed by the environment without causing negative impacts. This is particularly important in a world where sustainability is an increasingly pressing concern.

However, natural fibers present some drawbacks, such as lower mechanical strength when compared to synthetic fibers, poor resistance to moisture absorption, high variability in its microstructure, susceptibility to pests and microorganisms, and a hydrophilic behavior (SOOD; DWIVEDI, 2018; SMAIL *et al.*, 2021). These characteristics must be carefully considered and addressed in order to optimize their use in different applications.

However, some of these weaknesses can be prevented by fiber treatment (SOOD; DWIVEDI, 2018; QIAN *et al.*, 2015). The mechanical properties of natural fiber composites are strongly influenced by the processing techniques used to manufacture the composites. There are a lot of treatments that can easily modify the natural fiber and change its hydrophilic nature (ARDANUY *et al.*, 2015), providing them a better interface bonding, lower water absorption, and an improved performance (XIE *et al.*, 2010). The literature points out to different types of chemical and physical treatments available (SOOD; DWIVEDI, 2018) however, alkali treatment is the most used pre-treatment in natural fibers (XIE *et al.*, 2010).

Since natural fibers present some disadvantages, and the use of synthetic fibers must be reduced due to environmental issues, the use of hybrid composites (with natural and synthetic fibers) is increasing, taking advantage of the best qualities of each material (SANJAY;

YOGESHA, 2016).

There is a plethora of research presenting experimental data on composites reinforced with synthetic fibers, however, experimental data for natural fiber composites is not widely available due to proprietary research, limited publications, or the niche nature of the field. Consequently, the development of reliable numerical models to predict the behavior of these materials becomes a critical endeavor, and understanding the mechanical behavior and failure mechanisms is paramount for their successful application in various industries.

In the realm of composite materials, the development and characterization of novel compositions often necessitate extensive experimental testing. These tests involve time-consuming processes, the handling of chemical substances, and meticulous data collection through various mechanical tests, such as tensile testing. Such experimental endeavors, while invaluable for understanding material behaviors, can be resource-intensive and limit the scope of exploration. A numerical model calibrated to represent hybrid composites would reduce the need for extensive experimentation.

Overcoming these difficulties requires a combination of careful experimental design, a collaboration between researchers, meticulous data collection, and integration of the obtained data into numerical models that accurately represent the complex behavior of natural fiber composites.

As composite materials, whether natural or synthetic fiber reinforced, exhibit complex behavior influenced by various factors, such as fiber-matrix interaction, loading conditions, and environmental influences, it becomes essential to employ suitable failure theories and degradation models to capture their complex response accurately. In the context of natural fiber composites, selecting the most appropriate models to represent the intricate interplay between various failure mechanisms remains an ongoing challenge.

Within this context, the task of identifying suitable damage initiation criteria becomes a focal point of investigation. A range of established criteria have been proposed to capture different aspects of damage initiation in composite materials. However, their application to natural fiber composites requires careful consideration, given the unique characteristics and behaviors exhibited by these materials.

In light of these complexities, the present research embarks on an investigation into the suitability of some damage initiation criteria for natural fiber-reinforced hybrid composites. In summary, the incorporation of effective failure theories and degradation models tailored to the

unique characteristics of natural fiber composites is a pivotal step toward enabling their wider application. This research aims to provide a deeper understanding of the interplay between composite constituents and to analyze numerical models that accurately predict the response of these materials. Different failure theories and degradation models are used to describe the composite's behavior in numerical models. Thus, different damage initiation criteria (HASHIN; ROTEM, 1973; HASHIN, 1980; TSAI; WU, 1971; HILL, 1948; DANIEL *et al.*, 2006) are going to be studied in this research, and a numerical model will be tested to represent experimental data.

1.1 Objectives

This work's main goals were to perform experimental and numerical analysis of jute–glass hybrid-reinforced epoxy composites. Different composites were produced, and different tests were conducted to analyze and compare the properties of these composites. Important mechanical properties to numerical modeling were obtained experimentally. A failure initiation criterion was used to represent the mechanical behavior of these hybrid composites. For this purpose, the following specific objectives were set:

a) To assess the feasibility of producing hybrid composites (by manual lamination), using epoxy resin, jute, and glass fibers;
b) To carry out an experimental program to characterize fundamental mechanical properties of the hybrid composites and their constituents;
c) To perform a numerical analysis of the composites using Hashin's failure initiation criteria and damage evolution law based on fracture energy (G_f) and validate it with experimental results
d) To perform a parametric study involving different lamination schemes in terms of the ultimate strength of specimens with different geometries.

1.2 Organization of the text

Chapter 2 introduces important concepts about the mechanical behavior of laminated composites reinforced with fibers. Failure theories and damage models that will be used in this work are presented and discussed there.

Chapter 3 presents the materials that are going to be used in the experimental tests.

The treatments and the tests are also described.

Chapter 4 presents numerical and experimental results. Finally, Chapter 5 presents the concluding remarks.

2 LITERATURE REVIEW

2.1 Laminated Composites

Composite materials are the combination of two or more dissimilar materials, that together have better mechanical properties and higher performance that could not be reached by its constituents separated. These materials can be divided into four main types (JONES, 1998): (i) particulate composite materials (ii) fibrous composites material (iii) laminated, which consists of layers of different materials, and (iv) a combination of some or all of the other types. Types (i) to (iii) and variations of type (ii) are presented in Figure 1.

Figure 1 – Types of composites material.

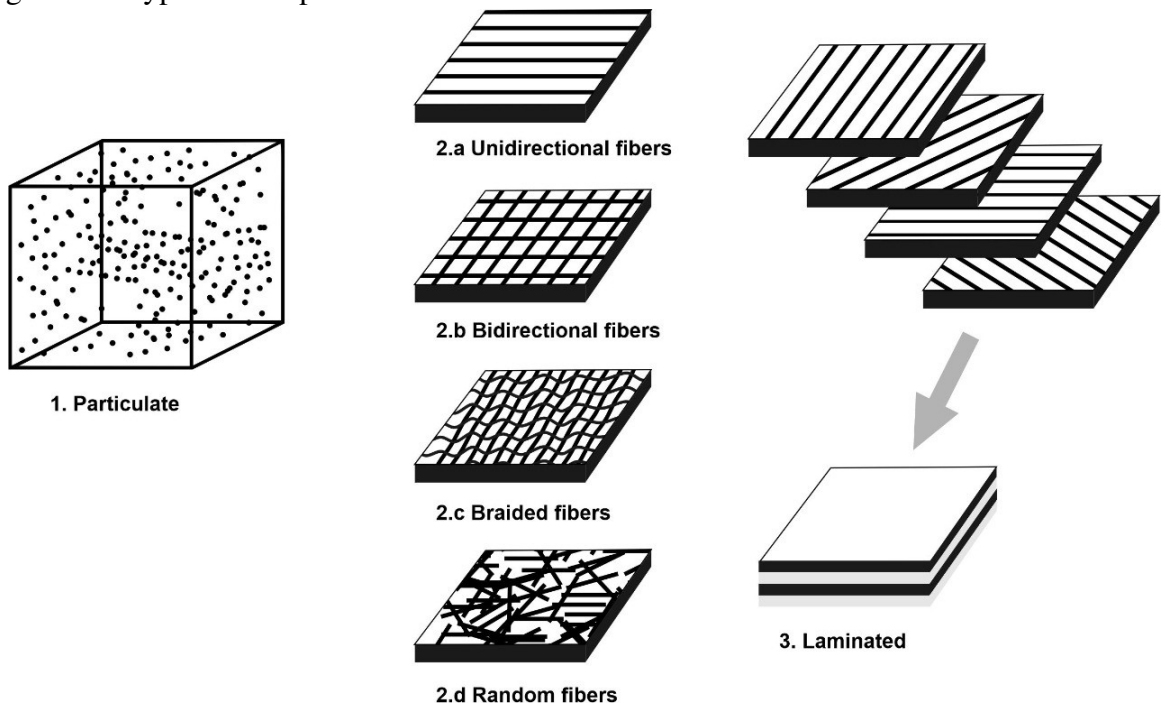

Source: Author.

This research centers around laminated composites, also referred to as fiber-reinforced materials, which encompass distinct layers or laminae of fibers incorporated within a matrix material. The mechanical characteristics of each lamina or ply vary based on the alignment of the fibers within the matrix.

Laminated composites find extensive application in high-performance structures. In recent decades, the demand for FRP composites has surged due to their remarkable strength, streamlined manufacturing process, exceptional performance attributes, and cost-effectiveness (MISHRA; BISWAS, 2013).

While inorganic options such as fiberglass and carbon fibers remain the predominant choices for fiber reinforcement, nonetheless there is a growing exploration of natural fibers due to their environmental advantages. Epoxy resin stands as a primary choice for the polymer matrix in which the fibers are immersed. This amalgamation yields a material endowed with superior mechanical properties, elevated resistance to corrosion and fatigue, minimal thermal expansion, and reduced weight. The ensuing combination delivers a versatile material with an array of desirable properties suitable for a wide range of applications (BARBERO, 2010).

2.1.1 Fiber Reinforced Hybrid Composites

Traditional synthetic fibers have lots of advantages for being created to be used as an engineering reinforcing material. They present high mechanical properties, such as tensile and flexural modulus and strength, and interlaminar shear strength (SANJAY; YOGESHA, 2016; GUJJALA *et al.*, 2014). However, it is very difficult to recycle this material (JOHN; NAIDU, 2004) and their production causes CO_2 emissions, which are responsible for the atmospheric greenhouse effect (MONTEIRO *et al.*, 2009).

Natural fibers, on the other hand, are a renewable and biodegradable material, cheap, completely or partially recyclable and it has been attracting researches that worry with environmental consciousness and sustainability concept (MONTEIRO *et al.*, 2009; MAJUMDAR, 2016; SANJAY; YOGESHA, 2016; MISHRA; BISWAS, 2013). Incorporation of natural fibers in composite materials is becoming attractive for the use of renewable resources encouraged by the issues of a safer environment, that have been increasing in both areas of engineering and research technology (SABA *et al.*, 2016). These fibers also present low weight, low density, high-specific strength, nonabrasivity, and nontoxicity (GUJJALA *et al.*, 2014).

Natural fibers can also boost local economies (MONTEIRO *et al.*, 2009), since some woven, like jute fabric, are manufactured and sold in local markets. When compared to traditional reinforcing material, natural fibers present acceptable specific strength properties, low density, low abrasion, good thermal properties, and cause less skin and respiratory irritation. When they are in a polymer matrix, they show a systematic potential as a useful resource for structural and non-structural applications (AJI *et al.*, 2013). Another advantage is that they allow the reduction of petroleum products dependence (KHALIL *et al.*, 2010).

However, natural fibers present lower mechanical performance when compared to synthetic fibers. Gujjala *et al.* (2014) points out that jute fibers present, on average, tensile

strength three times lower than glass fibers. Besides that, natural fibers have poor resistance to moisture absorption and present a hydrophilic behavior due to the hydroxyl existing in their constituents (SOOD; DWIVEDI, 2018). They also present random properties, since they are a natural material, their microscopic structures can not be strictly controlled while growing (SMAIL *et al.*, 2021). Also, the fabric is usually handmade, so it is expected that their production results in materials with variable mechanical properties. Barbero (2010) presents other drawbacks: limited processing temperatures, lower durability, and lower fire resistance.

To capitalize on the favorable attributes of both synthetic and natural fibers while mitigating their limitations, there is a growing inclination towards embracing hybrid composites, which blend the advantages of both fiber types. The availability of empirical evidence is crucial for a comprehensive evaluation of these materials. Equally vital is the need for the numerical modeling of these composites and determining the most effective numerical framework for achieving optimal outcomes. These hybrid composites hold the potential for applications in structural roles, particularly in scenarios where enhanced strength and prudent cost management, derived from the synergy of diverse fibers, assume paramount significance (SANJAY; YOGESHA, 2016).

Usual synthetic composites present high strength and high modulus fibers in a matrix material, where the fibers are the main load-carrying members, and the matrix keeps the fibers together (REDDY, 2003). The matrix acts as a load-transfer environment for the fibers, protecting them from being exposed to moisture, humidity, etc..

Rashid *et al.* (2020) presents the use of banana fiber-reinforced hybrid composites in the sports industry, aiming to introduce new materials for field hockey equipment to reduce manufacturing costs and the environmental impact of synthetic materials, without comprising the quality of the final product. In the aerospace industry, natural hybrid composite materials are steadily being introduced as substitute materials for aircraft component construction, which are already employed for aircraft radome and interior cabin components, representing innovation in line with the industry's growing sustainability goals (MANSOR *et al.*, 2019; PUTTEGOWDA *et al.*, 2018).

In automotive studies, Ramasubbu and Madasamy (2022) fabricated a car bumper with hybrid composite produced by hand lay-up process. In the study, an old car bumper was reinforced with sisal and kenaf fibers. Epoxy resin and hardener were applied gradually over the layers of natural fibers. Chandgude and Salunkhe (2021), Siengchin (2017), Ravishankar *et al.*

(2019) present recent reviews about the mechanical behavior and potential of natural fiber-based hybrid polymeric composites for application in automobile components.

2.1.2 Fiberglass

Fiberglass or E-glass fibers are a reinforcing material, in which "E" means suitability for electrical insulation, which was its former application (MAHLTIG; KYOSEV, 2018). Since it can be used more widely than the original intended electrical applications, it has become a standard material for the production of fibers all over the world, playing a special role when used as a reinforcing material with synthetic resins, due to its low cost and fire resistance (MAHLTIG; KYOSEV, 2018).

Fiberglass is derived from bulk glass and its main constituent is silica (SiO_2). Chemical composition control can result in different types of glass fibers, but all of them present typical glass properties of hardness, corrosion resistance, and inertness (BARBERO, 2010). They are also lightweight, strong, inexpensive and robust material, which is used in different industries due to their excellent engineering properties (SANJAY; YOGESHA, 2016; BARBERO, 2010). This material shows a linear elastic behavior up to fracture. Its tensile strength is approximately 3500 N/mm^2, and its elastic modulus is 70000 N/mm^2 (BöGNER-BALZ *et al.*, 2015).

2.1.3 Jute

Jute is a bast fiber, which means it is collected from the phloem (the living tissue in vascular plants that transports the soluble organic compounds) or bast surrounding the stem of certain dicotyledonous plants. Among the natural fiber reinforcing materials, jute appears to be a promising material because it is relatively inexpensive and commercially available in the required form, which is as an woven (SANJAY; YOGESHA, 2016). It is one of the cheapest natural fibers (SONG *et al.*, 2021) and it is currently the bast fiber with the highest production volume. The average tensile stress of a jute yarn in environmental temperature is 53 MPa (SMAIL *et al.*, 2021).

Jute polymer composites have begun finding applications in the automobile sector for parts such as interior door panels, seat back and trunk liner (CHANDEKAR *et al.*, 2020). It also has application in geotextiles, construction and furniture industries. Its use helps in ecological balance and also provide employment to the rural people in countries like Brazil, India and Bangladesh, where it is abundantly available (MISHRA; BISWAS, 2013).

Alves *et al.* (2010) presents an investigation centering on replacing glass fibers with jute fibers in the production of a structural frontal bonnet for an off-road vehicle (Buggy). This study encourages that jute fibers are part of a broader trend of integrating natural materials in automotive applications. This aligns with global efforts towards sustainability, as evident in initiatives such as Mercedes-Benz of Brazil's collaboration with the Federal University of Pará, aiming to incorporate renewable resources into vehicle components. The study concludes that jute fiber composites offer enhanced environmental performance for vehicle enclosures, contributing to overall efficiency, despite some unanticipated impacts related to production logistics and recycling scenarios identified by the Life Cycle Assessment analysis.

These fibers main constituents are cellulose, hemicellulose, pectin and lignin, besides a little amount of other organic and inorganic substances. Cellulose is the major constituent and it is responsible for the fibers strength, stability and stiffness. Hemicellulose is a branched polymer, lignin is an aromatic structure and pectin is constituted of polysaccharides (SOOD; DWIVEDI, 2018). Hemicellulose, lignin and pectin play the role of matrix, responsible for the cohesion between the micro-fibrils (SMAIL *et al.*, 2021).

2.1.4 Fiber treatment

Fiber treatment can improve some of the weaknesses of the natural fibers. Cellulose, hemicellulose, pectin, lignin and other organic and inorganic constituents are responsible for a hydrophilic behavior in the natural fibers due to the hydroxyl existing in these constituents (SOOD; DWIVEDI, 2018). This is a problem because matrices are mainly polymers like polypropylene, polyvinyl chloride and polylactic acid, which are hydrophobic (QIAN *et al.*, 2015; SOOD; DWIVEDI, 2018). This leads to a poor interface because fibers do not adhere well to hydrophobic polymer matrices and also absorb water from the moisture. Poor bonding causes losses on the composite mechanical properties, which is a big issue.

To try to mitigate this, there are a lot of treatments that can easily modify the natural fiber and change its hydrophilic nature (ARDANUY *et al.*, 2015). The main reason behind these treatments is to make natural fiber reinforced composites materials a good structural element, and for this, they should present a good behavior under flexural loading. That is why they should have a good interface bonding. There are different types of chemical and physical treatments available that turns possible to enhance the functionality of natural fiber polymer composites (SOOD; DWIVEDI, 2018).

The chemical treatment is a permanent process that improves the compatibility between the fiber and matrix (SOOD; DWIVEDI, 2018). They can improve the fiber's water absorption behavior, turning it more hydrophobic or hydrophilic. (ARDANUY *et al.*, 2015). For composite materials, the aim is to turn the natural fibers more hydrophobic to achieve better bonding and composites with better mechanical properties. Besides that, chemical treatment provides more dimensional stability to the fiber cell walls, reduces water absorption and increases resistance against fungal decay (XIE *et al.*, 2010).

Alkali treatments are the most used in natural fibers. They can remove the lignin, wax and oil and cover part of the natural fibers increasing its surface roughness, which leads to a better interlocking between fiber and matrix and promotes a critical improvement to fiber performance (XIE *et al.*, 2010). Figure 2 shows micrographic photos of jute fiber untreated (a) and reated (b). It is possible to see that the treatment increased the surface roughness, which provides better interaction with matrix (PRAHARAJ *et al.*, 2015).

Figure 2 – Scanning electron micrographs of untreated (a) and treated (b) jute fibers.

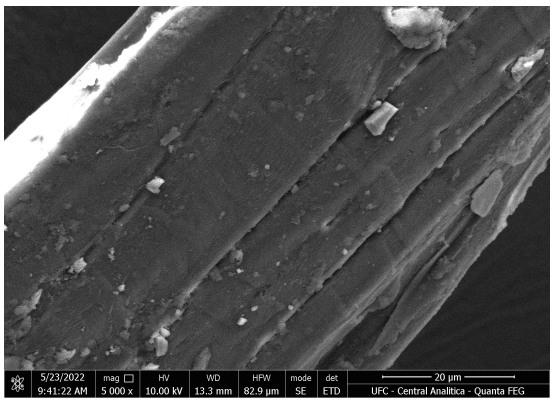

(a)

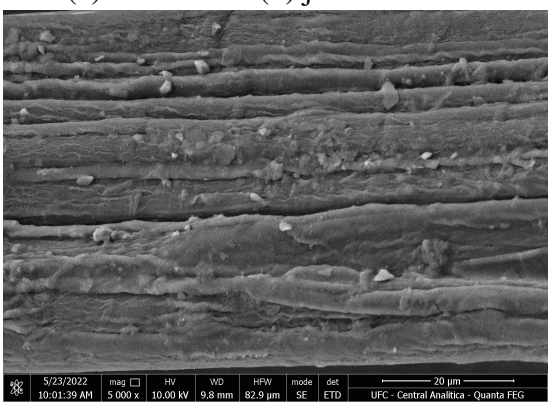

(b)

Source: Author

Many researchers used different alkali treatments to improve the flexural behavior of natural fibers. Xie *et al.* (2010) improved wood particles using glutaraldehyde and 1,3-dimethylol-4,5-dihydroxyethyleneurea. The chemical treatment reduced the wood water absorption and dimensionally stabilize the resulting composites. Bamboo fiber reinforced polyester composites with different levels of sodium hydroxide treatment (NaOH) were investigated (MANALO *et al.*, 2015). Enhancement in the adhesion between the bamboo fibers and the polyester resin was achieved. 6% of NaOH was found to be the optimum concentration, making it possible to reach a stiffness 25% higher than the untreated composites. With a higher concentration (8%) it was observed a reduction in mechanical properties, which shows the importance of using the

appropriate alkali concentration.

Sood and Dwivedi (2018) presents a review about chemical treatments in natural fibers. Bamboo, jute, pineapple, Arundo leaf, sisal, abaca, banana and other fibers are covered in this review. Focusing on jute fibers, that are going to be used in this work, treatments used NaOH, silane, peroxide, permanganate, among others.

Shanmugam and Thiruchitrambalam (2013) immersed jute fibers in 5% NaOH for 30 min. Later, the fibers have to be cleaned several times with distilled water and immersed in very dilute HCl in order to remove the NaOH adhering to the surface of the fibers. Finally, the fibers have to be washed several times again with distilled water and dried in an oven maintained at 70 °C. Composite flexural modulus increased 19% and its strength increased 56% with the treatment.

In order to improve the adhesion of jute fiber with polylactic acid matrix, Goriparthi *et al.* (2012) modified the jute fiber surface with alkali, permanganate, peroxide and silane treatments. All the treatments started by soaking the fibers for 1h in a 5% NaOH solution and then washing them in distilled water until a pH of 7 was reached. The other treatments were made in the alkaline-treated fibers, being the alkalization considered as a pre treatment for the other ones. In permanganate treatment, the fibers were dipped for 1 min in 0.125% parmanganate acetone solution. In benzoyl peroxide treatment ($(C_6H_5CO)_2O_2$), fibers were dipped in a 6% solution 30 min after the alkalization. In silane treatment, two kinds of coupling agents were used (3-amino propyl trimethoxy silane - silane 1 and trimethoxy methyl silane - silane 2). The fibers were soaked in a solution of acetone/water (50/50 by volume) with a concentration of 1% of silane for 2h. After alkalization and after the second treatment, the fibers were dried in the hot air oven at 80ºC for 5h to remove excessive solvent and moisture. All of the treatments improved the fibers mechanical properties, but alkali, permanganate and peroxide treated composites exhibited lower thermal stability. Silane 2 treated jute fiber composite was the one with the highest flexural properties and better abrasive wear resistance.

Sever *et al.* (2011) subjected jute fabric to oxygen plasma treatment. Low and Radio Frequencies plasma systems with different discharge powers were used for surface modification. Radio Frequency plasma-treated jute fibers presented composites with best improvements in terms of mechanical properties. These composites were made with the jute-treated fibers used as reinforcement into a high-density polyethylene matrix.

Hossain *et al.* (2011) achieved better interfacial bonding on jute fibers by using

detergent washing, dewaxing, alkali treatment and soaking with acetic acid. Detergent washing was used to remove the dirt from the fibers by keeping them into a 5% detergent solution at 30ºC for 1h and washing them subsequently with water. Dewaxing was made by keeping the fabric into a 5% ethanol solution to remove the pectin. To remove lignins and hemicelluloses the alkalization was performed with a 5% NaOH solution for 2h at 30ºC. Then, the alkali-treated fibers were soaked at a 2% acetic-acid solution for 1h. This acid reacts with the OH groups from the alkalization, converting hydrophilic surfaces into hydrophobic for better adhesion with a bipole matrix. This treatment turned the surface rougher and increased its effective area, resulting in better interaction between the fiber and matrix. These fibers showed better tensile properties compared to untreated ones.

Another pre treatment is to soak the jute fibers at a 0.1% H_2SO_4 solution at 55ºC for 1.5h (it has to be washed before the alkali treatment) (LIU *et al.*, 2009). Liu *et al.* (2009) the observed that surface modification as a result of alkali treatment exhibits fewer effects on flexural properties compared to tensile properties. Experimental results showed that surface modification can reduce the diameter of jute fibers. Besides that, among the treatments experimented by this author, the composite with better mechanical properties after treatment was the one subjected to a coupling agent (γ-methacryloxypropyltrimethoxysilane KH-570 with a molecular weight of 248.35): jute fibers were soaked in a solution of 2% NaOH, 0.2% Na_2SiO_3, 0.2% $Na_2P_3O_{10}$, 0.15% Na_2SO_3 and 0.2% penetrate JFC at 100ºC for 1 h, and then soaked in a solution of 1.5% coupling agent and 98.5% anhydrous ethanol at 20 ± 1ºC for 4h.

Most part of the treatments evolves drying the fibers in hot air oven with temperature around 80ºC. This step is important to avoid that water from the treatment interfere in the composite adherence. However, when it is heated, fibers lose mechanical properties (SMAIL *et al.*, 2021). It is not a problem, since the main goal of the treatments is to improve fibers adherence with the matrix, which will result in a composite with enhanced mechanical properties.

Even though the existence of many works showing that chemical treatments improve the quality of organic fibers, some authors prefer to not use such treatments. Castro *et al.* (2021) did not use chemical treatment and got satisfactory properties of jute fabrics compared to other ones in the literature. The jute fabrics were just dried at 50ºC for 2h. Acha *et al.* (2005) used jute fabric as reinforcement for a thermoset resin, the study investigated the effects of two simple inexpensive fiber treatments: (i) washed in acetone, and (ii) washed with detergent. It was concluded that these treatments did not significantly affect jute physical and thermal behaviors.

In summary, jute composites present improved mechanical properties when they are treated. All of the chemical treatments presented in the literature enhanced the mechanical properties, the only exception was in inadequate concentrations (MANALO *et al.*, 2015). Alkali treatment is the most used one, it was used as the main treatment and also as a pre treatment, improving the properties in both cases. More demanding treatments (GORIPARTHI *et al.*, 2012; HOSSAIN *et al.*, 2011; LIU *et al.*, 2009; SHIH *et al.*, 2014) presented better results when comparing to only using alkali treatment. Most of the treatments require the presence of an oven to dry the fabrics at a high temperature. It is also necessary to have distilled water to wash the fabrics after the treatments, Shanmugam and Thiruchitrambalam (2013) used also HCl to remove NaOH.

2.2 Epoxy resin

Epoxy resin has many different commercial applications in engineering: adhesives for general purposes, binders in cement and mortars, and fiber-reinforced composites, among others. These different applications are due to epoxy's superior properties as an insulating material, which leads to extremely versatile materials (SABA *et al.*, 2016). Saba *et al.* (2016) defines epoxy as a thermosetting matrix or resin material, having at least one or more epoxide groups in the molecule. Most of the commercial epoxy resins are composed of oligomers of diglycidyl ether of bisphenol A (SABA *et al.*, 2016). In composite structures, epoxy is used as a binder to hold the reinforcing materials in their places. Composites with natural fibers and epoxy resin present a unique combination of great versatility, and high performance (MISHRA; BISWAS, 2013).

Epoxy resins are also widely used as a polymer matrix for advanced composites where good stiffness, dimensional stability, and chemical resistance are required (KHALIL *et al.*, 2010). Besides being relatively inexpensive, easily available, impact- and corrosion-resistant, this material has many other advantages, such as minimum shrinkage during curing, improved mechanical and fatigue strength, high moisture and chemical resistance, good adhesion with many substrates, non-magnetic properties, no Volatic Organic Compounds (VOCs), long shelf life and high damage tolerance (SABA *et al.*, 2016). These are advantages that outstand epoxy resin from other traditional thermoplastic or thermoset resins.

In contrast, epoxy resins can be relatively brittle compared to some other polymer matrices. This brittleness can lead to reduced impact resistance and susceptibility to cracking

or delamination under certain loading conditions (KISIEL; MOSSETY-LESZCZAK, 2020). Moreover, epoxy resins offer high stiffness, they may lack the toughness needed to absorb energy in high-energy impact situations. This can lead to catastrophic failures in cases where the material experiences sudden impact loads. Additionally, epoxy resins are susceptible to moisture absorption, which can lead to dimensional changes, reduced mechanical properties, and the potential for delamination in humid or wet environments (MI *et al.*, 2022). This becomes a greater issue on natural fiber composites.

A lot of care must be taken when preparing laminated composites. Epoxy resin curing involves a chemical reaction that requires precise control of temperature, time, and mixing ratios. Deviations from the recommended curing process can result in incomplete curing, leading to reduced mechanical properties and durability. Another pressing issue has to do with the rheology (viscosity) of epoxy resins. They often have lower viscosity when compared to other thermosetting resins, which can make their impregnation into fibers during manufacturing more challenging. Special care needs to be taken to ensure proper wetting and consolidation of the laminate.

For particular uses, there are different modified epoxy resins, which are very frequently used in the fabrication of natural fiber-reinforced composites (SABA *et al.*, 2016). Green or sustainable epoxy resins and fire retardant epoxies are some examples of modified epoxies.

2.3 Stacking sequence

In fiber-reinforced composites, the laminate stacking sequence is a very important characteristic of the material. It can be classified into two types regarding the fiber orientation (GÜRDAL *et al.*, 1999):

1. Cross-ply: Laminate composite that contains fibers only at 0º and 90º alternately, for example: [90º, 0º, 90º, 0º];
2. Angle-ply: Laminate composite that contains at least one fiber with orientation different from 0º and 90º, for example: [0º, 30º, 90º, 30º, 0º].

Laminated composites can also be classified according to their symmetry about the midplane:

1. Symmetric: when the midplane (equidistant plane from the outer composite surfaces) is a mirror of the fiber orientations, material, and thickness, for example: [90º, 30º, 0º, 0º, 30º, 90º]. A subscript "s" is used to identify these composites: $[90º, 30º, 0º]_S$;

2. Anti-symmetric: material and thickness are symmetric, but fiber orientations are negative to its opposite layer (considering the midplane as a mirror), for example: [60º, 30º, -30º, -60º];
3. Assymetric: Laminate composite presenting no symmetry about the midplane;
4. Balanced: Laminate composite that has an equal number of $+\theta$ and $-\theta$ plies. For example: [30º, -30º, 60º, -60º].

The effects of stacking sequence in hybrid composites with glass and jute fibers were tested and discussed in different experimental studies (GUJJALA *et al.*, 2014; MAJUMDAR, 2016; SANJAY; YOGESHA, 2016).

Sanjay and Yogesha (2016) compared two different hybrid composites, with 7 and 8 layers each. Both were sandwich composites, but one presented jute as the outer layers (JJGGGJJ), and the other presented glass (GGJJJJGG). The tests of these composites were also compared with only jute and only glass layups. Both hybrid composites presented better mechanical properties than the composite containing only jute fabric. Tensile, flexural and impact tests were performed. The composite GGJJJJGG presented better results.

MAJUMDAR (2016) analyzed two different stacking types: one was a sandwich type, and the other was made by six layers of jute followed by six layers of glass. This work also compared the effect of using epoxy or polyester in the matrix. Besides the tests mentioned in the previous work, hardness test was also performed. It was also concluded that hybrid composites present better results than jute composites. The matrix affected the hardness value, which depends on the interfacial bonding between extreme fibers and the matrix. Flexural strength and modulus are controlled by the extreme layers.

Gujjala *et al.* (2014) studied the following stacking sequences: GGGG, JJJJ, GJGJ, JGGJ, GJJG. Similar tests and results were obtained. GJJG presented the maximum tensile and interlaminar shear strength, presenting 75% of GGGG tensile strength. However, the maximum flexural strength was observed in the JGJG, presenting 61% of GGGG flexural strength.

2.4 Numerical Analysis of Laminated Composites

Structural analysis of laminated materials involves several steps. It requires a knowledge of anisotropic elasticity, structural theories of laminates, analytical or computational methods to solve the equations, failure theories, modes of failures, and damage theories.

There are two approaches to analyzing FRPs mechanical behavior: micromechanical

and macromechanical. In micromechanics, the constituents are analyzed separately and their interaction is examined on a microscopic scale. In macromechanics, fibers, and matrix are treated as a homogeneous and orthotropic material.

In usual practical applications, the mechanical behavior of composite materials can be represented by a linear elastic model until very close to failure (JONES, 1998). Thus, constitutive relations can be described by the Generalized Hook's Law for orthotropic materials, where stress-strain relations are:

$$\begin{bmatrix} \varepsilon_{11} \\ \varepsilon_{22} \\ \varepsilon_{33} \\ \gamma_{13} \\ \gamma_{23} \\ \gamma_{12} \end{bmatrix} = \begin{bmatrix} S_{11} & S_{12} & S_{13} & 0 & 0 & 0 \\ S_{12} & S_{22} & S_{23} & 0 & 0 & 0 \\ S_{13} & S_{23} & S_{33} & 0 & 0 & 0 \\ 0 & 0 & 0 & S_{44} & 0 & 0 \\ 0 & 0 & 0 & 0 & S_{55} & 0 \\ 0 & 0 & 0 & 0 & 0 & S_{66} \end{bmatrix} \begin{bmatrix} \sigma_1 \\ \sigma_2 \\ \sigma_3 \\ \tau_{13} \\ \tau_{23} \\ \tau_{12} \end{bmatrix} \rightarrow \varepsilon_1 = S\sigma_1 \tag{2.1}$$

where $\mathbf{S}$ is the compliance matrix, ε is the vector of strains and σ is the vector of stresses. Subscript 1 means they are in the fiber local system. S_{ij} is obtained by:

$$S_{11} = \frac{1}{E_1}; S_{12} = \frac{-\nu_{12}}{E_1}; S_{13} = \frac{-\nu_{13}}{E_1}; S_{22} = \frac{1}{E_2}; S_{23} = \frac{-\nu_{23}}{E_2}; S_{33} = \frac{1}{E_3}; \\ S_{44} = \frac{1}{G_{12}}; S_{55} = \frac{1}{G_{13}}; S_{66} = \frac{1}{G_{23}} \tag{2.2}$$

where ν_{ij} are the Poisson coefficients, E_{ij} are the Young's modulus in the fibers orientation and G_{ij} are the transverse shear modulus.

2.4.1 Failure criteria

For being composed of two different materials, with different stiffnesses and strength, laminated composites are inherently anisotropic materials. Failure mechanisms vary greatly with material properties and type of loading. From the macromechanical point of view, the strength of a lamina varies with orientation because it is an anisotropic material (DANIEL *et al.*, 2006). Anisotropic failure theories have been proposed by Tsai-Hill (HILL, 1948), Tsai-Wu (TSAI; WU, 1971), Hashin (HASHIN; ROTEM, 1973; HASHIN, 1980), Puck (PUCK *et al.*, 2002), and others.

To characterize a lamina and apply failure theories, strength parameters shown in Figure 3 are going to be used. F_{1t} and F_{1c} are the longitudinal tensile and compressive strength, respectively. F_{2t} and F_{2c} are the transverse tensile and compressive strength, respectively. F_6 or F_{12} is the in-plane or intralaminar shear strenght.

Figure 3 – Main strength parameters of unidirectional lamina for in-plane loading.

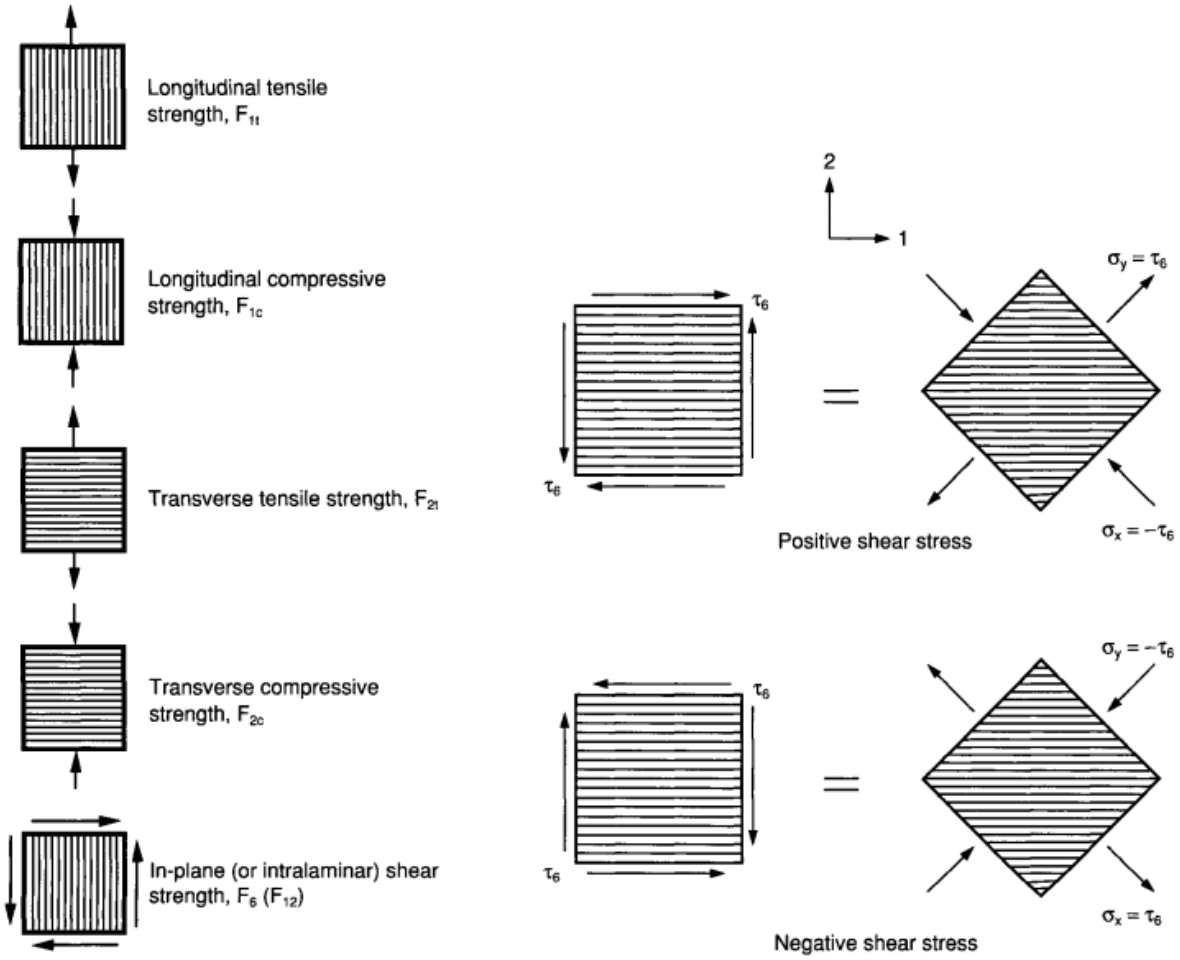

Source: Daniel *et al.* (2006).

In three-dimensional analysis, another four strength parameters are relevant: the out-of-plane or interlaminar tensile (F_{3t}), compressive (F_{3c}), and shear strengths ($F_4(F_{23})$ and $F_5(F_{13})$).

In a given state of stress, the principal stresses and their directions are obtained by stress transformation, which does not depend on the material properties. Since strength varies with orientation, anisotropic failure theories are needed to take into account stress and strength variation with orientation (DANIEL *et al.*, 2006).

In this study, experimental tests were performed to validate numerical models. In the experimental procedure, jute was characterized as treated and not treated. A hybrid composite

with treated jute fibers was prepared and submitted to tensile tests. The stacking sequence was chosen following previous experimental tests found in literature (GUJJALA *et al.*, 2014; MAJUMDAR, 2016; SANJAY; YOGESHA, 2016). Preliminary results of jute characterization and tests on the hybrid composites are presented herein.

Failure criteria for laminated composites can be classified into three categories according to the level of interaction between stresses in different directions:

1. Limiting or Non-interactive Criteria: consider stresses and strains individually for each direction (for example maximum stress and maximum strain theories).
2. Interactive Criteria: consider the interaction between directions. Overall failure is predicted without reference to particular failure modes (For example Tsai-Hill and Tsai-Wu theories).
3. Partially Interactive Criteria: consider all directions together, but analyze fiber and matrix failure separately (for example Puck theory).

2.4.1.1 Maximum Stress Theory

According to this theory, failure occurs when at least one of the stress components exceeds the strength in its corresponding direction. This theory does not take into account any stress interaction under a general biaxial state of stress. The stress acting on a unidirectional composite is resolved along the principal material axes and the failure condition is expressed in the following form:

$$\sigma_1 = \begin{cases} F_{1t} & \text{when} \quad \sigma_1 > 0 \\ -F_{1c} & \text{when} \quad \sigma_1 < 0 \end{cases} \tag{2.3}$$

$$\sigma_2 = \begin{cases} F_{2t} & \text{when} \quad \sigma_2 > 0 \\ -F_{2c} & \text{when} \quad \sigma_2 < 0 \end{cases} \tag{2.4}$$

$$\sigma_3 = \begin{cases} F_{3t} & \text{when} \quad \sigma_3 > 0 \\ -F_{3c} & \text{when} \quad \sigma_3 < 0 \end{cases} \tag{2.5}$$

$$|\tau_4| = F_4 \tag{2.6}$$

$$|\tau_5| = F_5 \tag{2.7}$$

$$|\tau_6| = F_6 \tag{2.8}$$

In a two-dimensional state of stress, $\sigma_3 = \tau_4 = \tau_5 = 0$. If the lamina is subjected to a biaxial normal loading, $\tau_6 = 0$ and the failure envelope takes the form shown in Figure 4. In a more general case, the stresses are transformed along the principal axes. Figure 5 presents the

variation of lamina strength of an E-glass/epoxy composite (DANIEL *et al.*, 2006) as a function of fiber orientation. This envelope can be divided into three different modes of failure:

1. fiber failure
2. in-plane shear interfiber failure
3. transverse normal stress interfiber failure

Figure 4 – Failure envelope for unidirectional lamina under biaxial normal loading.

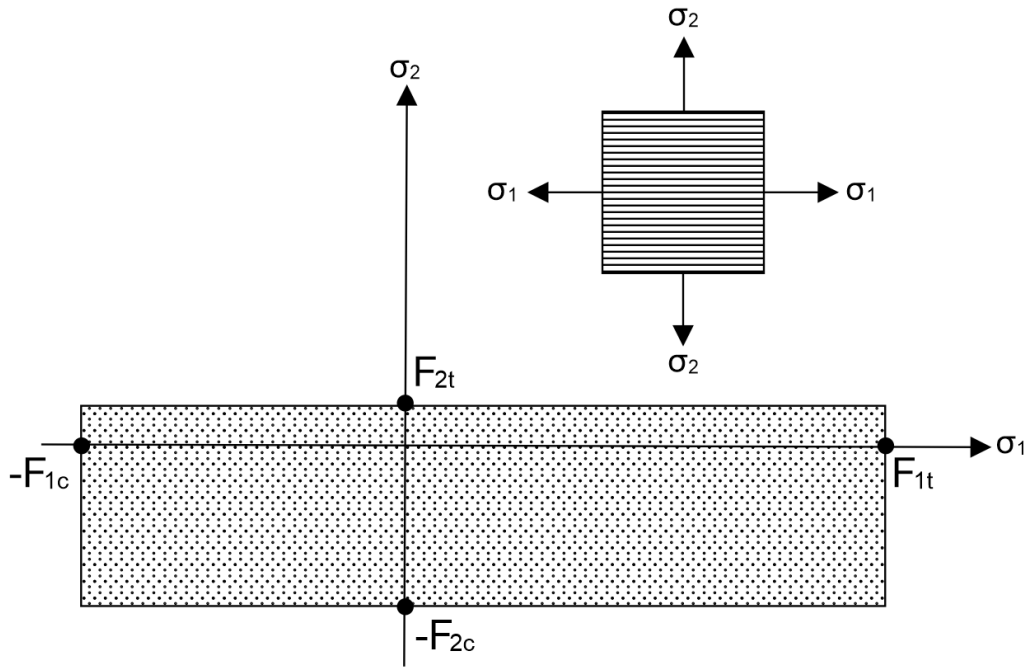

Source: Adapted from Daniel *et al.* (2006).

Figure 5 – Uniaxial strength of a unidirectional lamina as a function of fiber orientation.

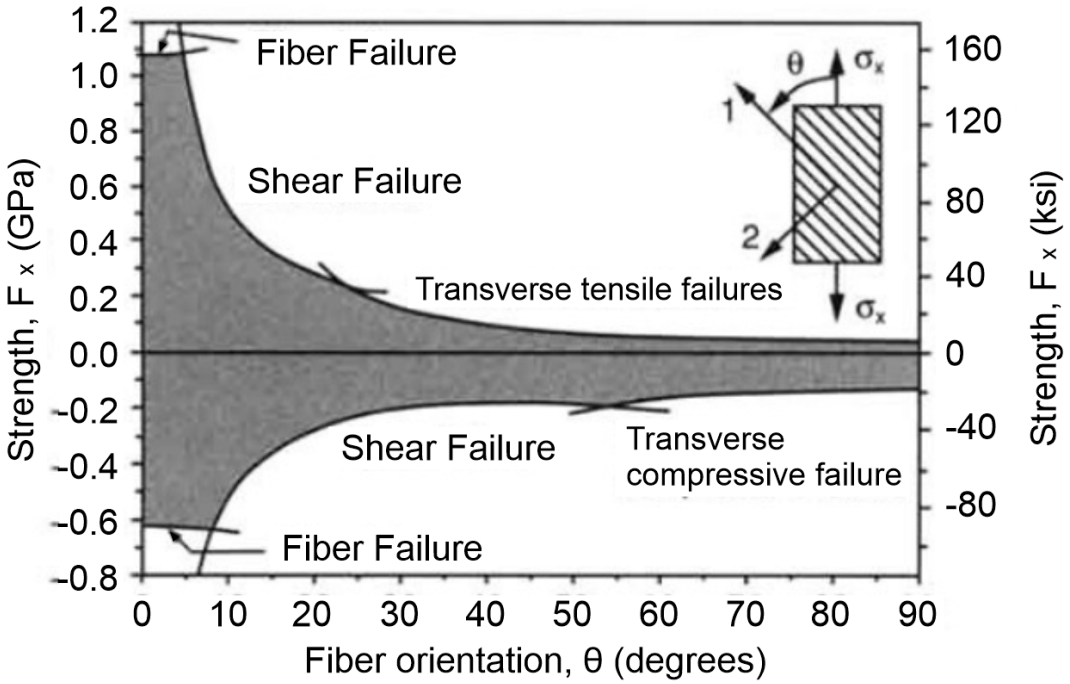

Source: Adapted from Daniel *et al.* (2006).

2.4.1.2 Maximum Strain Theory

According to this theory, failure occurs when at least one of the strain components exceeds the ultimate strain in its corresponding direction. It is expressed in the following form:

$$\varepsilon_1 = \begin{cases} \varepsilon_{1t}^u \text{ when } \varepsilon_1 > 0 \\ \varepsilon_{1c}^u \text{ when } \varepsilon_1 < 0 \end{cases} \tag{2.9}$$

$$\varepsilon_2 = \begin{cases} \varepsilon_{2t}^u \text{ when } \varepsilon_2 > 0 \\ \varepsilon_{2c}^u \text{ when } \varepsilon_2 < 0 \end{cases} \tag{2.10}$$

$$\varepsilon_3 = \begin{cases} \varepsilon_{3t}^u \text{ when } \varepsilon_3 > 0 \\ \varepsilon_{3c}^u \text{ when } \varepsilon_3 < 0 \end{cases} \tag{2.11}$$

$$|\gamma_4| = \gamma_4^u \tag{2.12}$$

$$|\gamma_5| = \gamma_5^u \tag{2.13}$$

$$|\gamma_6| = \gamma_6^u \tag{2.14}$$

In a given general state of stress, the stress components are obtained by stress transformation, and then the corresponding strains are obtained from the stress-strain relations:

$$\varepsilon_1 = \frac{\sigma_1}{E_1} - v_{21}\frac{\sigma_2}{E_2} - v_{31}\frac{\sigma_3}{E_3} = \frac{1}{E_1}(\sigma_1 - v_{12}\sigma_2 - v_{13}\sigma_3) \tag{2.15}$$

$$\varepsilon_2 = \frac{\sigma_2}{E_2} - v_{12}\frac{\sigma_1}{E_1} - v_{32}\frac{\sigma_3}{E_3} = \frac{1}{E_2}(\sigma_2 - v_{21}\sigma_1 - v_{23}\sigma_3) \tag{2.16}$$

$$\varepsilon_3 = \frac{\sigma_3}{E_3} - v_{13}\frac{\sigma_1}{E_1} - v_{23}\frac{\sigma_2}{E_2} = \frac{1}{E_3}(\sigma_3 - v_{31}\sigma_1 - v_{32}\sigma_2) \tag{2.17}$$

$$\gamma_4 = \frac{\tau_4}{G_{23}} \quad \gamma_5 = \frac{\tau_5}{G_{13}} \quad \gamma_6 = \frac{\tau_6}{G_{12}} \tag{2.18}$$

Since this theory considers Poisson's ratio effects, it allows for some interaction of stress components, which did not occur in the Maximum Stress Theory. In a unidirectional composite subjected to a uniaxial test, the basic strength parameters can be related to the material basic strength parameters presented on Figure 3. Then, the failure subcriteria presented in Equations (2.9) to (2.14) can be rewritten as:

$$\sigma_1 - v_{12}\sigma_2 - v_{13}\sigma_3 = \begin{cases} F_{1t} \text{ when } & \varepsilon_1 > 0 \\ -F_{1c} \text{ when } & \varepsilon_1 < 0 \end{cases} \tag{2.19}$$

$$\sigma_2 - v_{21}\sigma_1 - v_{23}\sigma_3 = \begin{cases} F_{2t} \text{ when } & \varepsilon_2 > 0 \\ -F_{2c} \text{ when } & \varepsilon_2 < 0 \end{cases} \tag{2.20}$$

$$\sigma_3 - v_{3!}\sigma_1 - v_{32}\sigma_2 = \begin{cases} F_{3t} \text{ when } & \varepsilon_3 > 0 \\ -F_{3c} \text{ when } & \varepsilon_3 < 0 \end{cases} \tag{2.21}$$

$$|\tau_4| = F_4 \quad |\tau_5| = F_5 \quad |\tau_6| = F_6 \tag{2.22}$$

In a two-dimensional state of stress ($\sigma_3 = \tau_4 = \tau_5 = 0$), and with $\tau_6 = 0$, the failure envelope takes the form of a parallelogram (Figure 6).

2.4.1.3 Tsai-Hill Theory

The von Mises yield criterion, which is applied to isotropic materials, has the following form:

$$\sigma_1^2 + \sigma_2^2 - \sigma_1\sigma_2 = \sigma_{yp}^2 \tag{2.23}$$

where σ_{yp} is the yield stress.

Figure 6 – Failure envelope for unidirectional lamina under biaxial normal loading in Maximum Strain Theory.

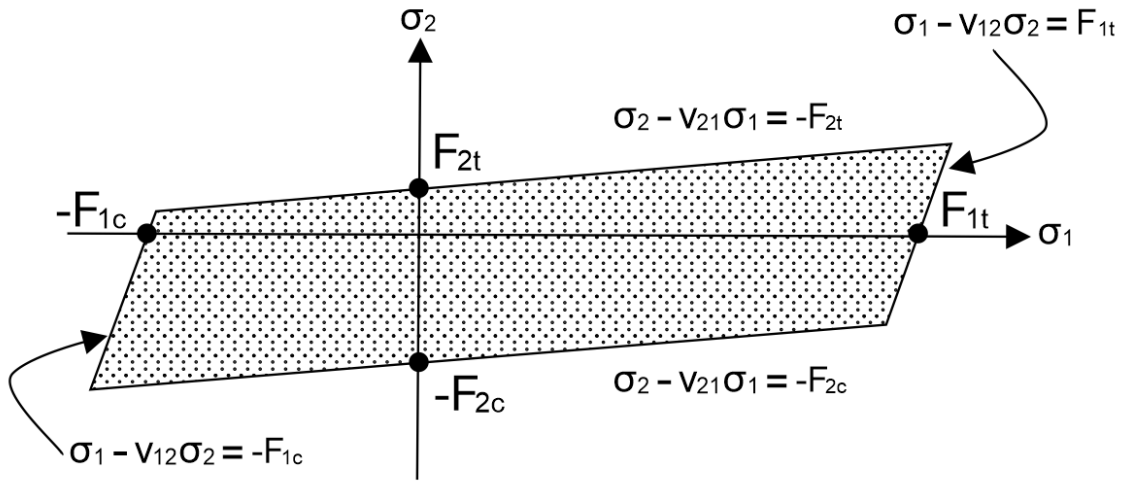

Source: Adapted from Daniel *et al.* (2006).

Also known as energy-based interaction theory, Tsai-Hill theory (HILL, 1948) is based on distortional energy as a failure criterion for anisotropic ductile metals. Hill (1948) modified Equation (2.23) for the case of ductile metals with anisotropy:

$$A\sigma_1^2 + B\sigma_2^2 + C\sigma_1\sigma_2 + D\tau_6^2 = 1 \tag{2.24}$$

where A, B, C and D are material parameters. In orthotropic composite materials, these parameters can be related to basic strength parameters of the lamina by conducting elementary experiments. Tsai-Hill criterion for a two-dimensional state of stress is given by:

$$\frac{\sigma_1^2}{F_1^2} + \frac{\sigma_2^2}{F_2^2} + \frac{\tau_6^2}{F_6^2} - \frac{\sigma_1\sigma_2}{F_1^2} = 1 \tag{2.25}$$

no distinction is made between tensile and compressive strengths, but the appropriate values can be used according to the signs of the normal stresses:

$$F_1 = \begin{cases} F_{1t} & \text{when } \sigma_1 > 0 \\ F_{1c} & \text{when } \sigma_1 < 0 \end{cases} \tag{2.26}$$

$$F_2 = \begin{cases} F_{2t} & \text{when } \sigma_2 > 0 \\ F_{2c} & \text{when } \sigma_2 < 0 \end{cases} \tag{2.27}$$

however, not distinguishing directly between tensile and compressive strengths is a disadvantage of this criterion.

The failure envelope of this theory is a closed surface in the $\sigma_1 - \sigma_2 - \tau_6$ space. The advantage of this theory when compared to the previous ones is that the Tsai-Hill criterion can be expressed in terms of a single criterion (a single equation). It also allows for considerable interaction among the stress components.

2.4.1.4 Tsai-Wu Theory

This is a criterion that was developed aiming to be a general failure theory for anisotropic materials without the limitations of the previous ones. It was proposed to adjust to experimental results and by assuming the existence of a failure surface in the stress space and can be written as follows:

$$f_{11}\sigma_1^2 + 2f_{12}\sigma_1\sigma_2 + f_{22}\sigma_2^2 + f_{66}\sigma_6^2 + f_1\sigma_1 + f_2\sigma_2 = 1 \tag{2.28}$$

the linear terms allow for distinction between tensile and compressive strengths, which was a problem in previous criteria. Tsai and Hahn (1980) proposed values for the constants, relating them to material strengths. These parameters and the value for F_{12} based upon von Mises isotropic criterion can be written as:

$$f_{11} = \frac{1}{F_{1t}F_{1c}} \tag{2.29}$$

$$F_1 = \frac{1}{F_{1t}} - \frac{1}{F_{1c}} \tag{2.30}$$

$$f_{22} = \frac{1}{F_{2t}F_{2c}} \tag{2.31}$$

$$F_2 = \frac{1}{F_{2t}} - \frac{1}{F_{2c}} \tag{2.32}$$

$$f_{66} = \frac{1}{F_{12}^2} \tag{2.33}$$

$$f_{12} = -\beta\sqrt{F_{11}F_{22}} \tag{2.34}$$

where β is the normalized interaction factor, which is in the range from 0 to -0.5 for most materials (KURAISHI *et al.*, 2004). For the generalized von Mises criterion, it is used $\beta = -0.5$.

The Tsai-Wu Criterion is widely used for fiber-reinforced composite materials because of its accuracy and relative simplicity (PANG *et al.*, 1992). With five strength parameter tests, failure strength for a lamina can be predicted for any generalized loading.

2.4.1.5 Hashin Criterion

There are two different failure modes in laminated composites: fiber and interfiber. For example, in the case of tensile off-axis loading, the interfiber failure mode is dominant. Thus, Hashin pointed out that the other failure criteria had the limitation of not considering these failure modes (LEE *et al.*, 2015). In his criterion, the failure of a lamina under an in-plane loading can be characterized by two failure criteria, one for fiber and the other for interfiber (HASHIN; ROTEM, 1973), as follows:

$$\frac{|\sigma_1|}{F_1} = 1 \tag{2.35}$$

$$\left(\frac{\sigma_2}{F_2}\right)^2 + \left(\frac{\tau_6}{F_6}\right)^2 = 1 \tag{2.36}$$

which can be extended to a three-dimensional state of stress:

$$\frac{|\sigma_1|}{F_1} = 1 \tag{2.37}$$

$$\left(\frac{\sigma_2}{F_2}\right)^2 + \left(\frac{\tau_4}{F_4}\right)^2 + \left(\frac{\tau_6}{F_6}\right)^2 = 1 \tag{2.38}$$

$$\left(\frac{\sigma_3}{F_3}\right)^2 + \left(\frac{\tau_4}{F_4}\right)^2 + \left(\frac{\tau_5}{F_5}\right)^2 = 1 \tag{2.39}$$

Hashin (1980) proposed a modification of this theory, considering four different damage initiation mechanisms: fiber tension (F_f^t), fiber compression (F_f^c), interfiber tension (F_m^t) and interfiber compression (F_m^c) in the general forms:

$$F_f^t = \left(\frac{\sigma_1}{F_{1t}}\right)^2 + \alpha\left(\frac{\tau_4}{F_4}\right)^2 \tag{2.40}$$

$$F_f^c = \left(\frac{\sigma_1}{F_{1c}}\right)^2 \tag{2.41}$$

$$F_m^t = \left(\frac{\sigma_2}{F_{2t}}\right)^2 + \left(\frac{\tau_4}{F_4}\right)^2 \tag{2.42}$$

$$F_m^c = \left(\frac{\sigma_2}{2F_6}\right)^2 + \left[\left(\frac{F_{2c}}{2F_6}\right)^2 - 1\right]\frac{\sigma_2}{F_{2c}} + \left(\frac{\tau_4}{F_4}\right)^2 \tag{2.43}$$

where α is a coefficient that determines the contribution of the shear stress to the fiber tensile initiation criterion. By setting $\alpha = 0$ and $S^T = Y^C/2$, the model of 1973 is used (HASHIN; ROTEM, 1973), and by setting $\alpha = 1$, the model of 1980 is used (HASHIN, 1980). Failure begins when these coefficients ($F_f^t, F_f^c, F_m^t, F_m^c$) are equal or higher than 1. This theory (HASHIN, 1980) is implemented on Abaqus/CAE. (MANUAL, 2012).

To estimate the compressive strength in cases where testing is not possible, the following empirical relationship exists:

$$F_{1C} = F_{1T}k \tag{2.44}$$

where the factor k can be obtained through one of the most common equations used for unidirectional composites present in Hashin's Law, which estimates the constant k in terms of the fiber volume fraction and individual properties of the fiber and matrix:

$$k = \frac{1}{1 - V_f/V_m} \tag{2.45}$$

where V_f is the fiber volume fraction and V_m is the resin volume fraction.

2.4.1.6 Puck Criterion

The Puck Criterion is a Partially Interactive Criteria. This criterion was one of the most accurate theories in the first and second worldwide failure exercises (WWFE-I and WWFE-II) (REINOSO *et al.*, 2017). It is based in Mohr-Coulomb, being strictly theoretical based. In others criteria, the models predict the failure initiation. The puck model enables to predict failure initiation and also the orientation of the fracture plane (PINHO *et al.*, 2005).

This criterion is an enhancement of Hashin failure criterion (LEE *et al.*, 2015). Besides distinguishing failure mechanisms (fiber and inter-fiber), it makes the distinction between damage development under tensile and compressive conditions (REINOSO *et al.*, 2017). Puck considered material properties of the ply and proposed an equation to determine the angle of the new fracture plane, which is generated during the fracture.

The Puck failure criterion can be written in five equations, and there is a condition for each one being valid. The equations and their respective application conditions are written as follows (LEE *et al.*, 2015):

1. Fiber failure in tension

$$\frac{1}{\varepsilon_{1T}}\left(\varepsilon_1+\frac{\nu_{f12}}{E_{f1}}m_{\sigma f}\sigma_{22}\right)=1 \tag{2.46}$$

Condition for validity:

$$\varepsilon_1+\frac{\nu_{f12}}{E_{j1}}m_{\sigma f}\sigma_{22}\geqslant 0 \tag{2.47}$$

2. Fiber failure in compression

$$\frac{1}{\varepsilon_{1C}}\left|\left(\varepsilon_1+\frac{\nu_{f12}}{E_{f1}}m_{\sigma f}\sigma_{22}\right)\right|+(10\gamma_{21})^2=1 \tag{2.48}$$

Condition for validity:

$$\varepsilon_1+\frac{\nu_{f12}}{E_{f1}}m_{\sigma f}\sigma_{22}<0 \tag{2.49}$$

3. Matrix failure in transverse tension

$$\sqrt{\left(\frac{\tau_{21}}{F_{21}}\right)^2+\left(1-p^+_{vp}\frac{F_{2t}}{F_{21}}\right)^2\left(\frac{\sigma_{22}}{F_{2t}}\right)^2}+p^+_{vp}\frac{\sigma_{22}}{F_{21}}+\frac{\sigma_{11}}{\sigma_{11D}}=1 \tag{2.50}$$

Condition for validity:

$$\sigma_{22}\geqslant 0 \tag{2.51}$$

4. Matrix failure in moderate transverse compression

$$\frac{1}{F_{21}}\left(\sqrt{\tau_{21}^2+\left(p_{vp}^{-}\sigma_{22}\right)^2}+p_{vp}^{-}\sigma_{22}\right)+\frac{\sigma_{11}}{\sigma_{11D}}=1 \tag{2.52}$$

Condition for failure:

$$\sigma_{22}<0 \text{ and } 0\leqslant\left|\frac{\sigma_{22}}{\tau_{21}}\right|\leqslant\frac{R_{vv}^{A}}{|\tau_{21c}|} \tag{2.53}$$

5. Matrix failure in large transverse compression

$$\left[\left(\frac{\tau_{21}}{2\left(1+p_{vi}^{-}\right)F_{21}}\right)^2+\left(\frac{\sigma_{22}}{F_{2c}}\right)^2\right]\frac{F_{2c}}{(-\sigma_{22})}+\frac{\sigma_{11}}{\sigma_{11D}}=1 \tag{2.54}$$

Condition for failure:

$$\sigma_{22}<0 \text{ and } 0\leqslant\left|\frac{\tau_{21}}{\sigma_{22}}\right|\leqslant\frac{|\tau_{21c}|}{R_{yv}^{A}} \tag{2.55}$$

where ε_{1T} and ε_{1C} are the tensile and compressive failure strains of a unidirectional layer in the x direction, respectively; ε_1 is the normal strain of a unidirectional layer; ν_{f12} and E_1 are Poisson's ratio and Young's modulus for the fiber in the x direction, respectively; $m_{\sigma f}$ is the stress magnification factor for the fibers in y direction; σ_{11} and σ_{22} are the normal stresses in a unidirectional layer; γ_{21} and τ_{21} are the shear strain and stress of a unidirectional layer in the elastic symmetry direction, respectively; F_{21} is the shear strength of a unidirectional layer transverse and parallel to the fiber direction; p_{vp}^{+}, p_{vp}^{-} and p_{vv}^{-} are the fracture plane angle-dependent parameters; σ_{11D} is the stress value for linear degradation; R_{vv}^{A} is the fracture resistance of the action plane against its fracture due to transverse shear stressing; and τ_{21c} is the shear stress at the "turning point" of the (σ_{22}, τ_{21}) fracture curve.

Some of these parameters are hard to obtain experimentally, Lee *et al.* (2015) present some formulae to obtain some of them and Puck *et al.* (2002) recommend values for inclination parameters.

2.4.2 Stiffness degradation

When a ply experiences damage, the composite begins to lose stiffness. After failure in one of the plies, further loading will degrade composite mechanical properties. Degradation of mechanical properties of a failed ply can be accomplished using different methods that are herein presented.

Table 1 – Degradation properties in ply discount method.

Failure mode	Degradation of mechanical properties
$(E_X, E_Y, \nu_{XY}, G_{XY}, F_{1t}, F_{1c}, F_{2t}, F_{2c}, F_{12})_{\text{intact}} \rightarrow (0,0,0,0,0,0,0,0,0)_{\text{failed}}$	Fiber breakage/buckling
$(E_Y, \nu_{XY}, G_{XY}, F_{2t})_{\text{intact}} \rightarrow (0,0,0,0)_{\text{failed}}$	Matrix tension
$(E_Y, \nu_{XY}, G_{XY}, F_{2c})_{\text{intact}} \rightarrow (0,0,0,0)_{\text{failed}}$	Matrix compression
$(\nu_{XY}, G_{XY}, F_{12})_{\text{intact}} \rightarrow (0,0,0)_{\text{failed}}$	In-plane shearing

Source: (RAFIEE *et al.*, 2018)

2.4.2.1 Ply Discount Method

In this method, certain mechanical and strength properties experience a sharp reduction to represent degradation (RAFIEE *et al.*, 2018). The extent of degradation depends on the failure mode. Catastrophic failure modes, such as fiber rupture, result in the mechanical properties being set to zero. As a result, the damaged ply becomes incapable of bearing any load. To prevent numerical instability (e.g., division by zero errors), negligible values are employed instead of zero.

For other failure modes, such as matrix tension or compression, the damaged ply can still bear loading in other directions. Therefore, Table 1 presents the strategy of reducing mechanical properties.

However, many projects still utilize the First Ply Failure criterion, which prohibits any failure. Additionally, the abrupt change in stiffness often leads to convergence issues in simulations. Nevertheless, due to its simplicity, this method serves as a valuable tool for representing damage in composite materials. Alternative approaches involves considering a gradual failure progression rather than an abrupt one.

2.4.2.2 Continuum damage mechanics (CDM)

In this approach, degradation rule is determined based on the assumption that the total energy needed to fail an element equals the energy needed to induce damage, so the element can not accommodate further loading (RAFIEE *et al.*, 2018). While in ply discount some of the ply parameters or all of them are suddenly set to zero, in CDM the effect of damage can be considered by reducing mechanical properties of the intact ply using a constitutive model

(RAFIEE *et al.*, 2018). Lapczyk and Hurtado (2007) proposed the following model:

$$\frac{1}{D}\begin{bmatrix} \left(1-d_f\right)E_x & \left(1-d_f\right)\left(1-d_m\right)\nu_{yx}E_x & 0 \\ \left(1-d_f\right)\left(1-d_m\right)\nu_{yx}E_x & \left(1-d_m\right)E_y & 0 \\ 0 & 0 & D\left(1-d_s\right)E_s \end{bmatrix} \tag{2.56}$$

where d parameters are damage variables defined as:

$$d_f = \begin{cases} d_{ft} & ;\sigma_x \geq 0 \\ d_{fc} & ;\sigma_x \prec 0 \end{cases} \tag{2.57}$$

$$d_m = \begin{cases} d_{mt} & ;\sigma_y \geq 0 \\ d_{mc} & ;\sigma_y \prec 0 \end{cases} \tag{2.58}$$

$$d_s = 1-\left(1-d_{ft}\right)\left(1-d_{fc}\right)\left(1-d_{mt}\right)\left(1-d_{mc}\right) \tag{2.59}$$

and D is defined as:

$$D = 1-\left(1-d_f\right)\left(1-d_m\right)\nu_{xy}\nu_{yx} \tag{2.60}$$

Fiber and matrix damage variables are independent, while shear damage variable depends on fiber and matrix ones. These values lie between zero (undamaged) and one (completely damaged). To alleviate mesh dependency during material softening, ABAQUS introduces a characteristic length into the formulation, so that the constitutive law is expressed as a stress-displacement relation. The damage variable will evolve such that the stress-displacement behaves according to the fracture energy set ($G_{I,C}$). Each damage parameter is related to its corresponding equivalent displacement, that are expressed as:

$$\delta_{ft,eq} = L_C\sqrt{\langle\varepsilon_{\mathrm{x}}\rangle^2+\varepsilon_s^2} \tag{2.61}$$

$$\delta_{fc,eq} = L_C\langle-\varepsilon_{\mathrm{x}}\rangle \tag{2.62}$$

$$\delta_{mt,eq} = L_C\sqrt{\langle\varepsilon_{\mathrm{y}}\rangle^2+\varepsilon_s^2} \tag{2.63}$$

$$\delta_{fc,eq} = L_C\sqrt{\langle-\varepsilon_{\mathrm{y}}\rangle^2+\varepsilon_s^2} \tag{2.64}$$

$$\langle\eta\rangle = \frac{1}{2}(\eta+|\eta|) \tag{2.65}$$

where L_C is the characteristic length, considered as the square root of the element reference surface area for membrane and shell elements. The value of damage parameter is obtained by calculating equivalent displacement at each increment:

$$d_I = \frac{\delta^E_{I,eq}\left(\delta_{I,eq} - \delta^0_{I,eq}\right)}{\delta_{I,eq}\left(\delta^E_{I,eq} - \delta^0_{I,eq}\right)} \quad I \in \{ft, fc, mt, mc\} \tag{2.66}$$

where $\delta^0_{I,eq}$ and $\delta^E_{I,eq}$ are the equivalent displacement in failure initiation and when the material is entirely damaged, respectively. $\delta^f_{I,eq}$ is obtained using a formulation based on linear softening behavior (LAPCZYK; HURTADO, 2007):

$$\delta^f_{I,eq} = \frac{G_{I,C}}{2\sigma^0_{I,eq}} \quad I \in \{ft, fc, mt, mc\} \tag{2.67}$$

where $G_{I,C}$ is the fracture energy and $\sigma^0_{I,eq}$ is the equivalent stress at initiation of failure obtained by:

$$\begin{aligned}
\sigma^0_{ft,eq} &= \frac{L_C\left(\langle\sigma_{\mathrm{x}}\rangle\langle\varepsilon_{\mathrm{x}}\rangle + \sigma_s\varepsilon_s\right)}{\delta^{ft}_{eq}\sqrt{F_{ft}}} \\
\sigma^0_{ft,eq} &= \frac{L_C\left(\langle-\sigma_{\mathrm{x}}\rangle\langle-\varepsilon_{\mathrm{x}}\rangle\right)}{\delta^{fc}_{eq}\sqrt{F_{fc}}} \\
\sigma^0_{mt,eq} &= \frac{L_C\left(\langle\sigma_{\mathrm{y}}\rangle\langle\varepsilon_{\mathrm{y}}\rangle + \sigma_s\varepsilon_s\right)}{\delta^{mt}_{eq}\sqrt{F_{mt}}} \\
\sigma^0_{mc,eq} &= \frac{L_C\left(\langle-\sigma_{\mathrm{y}}\rangle\langle-\varepsilon_{\mathrm{y}}\rangle + \sigma_s\varepsilon_s\right)}{\delta^{mt}_{eq}\sqrt{F_{mc}}}
\end{aligned} \tag{2.68}$$

where

$$\langle\eta\rangle = \frac{1}{2}(\eta + |\eta|) \tag{2.69}$$

Thus, linear damage evolution law is combined with the linear softening model to capture gradual degradation of material properties. In Abaqus, a viscous regularization scheme is employed to overcome convergence difficulties associated with small time increments (MANUAL, 2012). The values of $\delta^0_{I,eq}$ for the various modes depend on the elastic stiffness and the strength parameters specified as part of the damage initiation definition. For each failure mode you must specify the energy dissipated due to failure, $G_{I,C}$, which corresponds to the area

force-displacement curve. The values of $\delta^{E}_{I,eq}$ for the various modes depend on the respective $G_{I,C}$ values. Unloading from a partially damaged state occurs along a linear path toward the origin in the plot of equivalent stress vs. equivalent displacement.

The CDM has been successfully applied to a wide range of laminated fiber composites, including glass and carbon fibers. The model has been shown to provide accurate predictions of damage evolution, including the onset and progression of delamination, cracking, and matrix cracking. It has also been applied to multi-scale simulations, taking into account the microstructural characteristics of the material, such as the fiber-matrix interface, the fiber architecture, and the matrix properties. CDM has emerged as a promising approach to describing the progressive damage in laminated fiber composites. However, due to the complex nature of their microstructure, the prediction of their damaged behavior is a challenging task.

3 MATERIALS AND METHODS

3.1 Materials

The hybrid composites studied herein are composed by synthetic fiber, natural fiber, and epoxy. The synthetic fiber chosen was Glass fibers, due to their good engineering properties and availability. The natural fiber is jute, due to its low cost, and for being a material easily found in the woven form in Fortaleza - Ceará. Epoxy resin is a cheap and resistant material to compose hybrid composites. Two resins were used, but only data from the second resin was provided by the manufacturer, which is presented in Annex A.

In this work, the natural fibers are alkali-treated to enhance their properties. A 5% NaOH solution will be used to treat jute fibers, which will be immersed for 1h. After immersion, the fibers are going to be washed in current distilled water. Then, the fibers are going stay at ambient temperature, and before the layup is done they are going to dry for 5h at 80ºC.

3.2 Characterization

Tests are going to be performed in order to characterize materials separated and in the composite form. The effect of fiber treatment will also be analyzed by testing jute in both forms: treated and untreated.

3.2.1 Jute properties

To characterize the jute woven, its peak force was obtained by using statistical analysis with Weibull distribution. It allows for determining the spatial distribution of the properties. This is the most used analysis method for analyzing dispersion in natural yarns mechanical properties as a function of gage length (SMAIL *et al.*, 2021). In this study, the results were analyzed using the two-parameter Weibull model available in *Matlab* R2016a. The yarns failure probability ($P(y)$) is considered as follows:

$$P(y) = 1 - exp\left[-\left(\frac{y}{y_0}\right)^m\right] \tag{3.1}$$

where m is the Weibull modulus, or shape parameter; y_0 is a scale parameter representing the average value for each mechanical property y. m and y_0 are determined from the plot of a straight line of Weibull model approach.

The value of $P(y)$ is determined by an average value rank as:

$$P(y_i) = \frac{i - 0.3}{n - 0.4} \tag{3.2}$$

where n is the number of data points and "i" represents the i^{th} data point.

In order to obtain jute fibers tensile resistance, 60 specimen with the same number of longitudinal fibers (16) were prepared. The tensile tester force and displacement calibrations were performed before the test, the calibration curves are presented in AppendixA. The test followed the ASTM D 3039-76 standard procedure.

3.2.2 Abaqus parameters

To analyze composite structures in Abaqus, the composite properties are necessary as input data. So, tests on the composite must be performed.

Until very close to failure, a linear elastic model can be assumed. To represent this, Abaqus necessary input parameters are: E_1, E_2, ν_{12}, G_{12}, G_{13} and G_{23}.

To represent failure, Hashin failure criterion is the only model available on Abaqus, the following parameters are necessary as input: F_{1C}, F_{1T}, F_{2C}, F_{2T}, F_{12} and F_{23}. Besides Hashin criterion, other criteria that were previously mentioned, can be implemented in FORTRAN language as User Sub-routines (UMATS), in which the necessary input data is similar to the one necessary in Hashin Abaqus model.

E_1, E_2, F_{1T}, F_{2T} and ν_{12} can be obtained in a tensile test. F_{1C} and F_{2C} can be obtained with a compression test. To obtain F_{23}, Hashin and Rotem (1973) recommends to use F_{23}=F_{2C}/2. To obtain G_{12}, G_{13}, G_{23} and F_{12} an interlaminar shear strength should be performed following ASTM D2344-84 standard. It consists in a 45mm length specimen with square cross section subjected to a three-point bending. Since this is a short beam, it can be considered that bending effects can be neglected. To account for shear strength (SH), the following relation is used:

$$SH = \frac{0.75 P_B}{A} \tag{3.3}$$

where P_B is the breaking load (N) and A is the cross-section area.

Besides these important parameters to perform numerical analyses, there are others important parameters widely used to characterize composite materials. The most common to

characterize fibers is the effective diameter (d_e), which is the diameter of a circle with the same fiber cross section area. However, in natural fibers this parameter is difficult to obtain, since it presents fibers with different diameters.

The theoretical density of the composite (ρ_{ct}) can be obtained in terms of the weight fractions and densities of the constituents:

$$\rho_{ct} = \frac{1}{(W_f/\rho_f) + (W_m/\rho_m)} \tag{3.4}$$

where ρ and W are the density and weight fraction, respectively. f is for fibers, m for matrix, c for composites and t for theoretical. The actual density (ρ_{ex}) can be determined by water immersion technique, and then the volume fraction of voids is given by:

$$\Delta v = \frac{\rho_{ct} - \rho_{ex}}{\rho_{ct}} \tag{3.5}$$

GRÉDIAC (2004) brings a review of full-field measurement algorithms and software that automatically process images. This is an interesting type of tool in the field of composite material characterization. Among these full-field techniques, there are the interferometric, which uses the phenomenon of interference of waves, and the non-interferometric. (HE *et al.*, 2018) uses Digital Image Correlation (DIC) to perform composite characterization. Besides these advanced characterization devices, the standard ones are always important and necessary, such as tensile/flexural testing and fracture energy determination.

3.3 Tensile test in composites

This test is usually performed in a Universal Tester Machine (UTM), following recommendations of ASTM D 3039-76 standard. Longitudinal and transversal strain gauges are necessary. Composite must be prepared and the specimens to perform this test are easily obtained by cutting them with a utility knife. Gujjala *et al.* (2014) used 5 specimens with 125mm length to each composite. It is also necessary to protect specimen ends, so they will not be crushed by UTM tensile grips. In this study, this was made by adhering composite ends to aluminum with epoxy resin.

With the sample prepared, the next step is to apply a controlled load to the sample using the UTM. This can be done in a uniaxial tensile or compressive direction. Then, the load and deformation are measured. During the test, the UTM applies a controlled load to the sample and records the corresponding deformation. It is important to measure these two quantities at

regular intervals to get a complete picture of the material's behavior. This can be done either manually by reading the load and deformation values from the UTM's display or digitally by using data acquisition software.

Once the load and deformation data have been collected as elongation versus applied force in N, the elongation is transformed into strain by dividing it by the original length of the sample. Similarly, the force is transformed into stress by dividing it by the cross-sectional area of the sample where the composite material ruptured. Stress-strain curves can then be plotted by plotting stress against strain, and then it is possible to observe how the material responds to increasing loads, from initial loading to ultimate failure.

A smoothing technique was applied to the initial curved portion of the force-displacement curve obtained from tensile tests conducted on composite materials. This technique aimed to eliminate the non-linear variations present at the beginning of the curve, allowing for a more accurate representation of the material's elastic behavior.

To achieve this, a tangent line was determined at the point of transition from the curved region to the linear region of the curve. The slope of this tangent line was then extended to intersect the displacement axis, effectively smoothing and extending the linear portion of the curve towards the origin. This procedure helped to remove any initial irregularities or non-linear effects that could arise due to factors such as interfacial slippage or geometric imperfections. The resulting smoothed curve provides a clearer understanding of the material's elastic properties, enabling more reliable comparisons and analysis within the linear range.

The modulus of elasticity is then calculated as the slope of this linear region. It is important to choose the appropriate linear region to obtain an accurate value for the modulus of elasticity and to ensure that the sample is in its elastic region, avoiding plastic deformation.

With this test, the value of E_1 was obtained. E_2 was assumed to be $E2 = E1$. ν is the Poisson's ratio of the composite, which will be approximated as:

$$v = 0.5\left(\frac{L}{L+\Delta L}\right) \tag{3.6}$$

where δL was considered as the displacement in the maximum load.

3.4 Fracture Energy Test

Fracture energy is a measure of the amount of energy required to break or fracture a material. It is an important property because it allows to evaluate the material's resistance to fracture and, consequently, its ability to withstand external loads without failing. Fracture Energy Test, also known as the fracture toughness test, is an important technique for evaluating the fracture resistance of materials. The fracture energy test involves applying a load to a pre-cracked specimen, with the aim of measuring the amount of energy required to propagate the crack in the material (ASTM, 2019; ASTM, 2012).

The experimental procedure for the fracture energy test may vary depending on the type of material and equipment used. In this work, specimens were manufactured and then notched on their surface, creating a pre-existing crack of controlled size.

The specimen is fixed to a testing device, which applies an axial load in an increasing manner until crack propagation occurs in the material. The amount of energy absorbed by the material is measured during the test, from the area under the load versus displacement curve. The test results are analyzed to determine the fracture toughness of the material, which is the amount of energy required to propagate the crack in a unit area.

There are two different loading mods to perform this test: Mode I and Mode II. Mode I is characterized by a uniaxial loading that acts perpendicular to the crack direction. In other words, the loading is applied in the direction normal to the crack surface and is known as tensile loading (CALLISTER *et al.*, 2007). This type of loading is common in materials with flat surfaces, such as plates and sheets, and it was used in this work.

Mode II is characterized by a loading that acts parallel to the crack direction and is in a plane perpendicular to the tensile axis. This type of loading is also known as in-plane shear loading. It is common in materials with non-planar surfaces, such as curved laminates and sandwich structures (AVALLONE *et al.*, 2007).

This test in composites is not easily found in the literature. Most of the research herein cited did not perform this test. This may be due to the complexity of the specimen shape, which can be shown in Figure 7. A similar laboratory test was performed by Leonard *et al.* (2009), by following ASTM (2007). However, in this study, fibrous composites with unidirectional fibers were made, instead of laminated ones. As for the content of the article, it explores the fracture behavior of a composite material made of glass fibers and polyester resin. The researchers likely conducted experiments to measure how the material behaves when subjected to various stresses

and strains, and analyzed the results to gain insights into the material's strength and durability.

Figure 7 – Fracture Energy Specimen

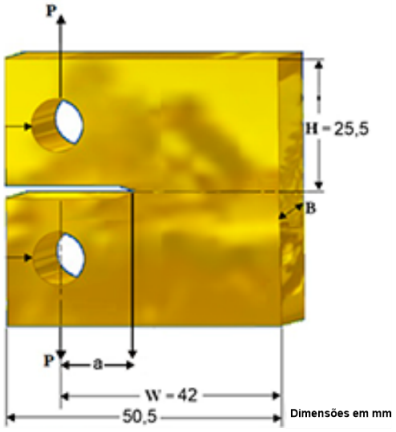

Source: Adapted from Leonard *et al.* (2009).

Fracture toughness (K_{1C}) and critical energy release rate (G_{1C}) were calculated by using the parameter shown in Figure 7 following equations:

$$K_{\mathrm{IC}} = \frac{P}{B\sqrt{w}} f\left(\frac{a}{w}\right) \tag{3.7}$$

where $f(a/w)$ is given by:

$$\begin{aligned} f\left(\frac{a}{w}\right) = & \frac{2+a/w}{(1-a/w)^{1.5}} \left[0.866 + 4.64\left(\frac{a}{w}\right)\right. \\ & \left. -13.32\left(\frac{a}{w}\right)^2 + 14.72\left(\frac{a}{w}\right)^3 - 5.6\left(\frac{a}{w}\right)^4\right] \end{aligned} \tag{3.8}$$

and for plane strain condition, the critical energy release rate is given by:

$$G_{\mathrm{IC}} = \frac{K_{\mathrm{IC}}^2}{E}\left(1-\nu^2\right) \tag{3.9}$$

in which Poisson's ration is given by Equation 3.6.

3.5 Shear Test

Shear strength test was performed based on ASTM B831 (ASTM, 2017). 4 specimens were tested at an average speed of 10.0 mm/min. Specimen is shown on Figure 8. Since its complexity, this test was performed just in one type of composite, which was the one containing only resin and jute fibers.

Figure 8 – J3 - Shear specimen

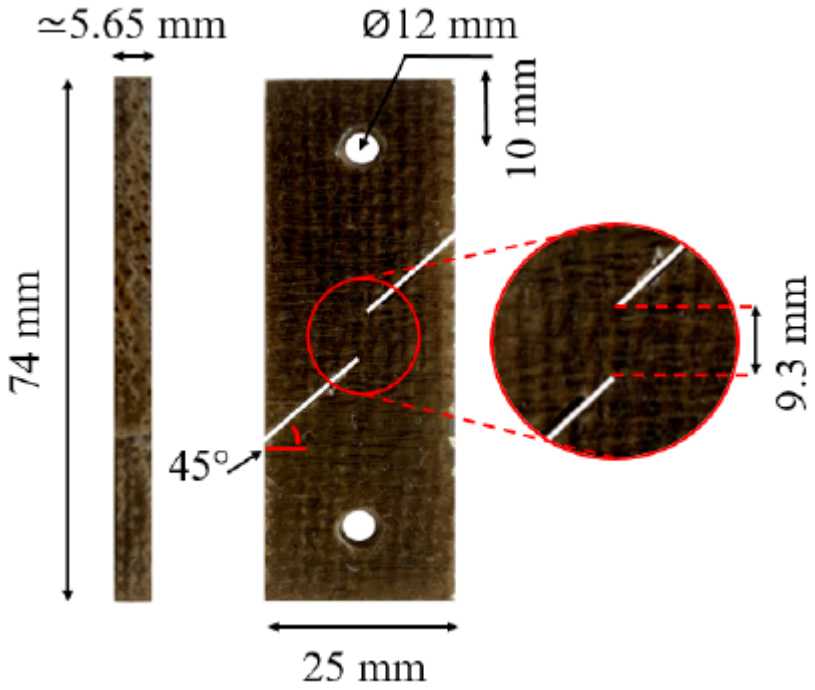

Source: Author.

The Equation 3.10 establishes the relationship between shear modulus (G), elastic modulus (E), and Poisson's ratio (Poisson). It is commonly used in solid mechanics to determine the shear modulus based on known elastic properties of a material, such as the elastic modulus and Poisson's ratio.

$$G = \frac{E}{2(1+\nu)} \tag{3.10}$$

4 RESULTS AND DISCUSSION

This section presents the results. Characterization was performed in treated and untreated jute fibers using an Educational Tester Machine, this is presented in Appendix B. Different composites were prepared and tested in a UTM machine for tensile tests and in an Educational Tester Machine for analyzing their fracture toughness. Fracture toughness tests were performed with precrack of 1mm. All tests were performed at room temperature.

4.1 Experimental results

Composites were prepared and they were subjected to tensile tests, fracture energy test, and shear tests. These composites were modeled in Abaqus, and their numerical results were compared with their experimental results, as will be presented throughout this chapter. In Table 2, the symbols G and J represent glass and jute fibers, respectively.

Table 2 – Description of Composite Subchapters

Subchapter	Fiber Composition	Resin	Description
GJJG	G+J+J+G	1	Results of a composite with one glass fiber, two jute fibers, and one glass fiber using resin 1.
GJJJJG	G+J+J+J+J+G	2	Results of a composite with one glass fiber, four jute fibers, and one glass fiber using resin 2.
J3	J+J+J	2	Results of a composite with three jute fibers using resin 2.
G8	G+G+G+G+G+G+G+G	2	Results of a composite with eight glass fibers using resin 2.

Source: Author

4.1.1 GJJG

The first composite was a hybrid composite with glass and jute fibers, with four laminae in this stacking sequence: GJJG, which is based on the results presented by Gujjala *et al.* (2014), being the stacking sequence with higher tensile and interlaminar shear strengths. Five specimens were prepared and tested in a Universal Tester Machine (UTM), at Laboratório de Materiais de Construção Civil (LMCC - UFC).

The five specimens are presented in Figure 9. The average dimensions of the five GJJG composite specimens are 96.17mm for length, 3.36mm for thickness, and 24.67mm for width. Figure 10 shows the specimens in the UTM and Figure 11 shows the results. It is possible to see that good behavior was presented in the 5 specimens, presenting almost linear stress-strain relationships. The results showed a range of ultimate strength from approximately 30 to 35MPa and a corresponding strain at failure ranging from 0.34 to 0.56. They presented varied Young's modulus, which is expected since natural fibers present varied properties, and in the composite exists a slight variation in the epoxy percentage.

Figure 9 – Specimens after failure in the tensile test.

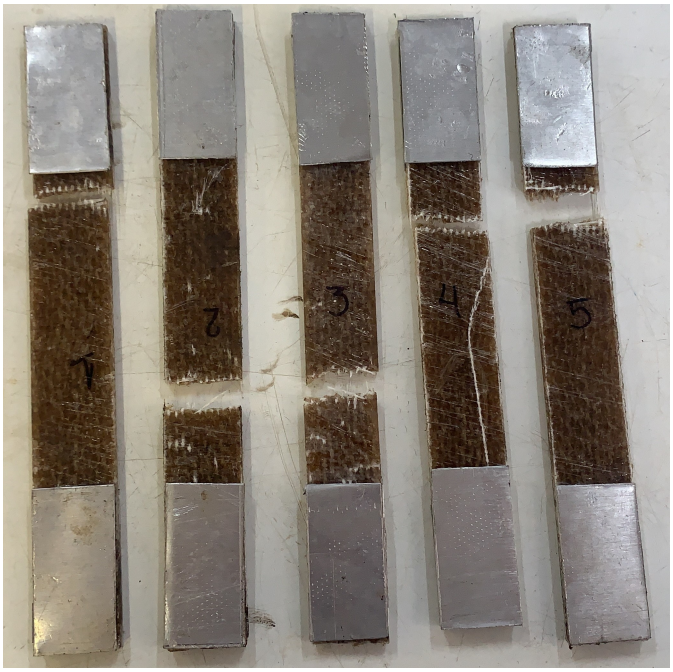

Source: Author.

However, these values are below the expected range when compared to the results reported by Gujjala *et al.* (2014), which showed strengths of approximately 85 MPa for composites with the same fiber configuration. The most plausible reason for this difference was believed to be the type of resin used. The low tensile strength of jute fibers makes the resin a critical factor in determining the overall strength of the composite, which is not typical of traditional composites but is an essential consideration for those made with natural fibers. Since the results are being compared to the ones obtained by Gujjala *et al.* (2014), it is worth mentioning that this research also used 5 samples, but it did not show sample results, only their average was presented. No further comments about results deviation from the average were made either.

Table 3 presents the Young Modulus obtained for GJJG composite, which is an

Figure 10 – Specimen after failure in the tensile test in the UTM.

Source: Author.

Table 3 – GJJG Composite - E_1 values

Specimen	E1 (MPa)
1	888.2
2	666.7
3	625.0
4	854.3
5	718.4
$\bar{E}_1$	750.5

Source: Author

important parameter for numerical modeling in Abaqus.

Figure 11 – Results of tensile test on composite.

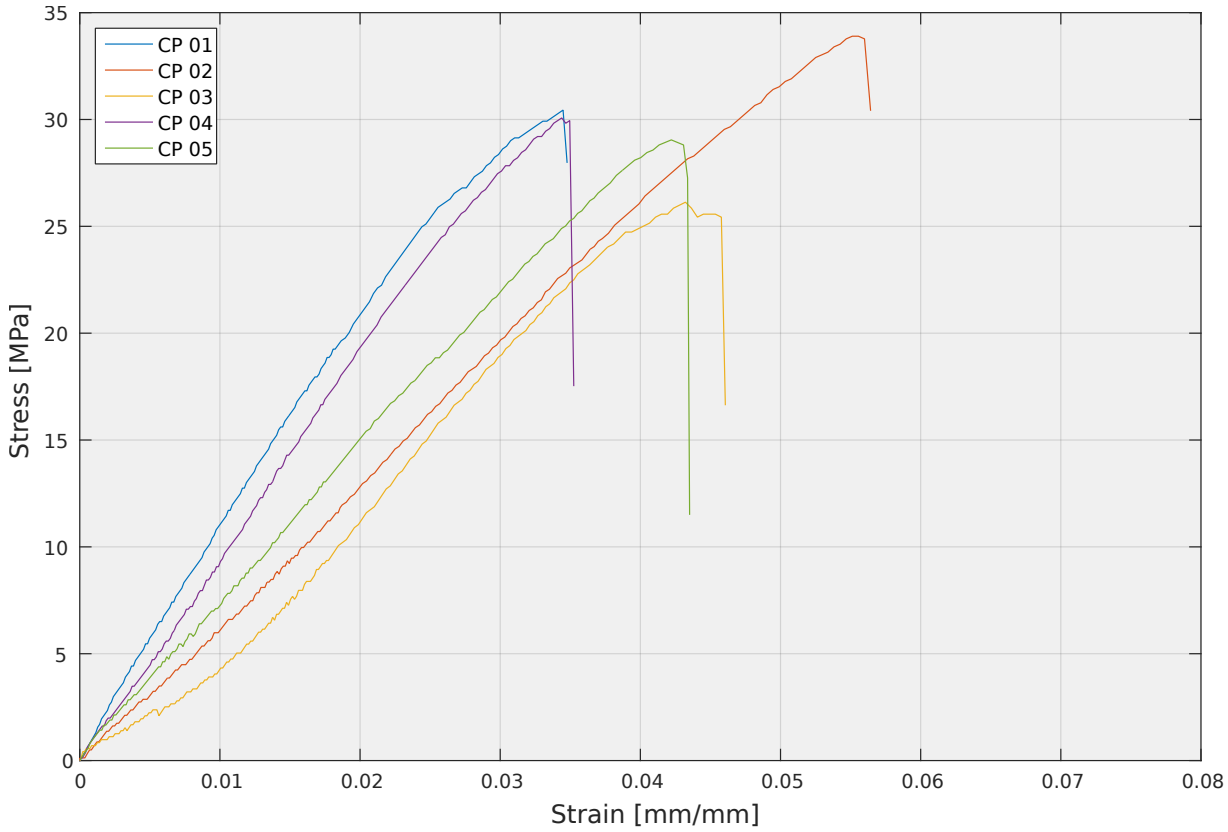

Source: Author.

4.1.2 GJJJJG

The second composite was using a different type of resin and two additional layers of jute fibers. The stacking sequence was GJJJJG and six specimens were tested. This sequence was chosen to study the influence of adding two additional external layers of glass fibers in the composite since a composite with 4 layers of jute and the same resin was also tested.

The six specimens are presented in Figure 12. All six specimens presented lengths of 163 mm, thickness of 7mm, and width of 10.5mm, the measurements were more consistent than those of the specimens in the previous test because these were cut with more precise cutting devices.

Figure 12 – GJJJJG specimens.

Source: Author.

The graph presented in Figure 14 shows the results for the tensile test with the GJJJJG composite. Initially, it can be observed that specimens 1 and 2 obtained results well below the others, which was expected since the resin did not adhere well to some layers of the composite, as can be seen in Figure 13. This significant difference in results highlights the importance of careful manufacturing. These composites were produced manually and methodologically, and even so, certain problems occurred during the manufacturing stage that caused these failures, such as the resin drying earlier, making it harder to spread it throughout the laminate, or the effect of gravity, which pulled the resin towards the lower layers of the composite, leaving the

upper layers drier. In specimens 3 to 6, visually, these problems did not occur, and a much better tensile strength result is observed. However, since specimen 3 yielded significantly higher results compared to the average, it was also discarded. Therefore, the average values used for modeling will be based on specimens 4 to 6, which exhibited an average elastic modulus of 463.3 and a maximum ultimate stress of 21.59. Figure 15 shows the 6 specimens after tensile test.

Figure 13 – GJJJJG - poorly bonded part of specimens 1 and 2

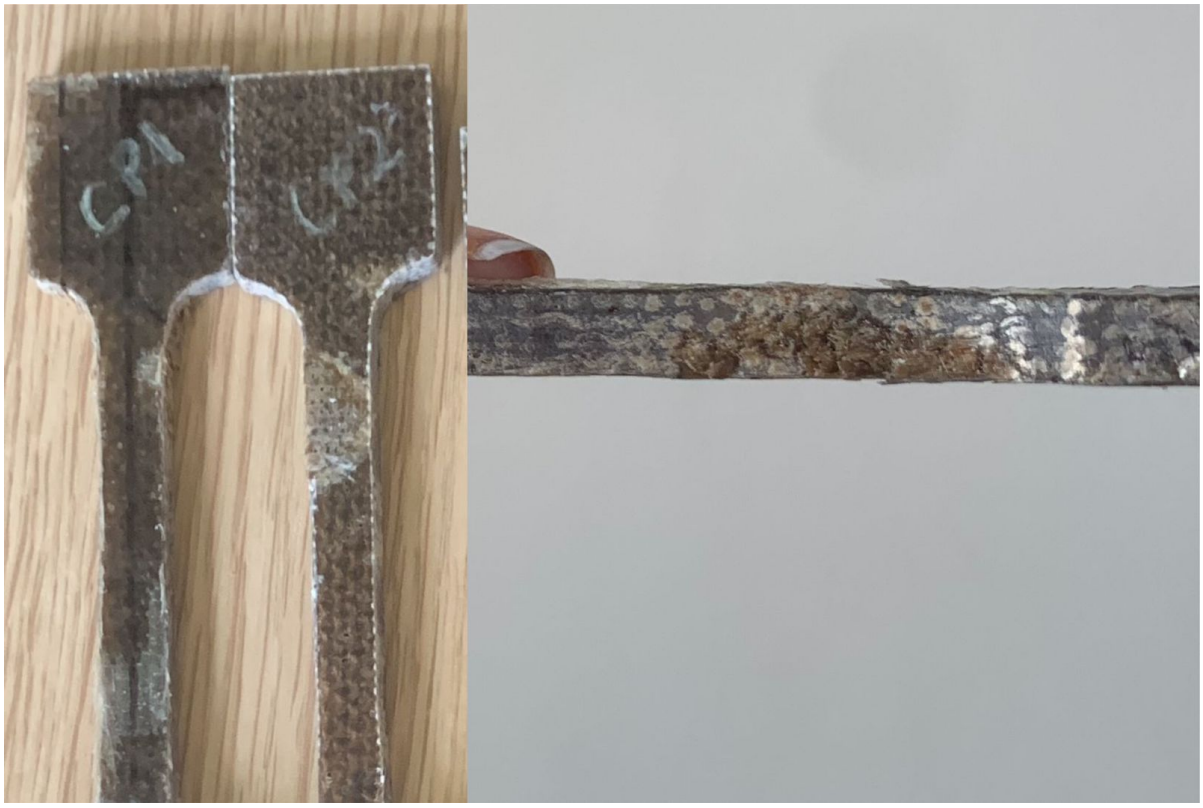

Source: Author.

Upon analyzing CPs 4 to 6, it is observed that even with the change in resin and the addition of two jute plies, the average ultimate tensile strength value was slightly lower, with an average of 21.59 MPa for this composite. This is coherent, as stress is inversely proportional to area, and the cross-sectional area of the material increased by including two plies of the less resistant material in this composite. Therefore, it can be concluded that the difference between the results presented here and those in the literature was not caused by the type of resin, considering that two different resins were used and there was no significant variation in the results. Hence, what makes more sense is that the difference in results is attributed to the jute; being a natural fiber, there is a significant possibility that its properties vary from the jute utilized in the other study.

Poisson's ratio average for this composite was 0.47. Table 4 presents Youngs

Figure 14 – GJJJJG - Tensile Test Results

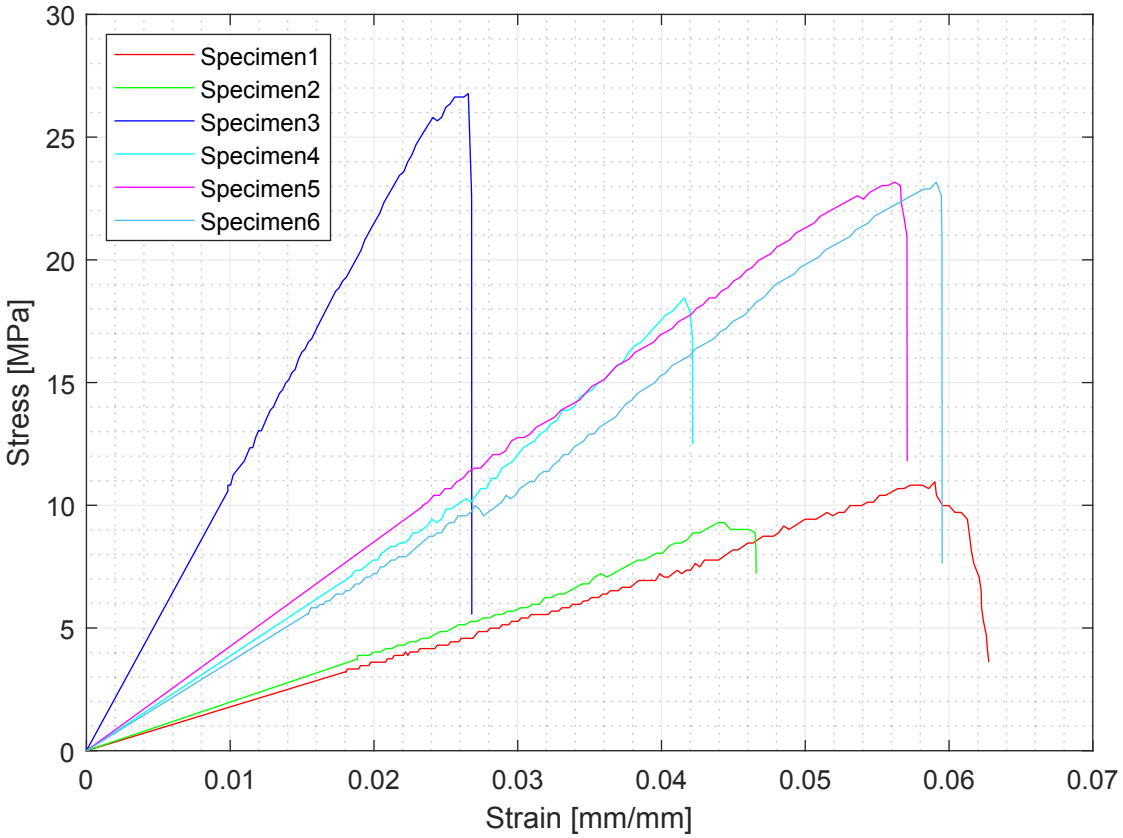

Source: Author.

Figure 15 – GJJJJG - Specimens after tensile test

Source: Author.

Modulus for GJJJJG composites. To calculate the average $\bar{E}_1$, the samples from specimens 1 to 3 were discarded as they deviated significantly due to manufacturing problems.

For this composite, 3 specimens for fracture energy test were prepared. They are

Table 4 – GJJJJG Composite - E_1 values

Specimen	E1 (MPa)
4	500.0
5	450.0
6	440.0
$\bar{E}_1$	463.3

Source: Author

shown in Figure 16. Unfortunately, the test did not work on specimen 2, as can be seen in Figure 17. It did not crack and ended up breaking at the part connected to the testing machine. Figure 17 also shows how the crack effectively occurred in specimen 1.

Figure 16 – GJJJJG - Specimens for fracture energy test

Source: Author.

Figure 18 presents the curves Force x Displacement of fracture energy tests. It can be noted that good behavior was presented by specimens 1 and 3. Specimen 2 presented an outlier result as expected. Results can be seen in Table 5. Since the test on specimen 2 did not break as expected, its result will be discarded, and the average will be adopted as the average of specimens 1 and 3 ($\bar{G}_{1C} = 29.92(MPa\sqrt{m}$ and $\bar{K}_{1C} = 3.22MJ/m$). The only literature reference of this test was performed in composites that are not laminated, but are fibrous (with only glass fibers) (LEONARD *et al.*, 2009). This experiment compared composites with different fiber content. Fibers content was not analyzed here in this work, but Gujjala *et al.* (2014) presented a fiber content of 17.5% for the GJJG composite, which is the closest to the GJJJG herein being studied. For this fiber content, Leonard *et al.* (2009) presented approximately $\bar{K}_{1C} = 4.20MPa\sqrt{m}$.

Figure 17 – GJJJJG - Specimens after fracture energy test

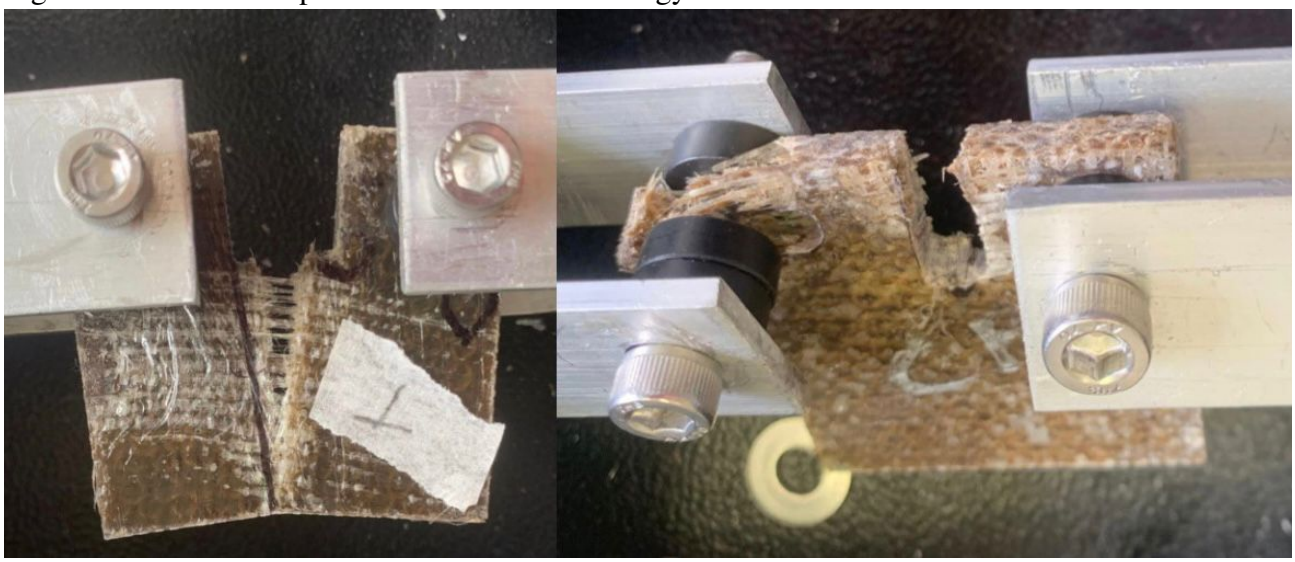

Source: Author.

Figure 18 – GJJJJG - Fracture - Load displacement curves

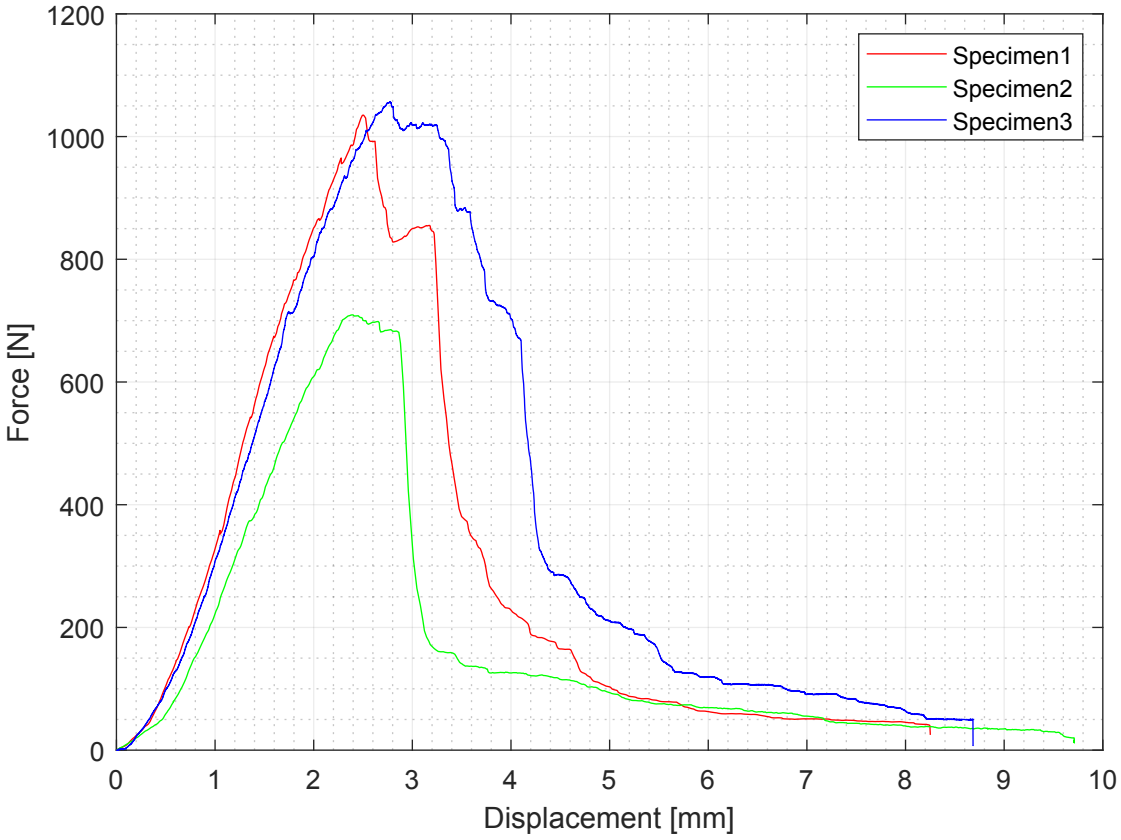

Source: Author.

Thus, it is analyzed that the results obtained here are consistent since the same order of magnitude was obtained. The composite analyzed here (GJJJJG) presented an average of approximately 30.43% lower than the fibrous composite from the literature. Considering that the

Table 5 – GJJJJG Composite - G_{1C} and K_1C values

Specimen	$G_{1C}(MJ/m)$	$K_{1C}((MPa\sqrt{m})$
Specimen 1	27.20	3.15
Specimen 2	11.75	2.10
Specimen 3	32.64	3.28

Source: Author

literature used only glass fibers and this composite contains jute, this result is consistent.

4.1.3 J3

A composite with just jute fibers and resin was produced, using three jute layers. The average dimensions of the five J3 composite specimens to tensile tests are 82.25mm for length, 5.21mm for thickness, and 10.91mm for width. Tensile tests for these composites are presented in Figure 19 and Table 6. Specimen 2 test was disregarded, since it deviated from the other results

Figure 19 – J3 - Tensile Test Results

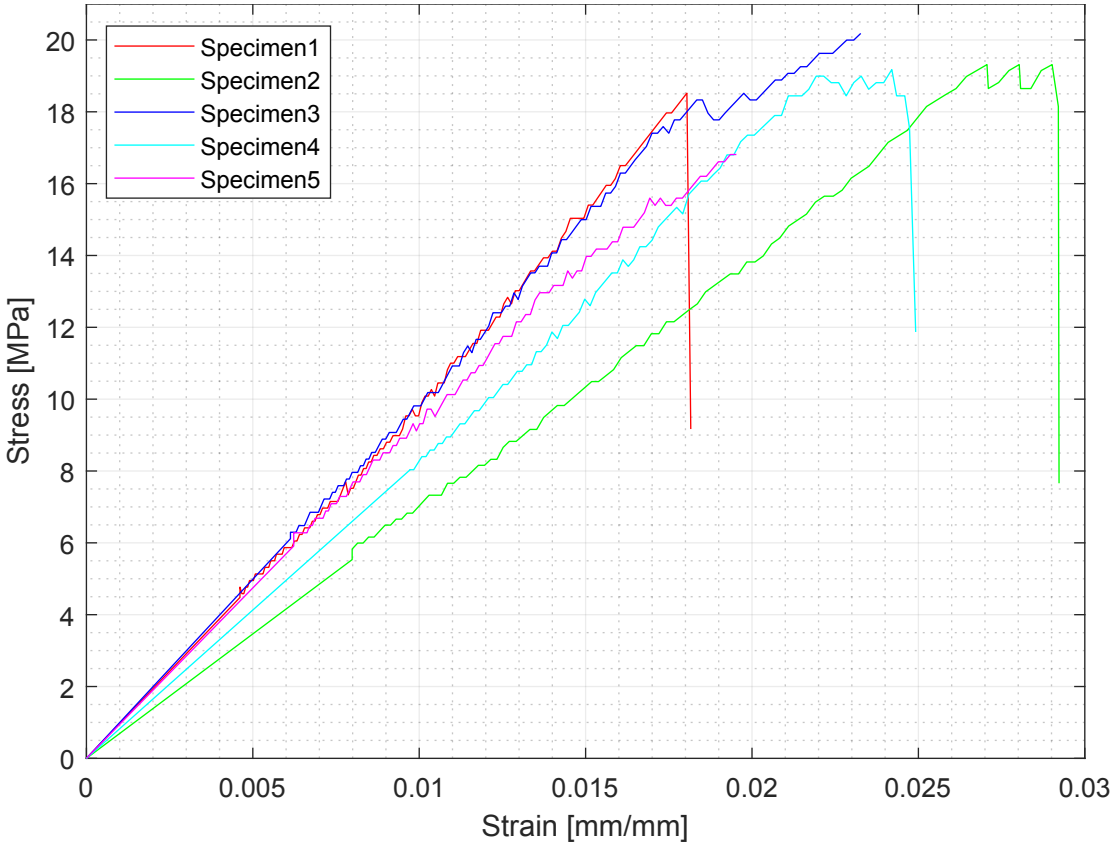

Source: Author.

The ultimate tensile stress average for J3 was approximately 18.80 MPa, which is lower than the other composites herein tested, which is expected since it contains only jute fibers. For a similar composite with 4 jute layers, Gujjala *et al.* (2014) obtained 52.00 MPa. The same occurred with GJJG composite, which leads to confirm the hypothesis that the jute used in this study is the limiting strength material. When compared to the existing reference, the results are consistently lower when the jute is present, but when the material is absent, the results are higher than expected, discarding the possibility of the resin being the problem. The poisson ratio average was 0.49.

Table 6 – J3 Composite - E_1 values

Specimen	E1 (MPa)
1	1024.92
3	999.09
4	848.72
5	884.74
$\bar{E}_1$	795.6

Source: Author

For this composite, only 2 specimens for the fracture energy test were prepared, due to problems that occurred in the laboratory. They are shown in Figure 20. It is observed that the curves had very similar behavior, which is very positive from the perspective of the effectiveness of this test and the preparation of the specimens, since it is a material with many variations, and in the other tests presented here, there were scattered results. Specimen 1 and 2 presented $K_{1C} = 3.35MJ/m$ and $\bar{K}_{1C} = 3.99MJ/m$, respectively. The average was $\bar{K}_{1C} = 3.67MJ/m$. Comparing to GJJJJG results, they were very close, which shows that the presence of glass fibers did not influence fracture results significantly.

Figure 20 – J3 - Fracture - Load-displacement curves

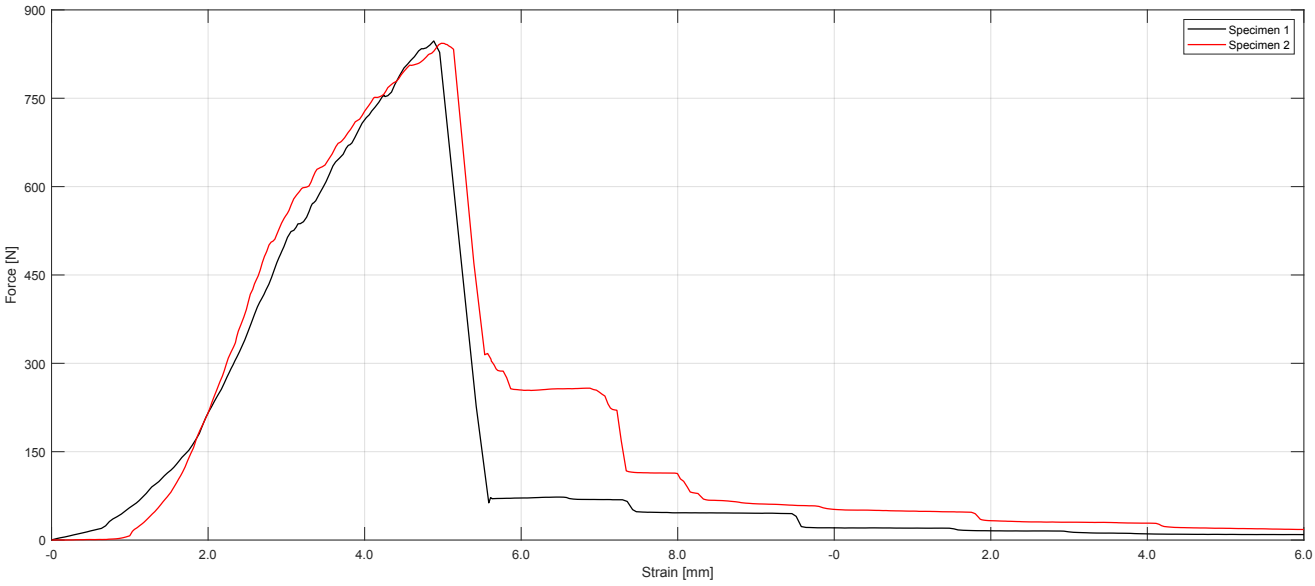

Source: Author.

For this composite, a shear test was conducted. This test is very complex, due to the complexity of cutting the specimen. As this was the only composite without the presence of fiberglass (which made cutting difficult), three specimens were prepared for the shear test. Table 7 presents composites' maximum shear stress results. Figure 8 presents specimens' average measures. The average maximum stress was 16.79 MPa and the average shear modulus was

Table 7 – J3 Composite - Shear test

	Specimen 1	Specimen 2	Specimen 3	Specimen 4
Maximum Stress (MPa)	13,58	14,18	17,70	21,68
Shear Modulus (MPa)	586.69	743.51	1155.55	1146.93

Source: Author

908.17 MPa. Due to the complexity of this test, none of the references herein studied presented shear test results to be compared to the one herein performed.

4.1.4 G8

A composite with just glass fibers and resin was produced. In literature, there is data about glass fibers and resin (GUJJALA *et al.*, 2014) using four layers. A composite with 4 layers of glass and resin was produced to be compared with the ones in the literature, but this composite was too flexible and thin, so it was discarded and one with twice as many layers was produced. 5 specimens were produced, and they are presented in Figure 21. The average dimensions of the five G8 composite specimens are 163.00mm for length, 1mm for thickness, and 15.90mm for width.

Tensile tests for these composites are presented in Figure 22 and Table 8. For tensile modulus, Specimens 2 and 4 were disregarded for presenting deviated slopes. It can be observed that, as expected, the G8 composite is much stronger. The thickness of these specimens is only 1mm, and they showed a strength up to nine times higher than the glass-jute sandwich composites (with 3.4mm and 7mm thickness), emphasizing one of the biggest challenges for the use of natural resins in sectors such as aerospace, where strength combined with slenderness is sought, which is what fiberglass offers.

The ultimate tensile stress average for G8 was approximately 176 MPa. Gujjala *et al.* (2014) obtained an average of 118 MPa, so the result herein obtained was approximately 50% higher. Factors that may explain the discrepancy include the use of double the amount of layers, and since the thickness of the fiberglass is minimal, this does not alter the area, increasing the ultimate tensile force while keeping the cross-sectional area close to the original, really results in a higher ultimate stress. Another difference may lie in the type of resin, which could have impacted the divergence. The tensile modulus obtained for G8 was approximately 7 times higher than that of J3. In the literature, Gujjala *et al.* (2014) found a modulus of synthetic fiber 3 times higher. Such discrepancy is, once again, due to the high variability in the properties of jute. The Poisson ratio average was 0.48.

Figure 21 – G8 - Specimens after tensile test.

Source: Author.

Analyzing the other composites herein tested, we can have a better understanding of the influence of the resin type. The GJJG and GJJJJG composites used different resin types, yet this did not impact the results significantly. The same resin used in the GJJJJG composite was used in the G8 composite, the latter showed highly satisfactory results, much higher than those reported in the literature, while the former presented results below expectations.

This leads to the conclusion that the jute fiber had a greater impact, considering that it is a natural fabric that depends on many factors such as diameter, manual manufacturing, and spacing between the fibers in the fabric, leading to divergences between the tests carried out here and those reported in the literature. This shows a significant difficulty in studying this material for engineering applications, given that in each region and by each manufacturer, small details lead to significantly different resistance characteristics.

For this composite, 3 specimens for fracture energy test were prepared. They are shown in Figure 23. Unfortunately, in all composites, the crack occurred but the test did not occur in the plane of the crack (Figure 24), so all specimens are invalidated and this test was discarded. This occurs due to the slenderness of the material and the difficulty of performing the test without

Figure 22 – G8 - Tensile Test Results

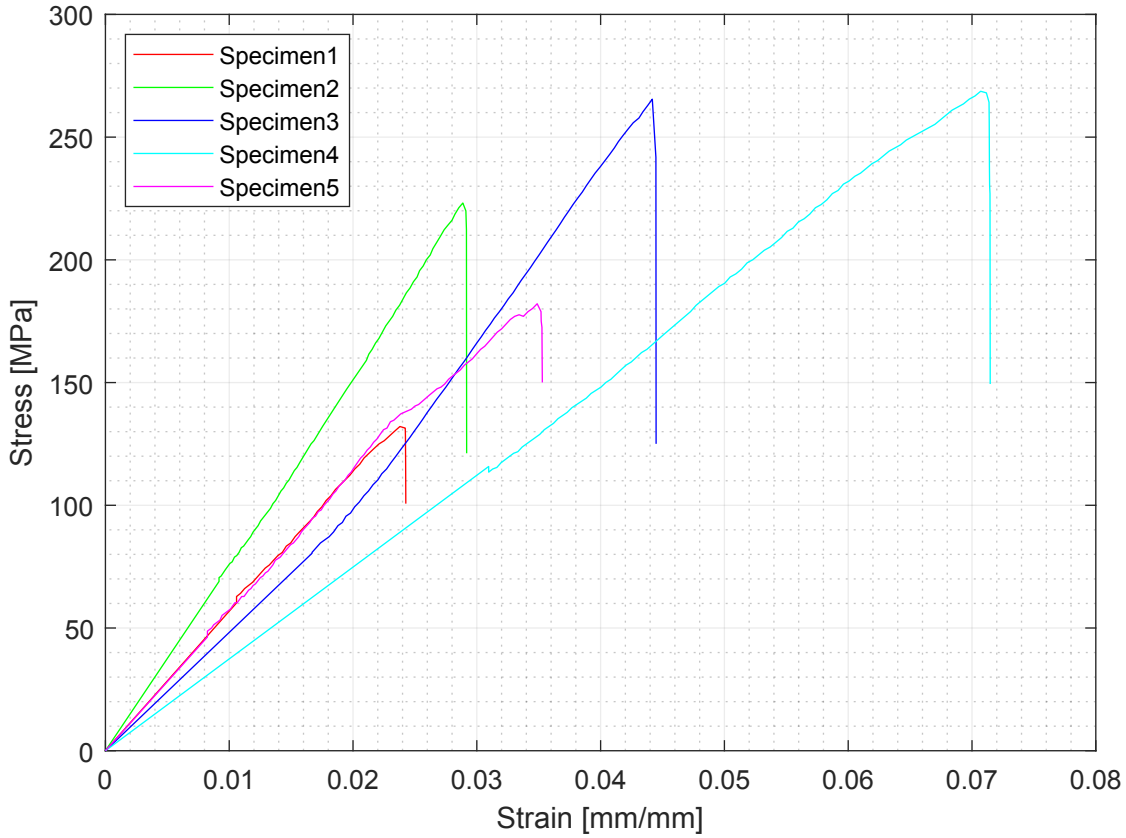

Source: Author.

Table 8 – G8 Composite - E_1 values

Specimen	E1 (MPa)
1	5553.00
3	6001.78
5	5766.54
$\bar{E}_1$	5773.77

Source: Author

going into the three-dimensional plane. Figure 25 presents the results in G8 composites. Table 9 presents G8 results, the average was $\bar{G}_{1C} = 438.29(MPa\sqrt{m}$ and $\bar{K}_{1C} = 4.82MJ/m$. For a similar fiber content, Leonard *et al.* (2009) presented approximately $\bar{K}_{1C} = 4.20(MPa\sqrt{m}$, which is 12.89% lower than the result herein obtained. Although the results were very close, it is important to note that the procedures used, both for the tests and for the data treatment following Equations 3.7 and 3.9, are valid for testing in the plane, which is not what happened here, as can be seen in Figure 24. Although the deformations occurred outside the plane, the obtained results cannot be dismissed as they provide valuable information about the material's fracture behavior. The deviation from the expected deformation behavior can provide insights into the composite's anisotropic properties, which may influence its structural performance under different loading

Table 9 – G8 Composite - G_{1C} and K_1C values

Specimen	$G_{1C}(MJ/m)$	$K_{1C}((MPa\sqrt{m})$
Specimen 1	278.32	4.70
Specimen 2	320.87	4.93
Specimen 3	715.67	4.82

Source: Author

conditions. As such, the results obtained from this test can be used to improve the design and performance of composite structures, making them safer and more reliable.

Figure 23 – G8 - Specimens for fracture energy test.

Source: Author.

Figure 24 – G8 - Specimens after fracture energy test.

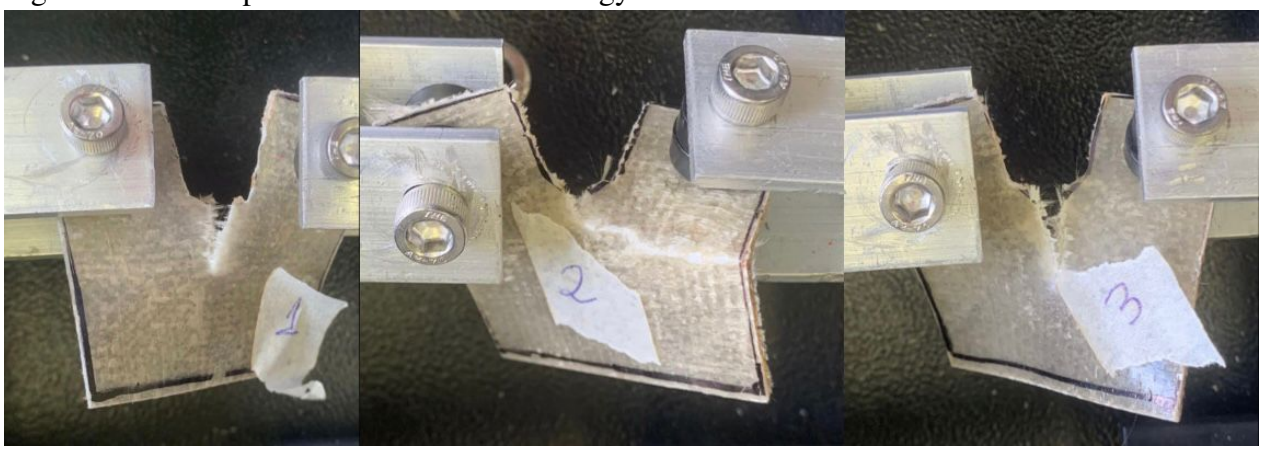

Source: Author.

Figure 25 – G8 - Load-displacement curves

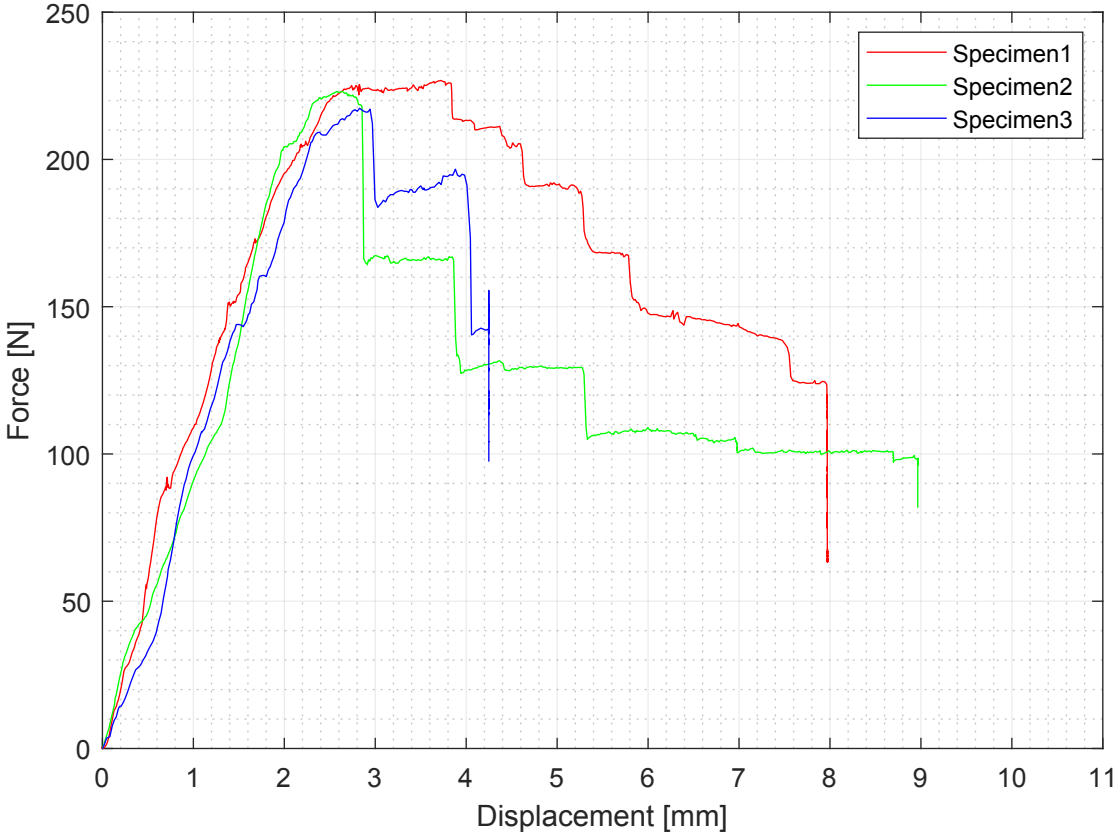

Source: Author.

4.2 Numerical Analysis Results

All the modeling was conducted in Abaqus version 6.11. Initially, the tensile tests of the J3 and G8 composites were simulated to verify if the properties obtained from experimental testing accurately represented the materials. Subsequently, two different models were developed for the GJJJG composite: firstly, a homogeneous material model will be considered using the data obtained for the GJJJG composite. Then, a laminated material model will be created, incorporating the data of the glass-only composite (G8) for the glass layers and the data of the jute-only composite (J3) for the jute layers.

As the fibers are braided (both jute and glass), it will be assumed $E_2 = E_1$, and $E_3 = 0.1E_1$, Since the deformations perpendicular to the plane in this test are negligible, a low value was adopted instead of using zero, which could cause convergence problems.

For the shear properties, simulations were performed using the experimental results of the J3 composite, but the obtained curves were not satisfactory. It was observed that the shear modulus result for J3 was significantly different from what would be expected using Equation 3.10. Therefore, for the shear analysis, Equation 3.10 was followed in all simulations. A parametric study was conducted to investigate the influence of Poisson's ratio, while maintaining all the experimentally obtained properties, a Poisson's ratio of 0.2 and a shear modulus calculated using the Equation 3.10 provided excellent results.

To estimate the compressive strength, Equations 2.44 and 2.45 suggested by Hashin were used. For all composites, a volume fraction of 17.5% was adopted (based on Gujjala *et al.* (2014)), which leads to a k factor of 1.27.

Apart from the material properties, the entire numerical modeling was the same, with the same boundary conditions, finite element mesh, and loading applied to both models. The boundary conditions used are presented in Figure 26. Both ends were fixed, leaving only the U2 displacement free at one end to simulate the tensile strength test in the UTM machine. The finite element mesh used the S4R plate element, and to generate the mesh presented in Figure 27 the Abaqus mesh generator was used with a global size approximation of 1.

For the thicknesses of each ply in Abaqus, it was adopted 1.74mm for each jute ply and 0.125mm for each glass ply. These thicknesses were obtained by dividing the thicknesses of the composite materials tested in the laboratory, J3 and G8, by the number of plies in each of them.

Figure 26 – Boundary conditions

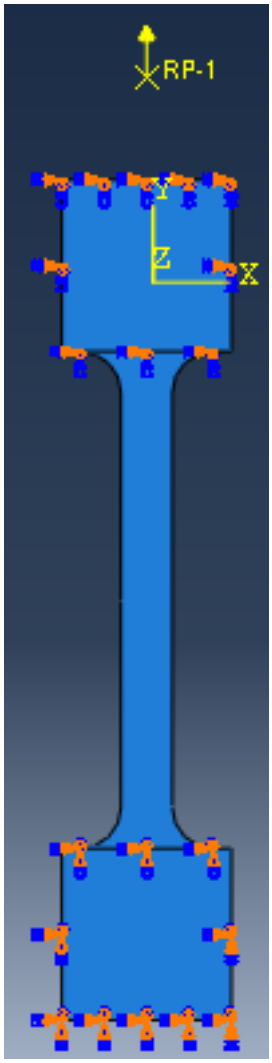

Source: Author.

Figure 27 – Specimen - S4R Mesh

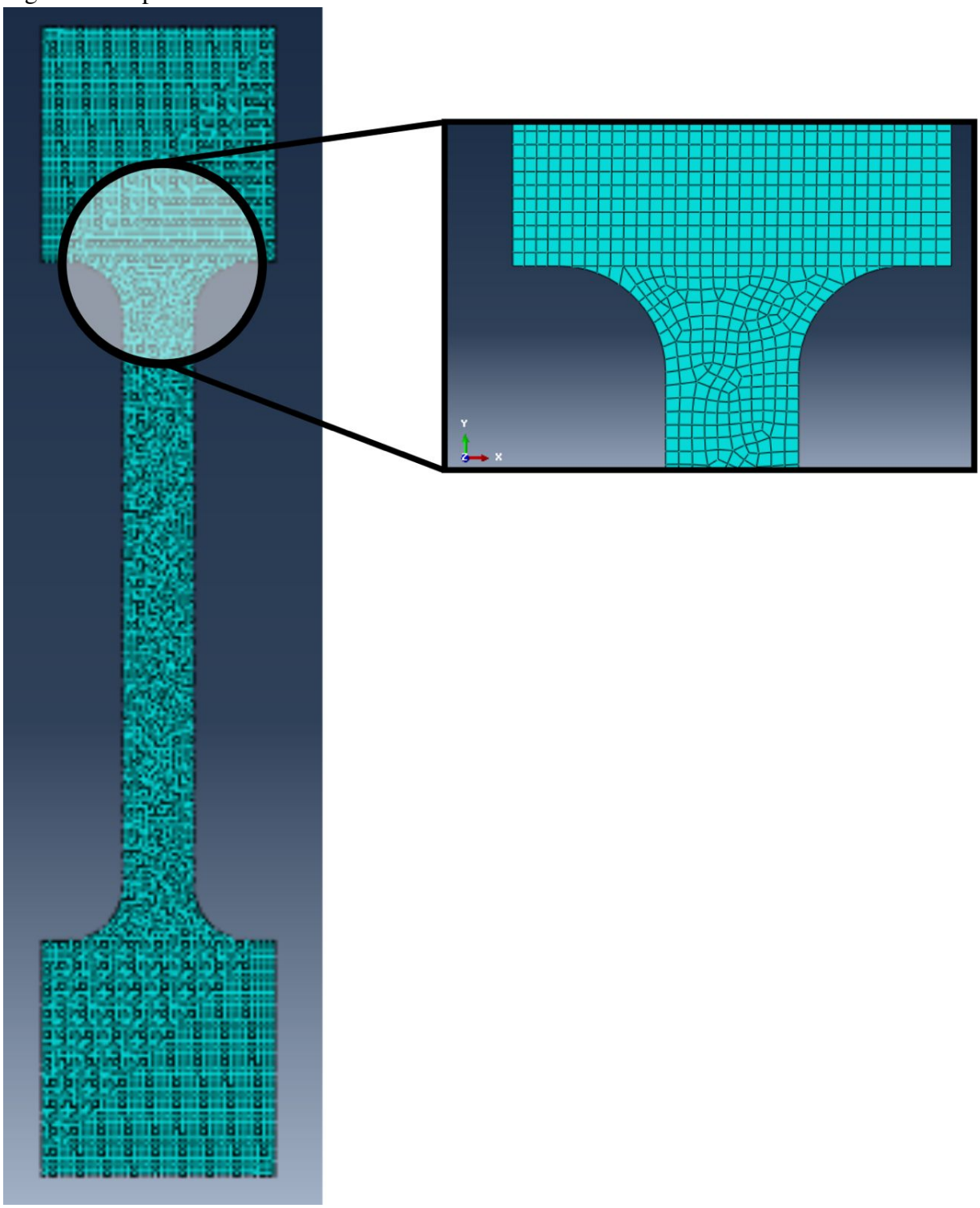

Source: Author.

4.2.1 J3 - Numerical results

The simulation of the J3 composite, following the modeling parameters described earlier, using the average dimensions and properties from the experimental tests (excluding shear) were used in the simulations. It presented excellent results, as shown in Figure 28. It can be observed that the numerical results are highly consistent with the experimental findings.

Figure 28 – J3 - Numerical tensile test results

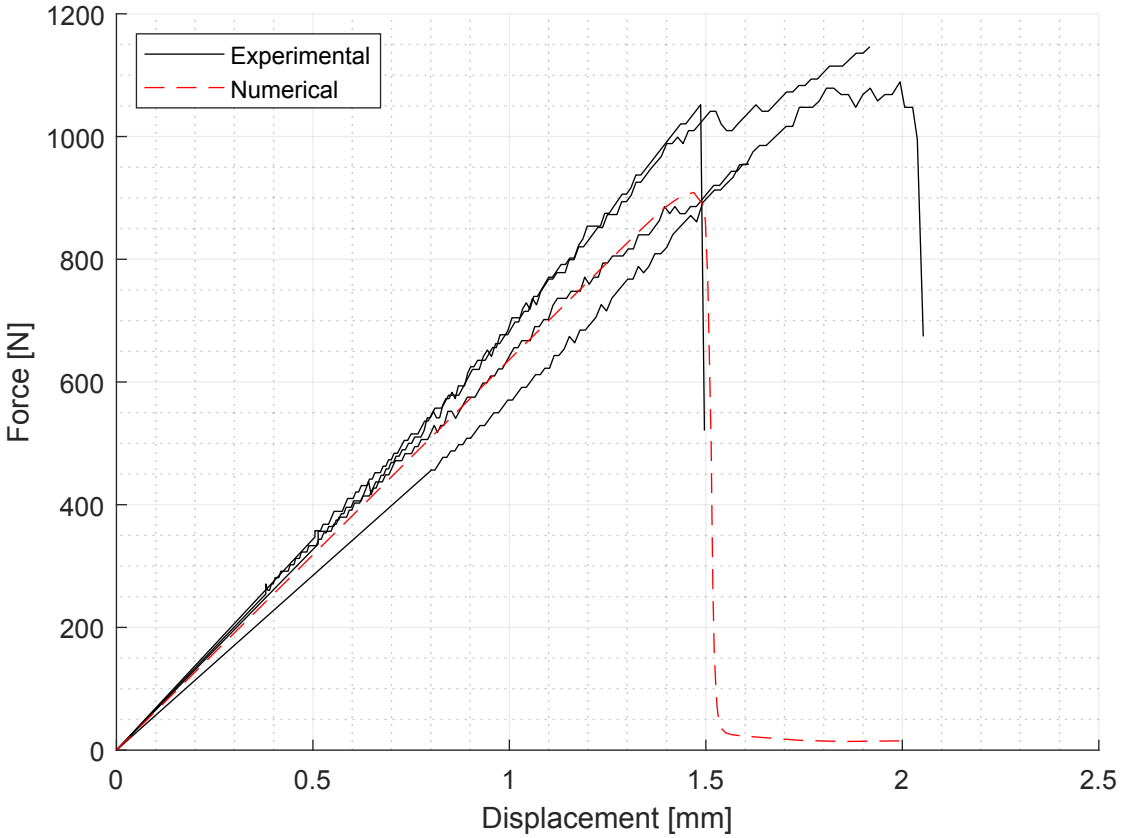

Source: Author.

4.2.2 G8 - Numerical results

As J3, simulation, G8 modeling was made by using parameters described earlier, the average dimensions and properties from the experimental tests (excluding shear). It also presented excellent results, as shown in Figure 29.

In this modeling, it is observed that the fracture energy from the numerical simulation is much higher than that from the experimental results when observing the area under the curve after reaching the maximum tensile force. This was expected since the numerical fracture energy results for this composite showed out-of-plane displacements, which was not ideal. As seen

Figure 29 – G8 - Numerical tensile test results

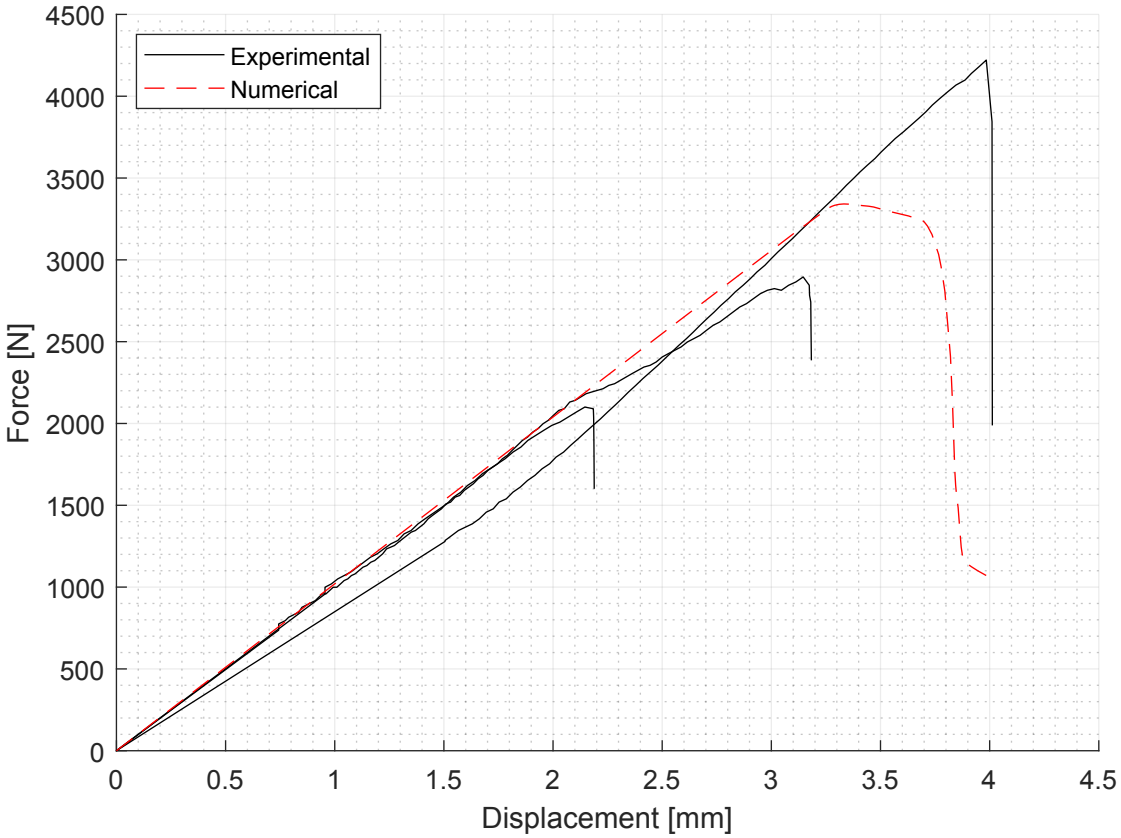

Source: Author.

in the experimental results, G8 exhibits an abrupt fracture, which is inconsistent with a high fracture energy. Therefore, to parameterize the glass, a numerical approach was tested using 50% and 10% of the fracture energy obtained from experiments. This was done to visually demonstrate the influence of fracture energy in the modeling after reaching the material's peak load. As shown in Figure 30, the result using 10% of the fracture energy was the closest match to the experimental results and will be used to represent the glass in the modeling of composites with different materials.

Figure 30 – G8 - Fracture Energy influence

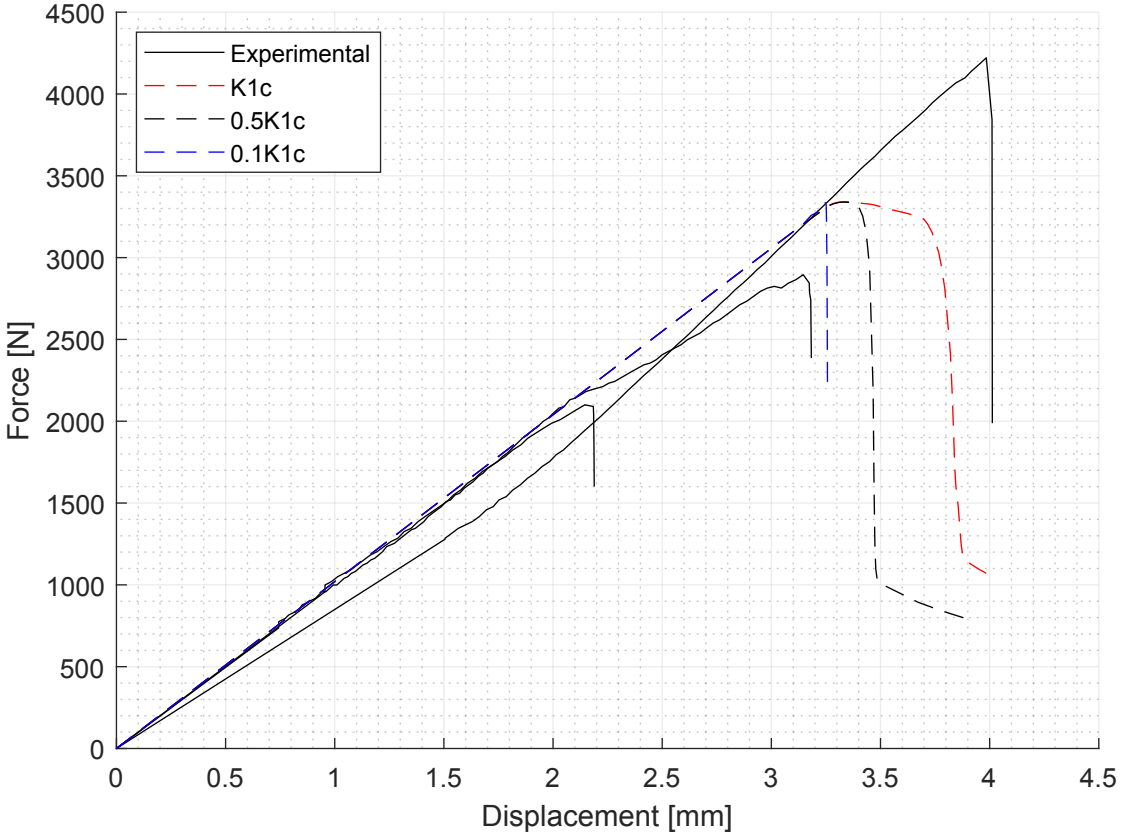

Source: Author.

4.2.3 GJJJJG - results

A tensile test specimen with the same dimensions as the GJJJJG composite was modeled in Abaqus software version 6.11. Two models were created, changing only the way the properties were represented. In the first model, the properties obtained from the GJJJJG composite test were used, considering a 3-ply composite in the same direction (0º), with each ply having the same thickness (one-third of the total composite thickness, which is 7mm). In the second model, the composite was divided into three plies, with the two external plies having the same properties as the G8 composite and a thickness of 0.02mm each, and the internal ply having the properties of the J3 ply with a thickness of 6.98mm (summing up to the 7mm thickness of the tested GJJJJG composite).

Figure 31 – GJJJJG - Experimental x Numerical results

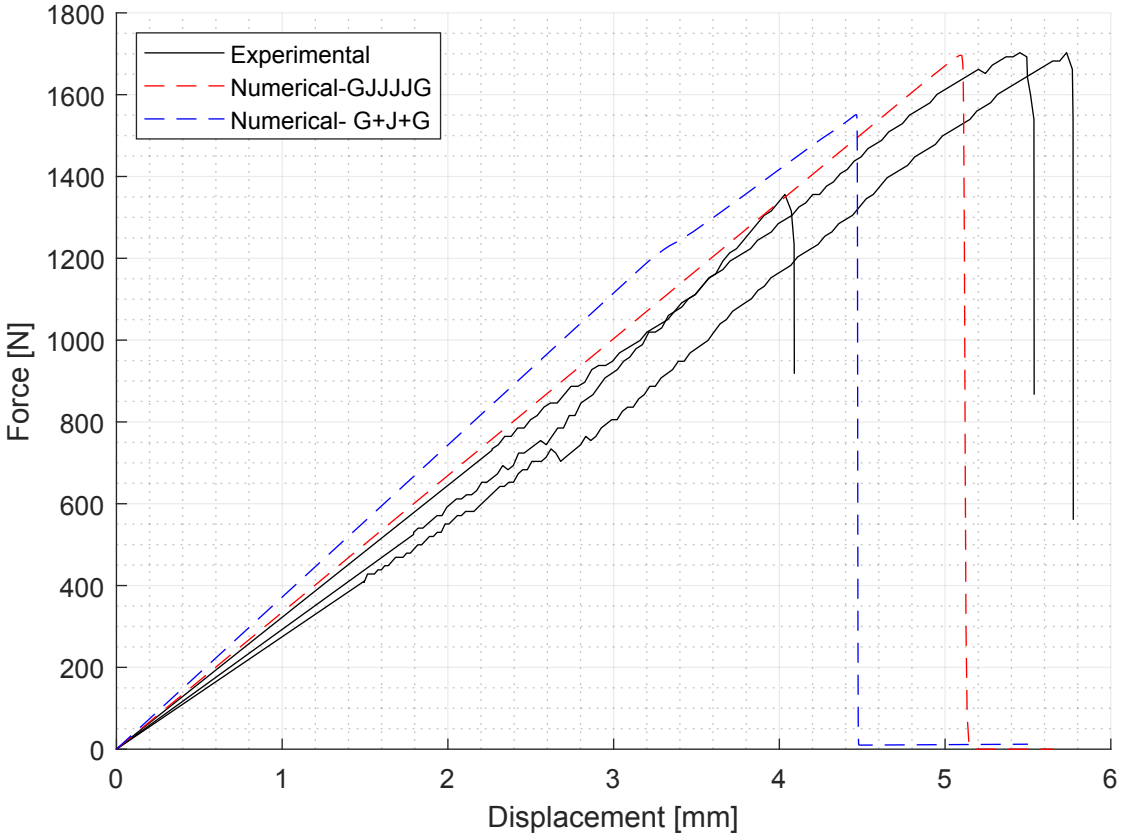

Source: Author.

In Figure 31, it can be observed that the numerical models yielded promising results. The model utilizing the properties of the GJJJJG composite showed the best outcomes, with the curve's slope between the experimental curves. The curve generated by the model using the separate properties of jute (J3) and glass (G8) was very close to the experimental data,

but it presented a modulus that was slightly more accentuated modulus. This model with separate properties presented a challenge in defining the thicknesses. Since the definition of each composite's thickness involves both fiber and resin, in the case of the GJJJJG composite, the precise thickness of each layer remains uncertain. To address this issue, an approach was employed by taking the thickness of the J3 composite, dividing it by 3, and using that value as the thickness for one layer of jute. As for the glass component, the difference from the total thickness of the hybrid composite was determined and assigned as the thickness for the glass layers.

4.2.4 Parametric study - Stacking sequences

Extensive experimental testing was conducted to characterize the mechanical behavior of different combinations, including jute-reinforced composites, glass-reinforced composites, and hybrids with both fiber types. The experimental results yielded valuable insights into the composite properties, enabling a comprehensive understanding of their performance under various loading conditions. Building upon this experimental foundation, numerical modeling techniques were employed using the Abaqus software. The same boundary conditions presented in Figure 26 were used. The developed model successfully simulated the mechanical behavior of the jute and glass fiber-reinforced composites. This achievement validated model's capability to predict material responses and provided confidence in its accuracy.

One of the most significant advantages of the developed model is its potential to simulate and predict the mechanical properties of laminated composites with different stacking sequences, without the need for extensive experimental tests. This approach leverages the knowledge gained from individual fiber-reinforced composites and hybrid materials to extrapolate the behavior of novel stacking sequences.

By avoiding additional experimental tests for each specific stacking sequence, the modeling approach drastically reduces the time and resources required for material characterization. This is very advantageous in scenarios where rapid assessment of multiple configurations is essential. It also eliminates the need to handle chemical substances for fiber treatment, reducing potential health and safety risks associated with experimental testing.

The modeling allows exploring unconventional stacking sequences and configurations that may not have been practical to investigate experimentally. This promotes innovation and the identification of optimized designs for specific applications, besides facilitating sensitivity analyses to understand the influence of various factors, such as fiber orientation and material properties, on composite behavior. Furthermore, optimization studies can be conducted to identify the most favorable stacking sequences based on specific performance criteria.

With the results obtained for J3 and G8, different layups were herein evaluated. After parametric studies and parameter adjustments, the final values adopted for the parameters of each material, which will be used in this lamination study, are presented in Table 10. The chosen sequences were the same as those used by Gujjala *et al.* (2014), aiming to compare the numerical results with the literature. Therefore, the analyses were conducted for the following sequences: GGGG, JJJJ, GJJG, JGGJ, and GJGJ. Figure 32 presents force x displacement results

for different stacking sequences and Figure 33 presents tensile strength values.

Table 10 – Jute and glass fibers parameters adopted in Abaqus

Parameter	Jute	Glass
Longitudinal Tensile Strength (MPa)	25.6	213.41
Longitudinal Compressive Strength (MPa)	29.07	271.00
Transverse Tensile Strength (MPa)	25.6	213.41
Transverse Compressive Strength (MPa)	29.07	271.00
Longitudinal Shear Strength (MPa)	16.79	113.00
Transverse Shear Strength (MPa)	16.79	113.00
E_1 (MPa)	463	5774
E_2 (MPa)	463	5774
ν_{12}	0.3	0.3
G_{12} (MPa)	193	2406
Viscosity coefficient in all directions:	0.0001	0.0001
Longitudinal Compressive/Tensile Fracture Energy $(MPa\sqrt{m})$	3.22	4.37
Transverse Compressive/Tensile Fracture Energy $(MPa\sqrt{m})$	0.2	0.2

Source: Author

Analyzing Figures 32 and Figure 33, expected behaviors for the different laminations are observed: GGGG exhibited the highest breaking strength, whereas JJJJ displayed the lowest. Among the variations in lamination for the other samples, it is noteworthy to observe that glass acts as the limiting layer for the maximum displacement of these materials, while jute exhibits greater flexibility. Additionally, it is evident that all combinations of glass and jute demonstrate intermediate behaviors between composites composed of a single fiber type. Gujjala *et al.* (2014) obtained similar results in experimental tests, the only difference is that GJJG and JGGJ in their tests obtained slightly different values.

In this example, damage propagation was analyzed. Figure 34 shows where the damage occurs and how it develops in the GJJG composite. In the other laminations, the damage occurred in a similar manner and in the same position. In the experimental tests, the damage also occurred in the same location, relatively close to the machine's claws. Figures 35 and 36 display the damage in the individual layers. Figure 35 depicts the damage in the outer (glass) fibers, while Figure 36 shows it in the inner (jute) fibers. An intermediate point was chosen where the damage had not yet reached 100%. It can be observed that the glass fiber has more advanced damage compared to the jute fiber. This outcome is consistent, considering that glass fiber is much stronger, thus absorbing a greater portion of the load. Additionally, as seen in Figure 32, jute fiber can displace more than glass fiber.

Figure 32 – Force x displacement curves for different stacking sequences

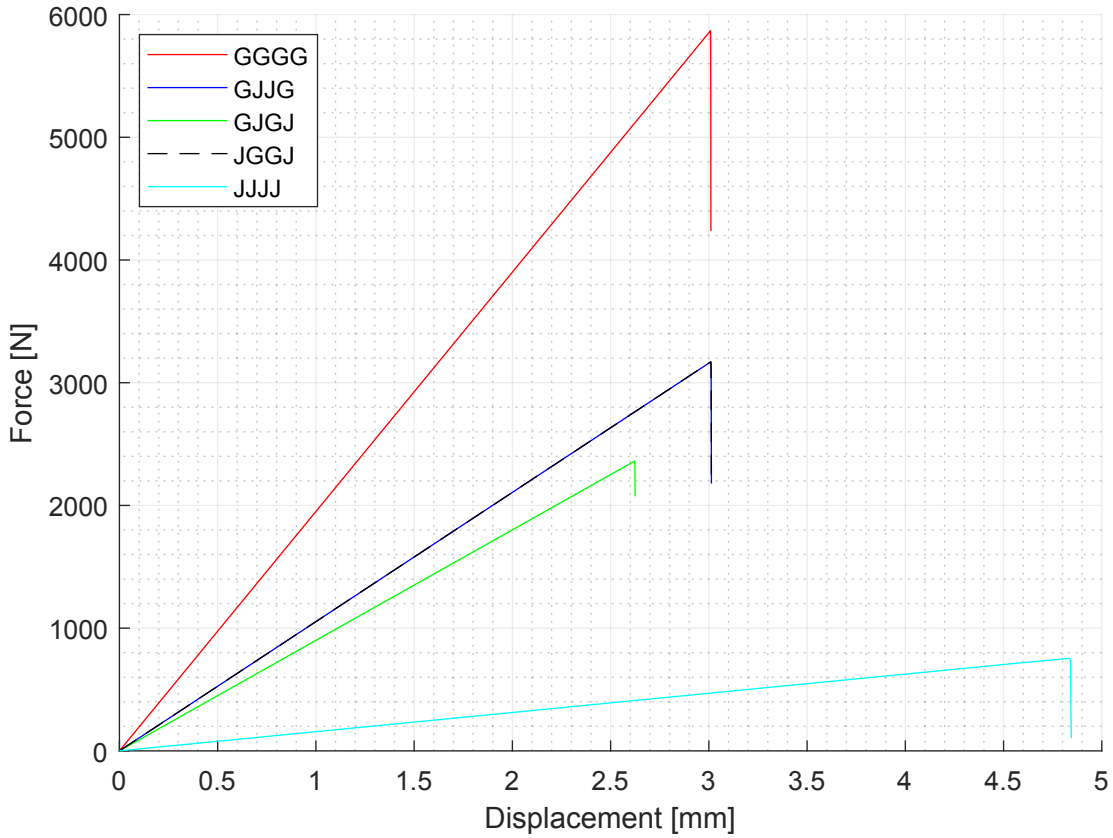

Source: Author.

Figure 33 – Numerical tensile strength of jute–glass fiber epoxy composite with different layups

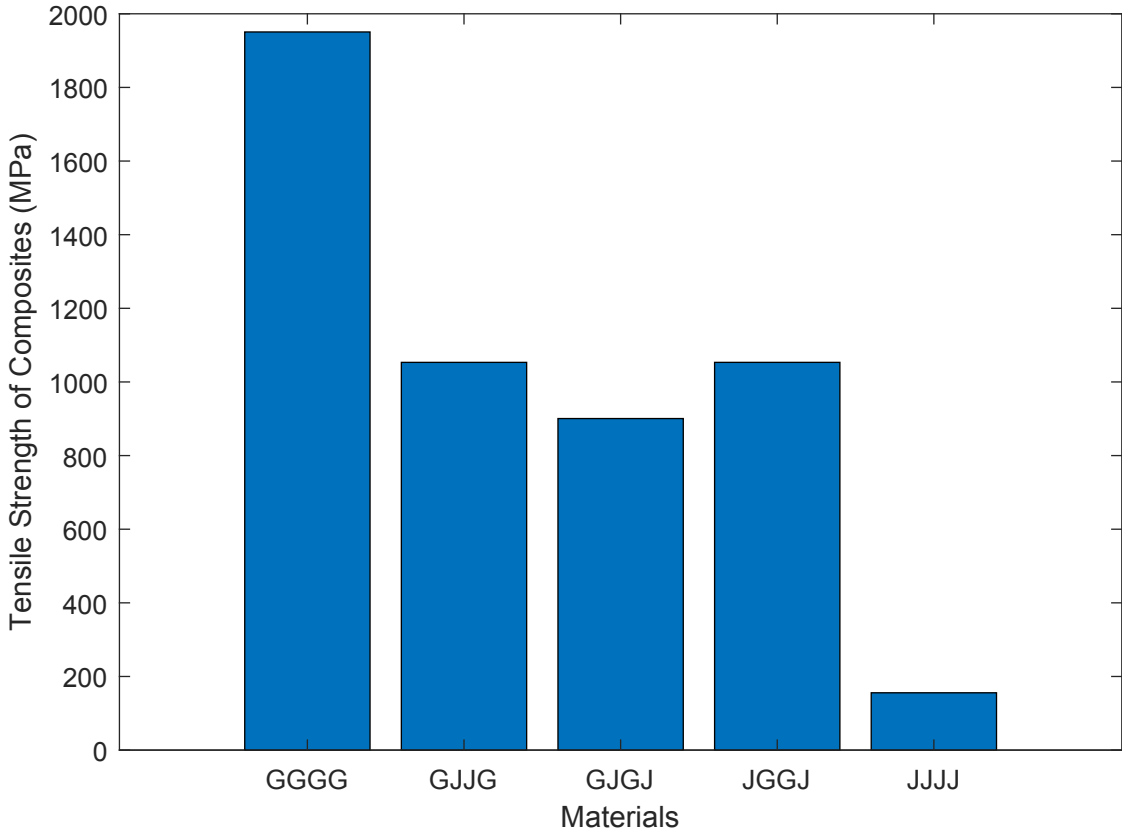

Source: Author.

Figure 34 – Damage in GJJG composite.

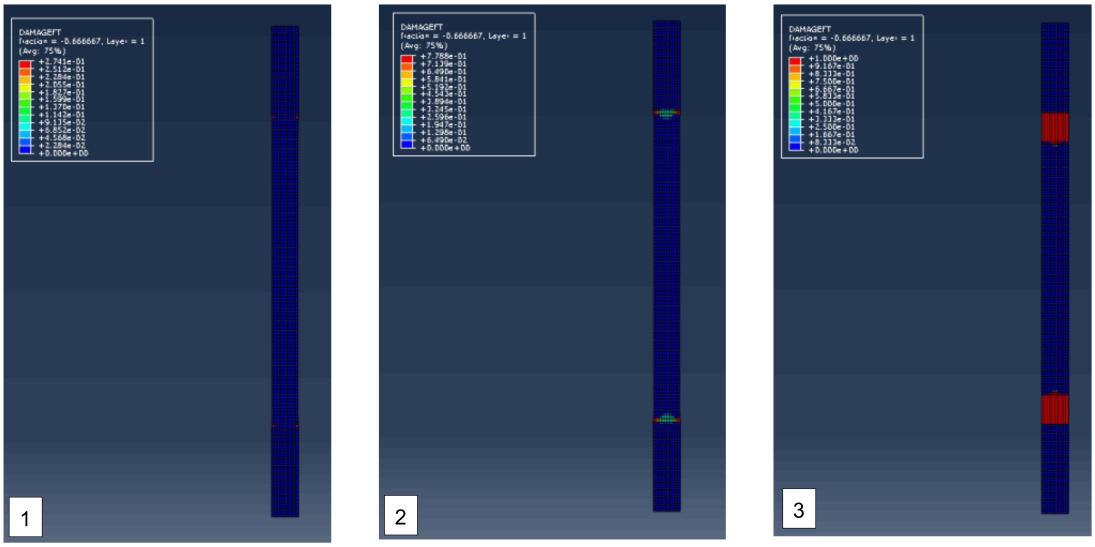

Source: Author.

Figure 35 – Glass plies behavior after damage initiation

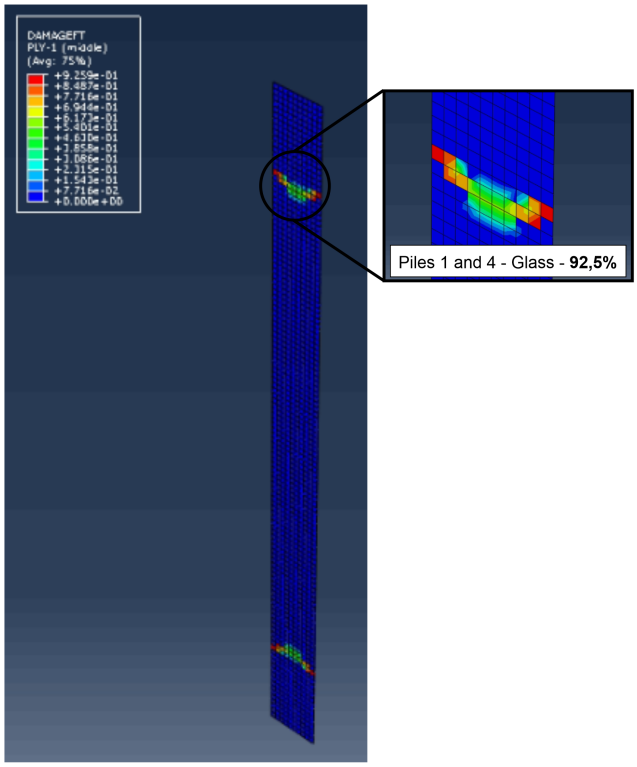

Source: Author.

Figure 36 – Jute plies behavior after damage initiation

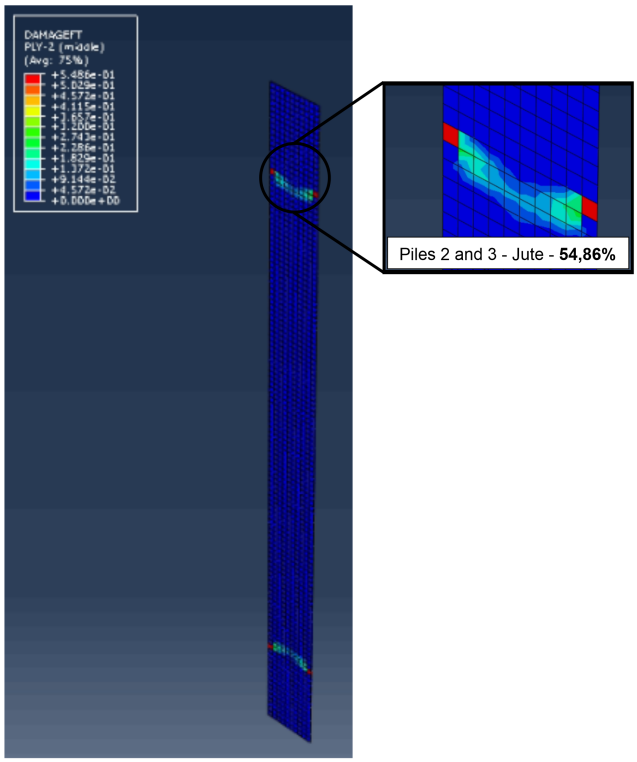

Source: Author.

Another parametric analysis was performed involving the study of a plate with a hole, having the same dimensions as the test specimens used in the parametric study of layup effects. A model was created with a hole of 2mm radius at the center of the component. Due to the presence of the hole, a finer mesh was required, as presented in Figure 37. The results are presented by ply in Figures 38 to 40. In the composite materials GJJG and JGGJ, it can be observed that the outer plies bear the majority of the load, with S22 representing the longitudinal stress in the component. This indicates that for components with varying geometries, where the loading is not simply a direct tension, the outermost fibers play a crucial role in the material's strength, as expected. In the GJGJ composite (Figure 40, for instance, which comprises an outer layer of jute and an outer layer of glass, distinct load distributions are evident among the material plies, consistently with the outermost material ply bearing the highest load. However, it is worth noting that the results for the GJGJ composite may be distorted due to the non-symmetry of the component along its thickness. Ideally, experimental testing of this composite should be conducted in the laboratory to validate the findings obtained through the finite element analysis program.

Figure 37 – Composite with a hole- mesh

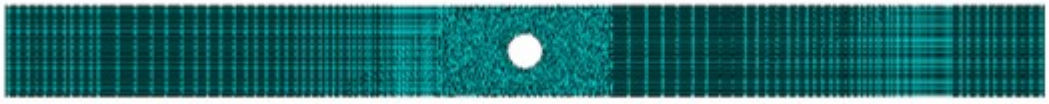

Source: Author.

Figure 38 – GJJG - Fiber damage per ply in composite with a hole

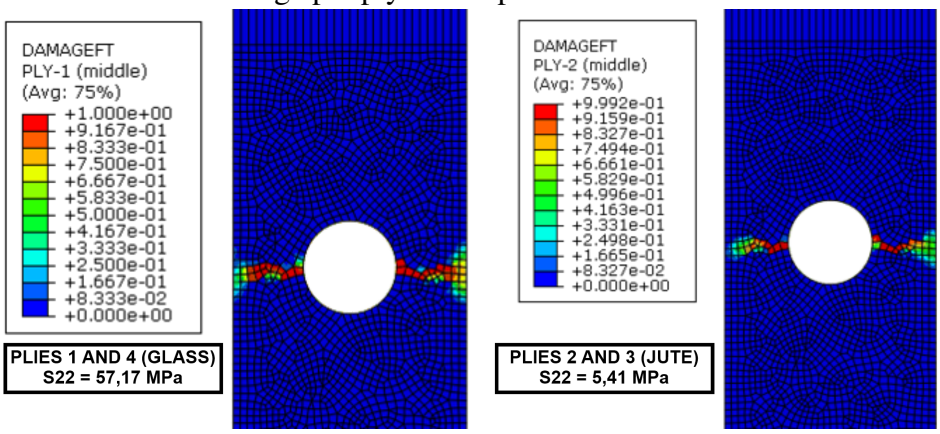

Source: Author.

In addition to studying the stress distribution in each ply, the radial and tangential stresses across the plate at the hole's height, as depicted in Figure 41, were also analyzed. The

Figure 39 – JGGJ - Fiber damage per ply in composite with a hole

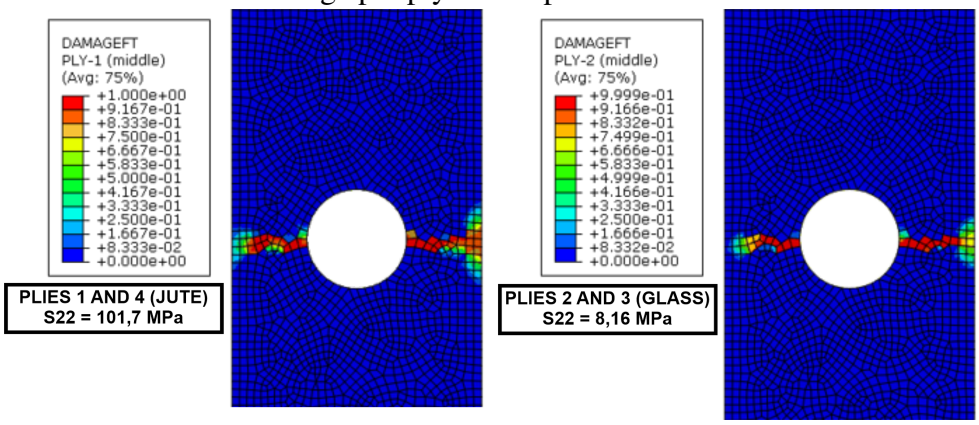

Source: Author.

Figure 40 – GJGJ - Fiber damage per ply in composite with a hole

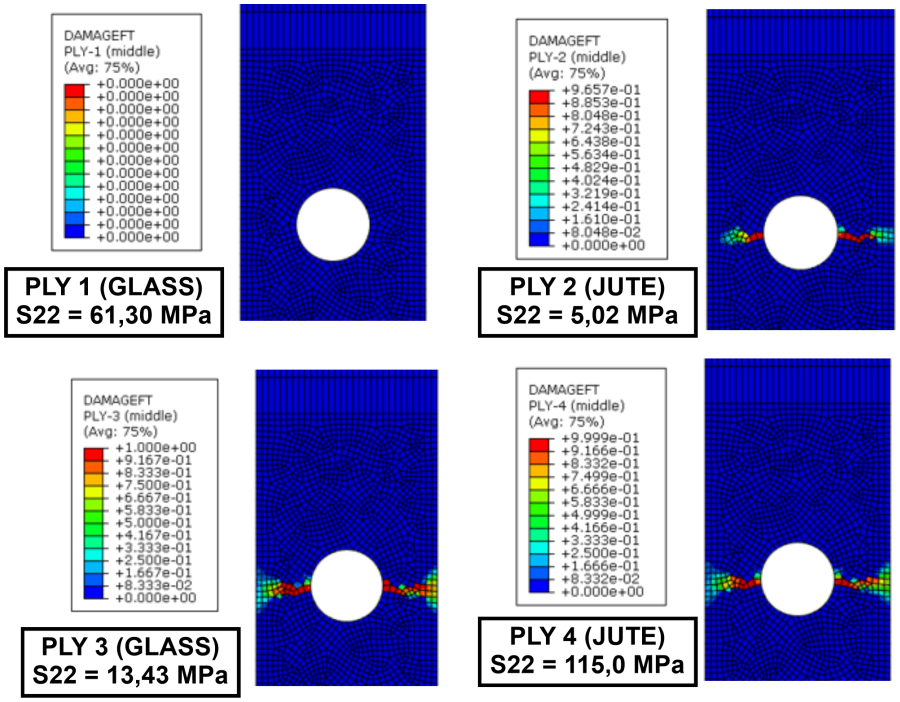

Source: Author.

outcomes are illustrated in Figures 42 and 43, where σ_r stands for radial stress and σ_θ denotes tangential stress. As anticipated, the composites exhibited behavior influenced by the outermost fibers. Since the results are normalized by σ_0, it can be observed that all of them displayed quite similar behaviors, except for the GJGJ composite, which is the only configuration featuring outer fibers made of different materials.

Figure 41 – Graphic representation - stresses at the composite with a hole

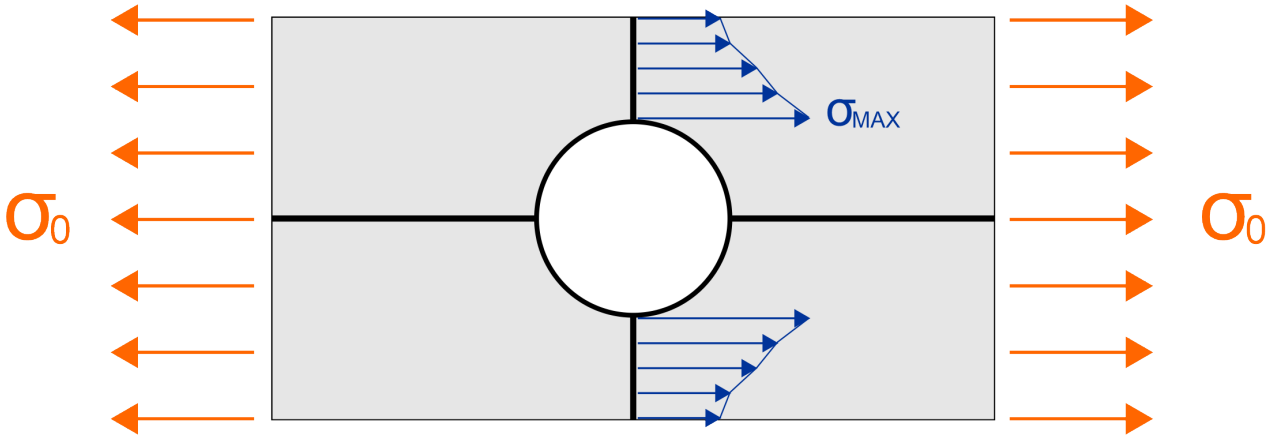

Source: Author.

Figure 42 – Radial stresses distribution in different layups

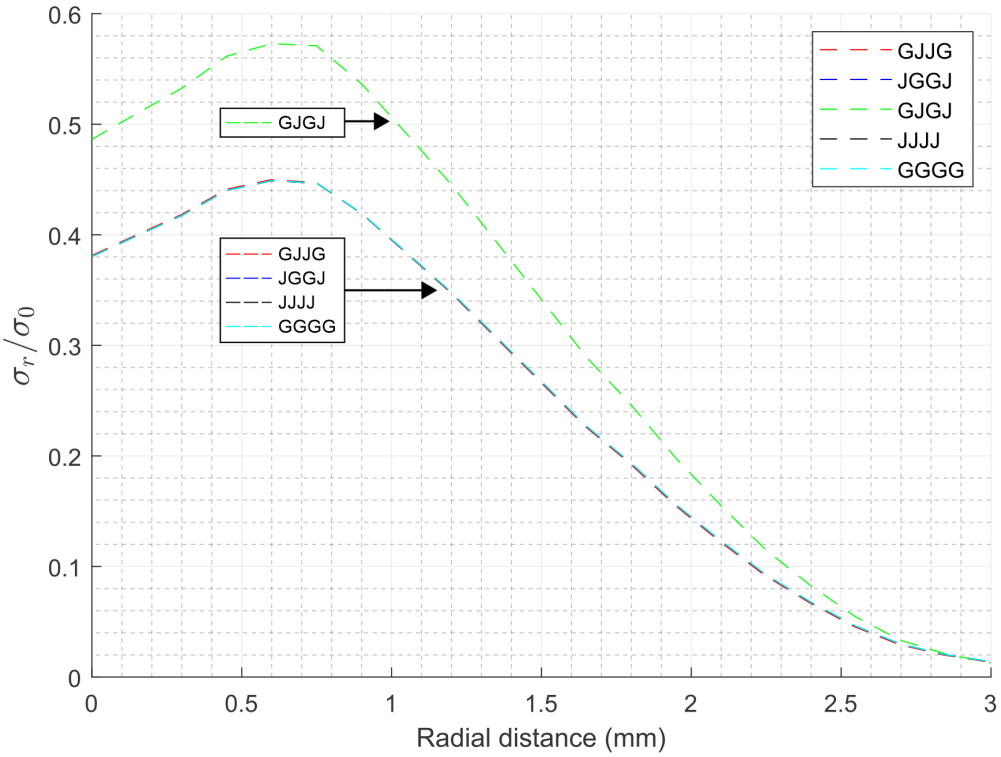

Source: Author.

Figure 43 – Tangential stresses distribution in different layups

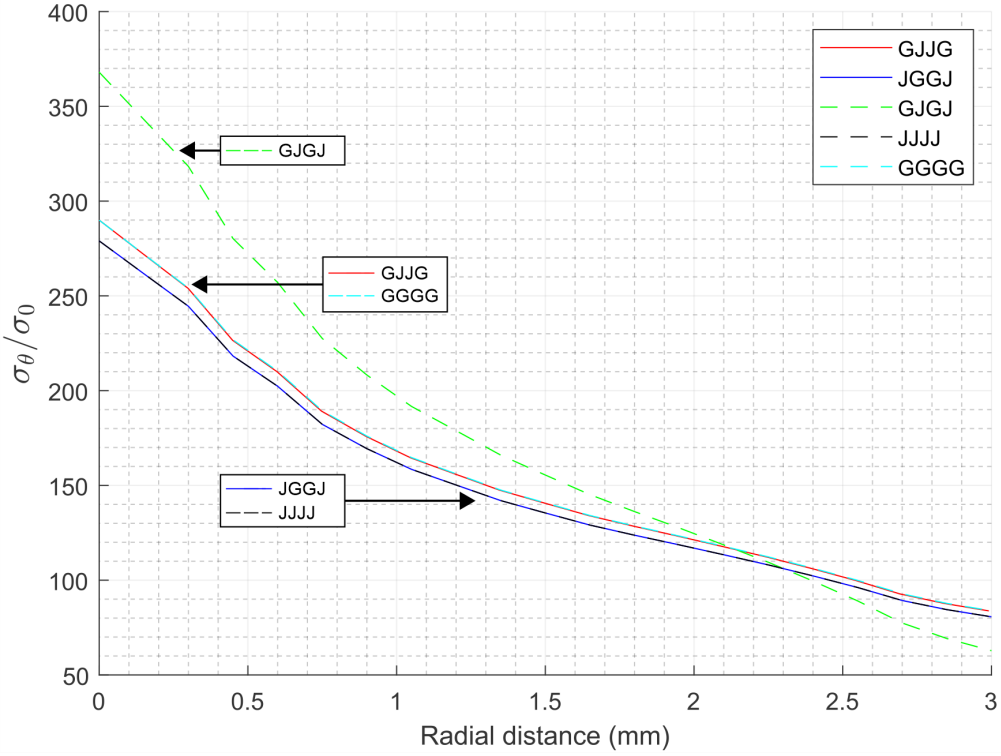

Source: Author.

5 CONCLUSION

In this study, jute-glass hybrid-reinforced epoxy composites were investigated through a combination of experimental and numerical analyses. The research aimed to explore the mechanical behavior of these composites, considering their potential applications in various industries as eco-friendly alternatives to traditional synthetic fiber composites.

The experimental characterization of jute fibers and the produced jute-glass hybrid composites provided valuable mechanical properties essential for the numerical modeling. Jute properties and different treatments were studied. Tensile properties of jute fibers were obtained. Impacts of alkali treatment were observed. It was possible to analyze that jute behavior was more ductile, but its tensile strength was reduced. The results demonstrated the feasibility of producing hybrid composites using manual lamination techniques. The combination of jute and glass fibers exhibited promising mechanical properties, showing the potential advantages of using natural fibers in conjunction with synthetic fibers.

The numerical analysis using Abaqus software allowed the simulation of the mechanical behavior of the jute-glass hybrid composites. A homogeneous material model and a laminated material model were developed, incorporating the properties of jute and glass fibers separately. The numerical simulations showed good agreement with the experimental results, validating the effectiveness of the models in representing the mechanical behavior of the hybrid composites.

Hashin's failure initiation criteria were found to be suitable for the numerical representation of jute-glass hybrid-reinforced composites in this study. Different failure and damage theories were studied. The next step of this work is to apply the experimental results to these different models to analyze which one better represents the hybrid composites studied herein. However, due to time constraints, it was not possible to complete this analysis in the current study. Nonetheless, it remains as a suggestion for future research to apply the experimental data to various models and evaluate their effectiveness in representing the behavior of the hybrid composites.

The outcomes of this research contribute to the understanding of jute-glass hybrid composites' mechanical properties and behavior. These composites offer a promising combination of mechanical performance, environmental advantages, and cost-effectiveness, making them attractive materials for applications in industries such as aerospace and automotive, where weight reduction and sustainability are crucial factors.

As with any research, this study had some limitations. The numerical modeling focused on the mechanical behavior of the hybrid composites, and other factors such as different failure and damage theories were not extensively explored. Further research is needed to address these aspects and to optimize the manufacturing processes and material compositions for specific applications.

In conclusion, jute-glass hybrid-reinforced epoxy composites demonstrate great potential as eco-friendly alternatives to traditional synthetic fiber composites. The integration of experimental and numerical analyses provides a comprehensive understanding of the material's behavior, opening up opportunities for its application in various industries. With ongoing research and development, jute-glass hybrid composites hold the promise of contributing to a more sustainable and environmentally conscious approach to composite materials in the future.

REFERENCES

ACHA, B. A. *et al.* Physical and mechanical characterization of jute fabric composites. **Journal of Applied Polymer Science**, Wiley Online Library, v. 98, n. 2, p. 639–650, 2005.

AJI, I. *et al.* Mechanical properties and water absorption behavior of hybridized kenaf/pineapple leaf fibre-reinforced high-density polyethylene composite. **Journal of composite materials**, Sage Publications Sage UK: London, England, v. 47, n. 8, p. 979–990, 2013.

ALVES, C. *et al.* Ecodesign of automotive components making use of natural jute fiber composites. **Journal of cleaner production**, Elsevier, v. 18, n. 4, p. 313–327, 2010.

ARDANUY, M. *et al.* Cellulosic fiber reinforced cement-based composites: A review of recent research. **Construction and Building Materials**, Elsevier, v. 79, p. 115–128, 2015. Available at: <https://www.sciencedirect.com/science/article/pii/S0950061815000550>. Accessed on: 28 jun. 2023.

ASTM. **ASTM E399-90(2012) Standard Test Method for Linear-Elastic Plane-Strain Fracture Toughness KIC of Metallic Materials.** [S.l.]: ASTM International West Conshohocken, PA, 2012.

ASTM. **Standard test method for measurement of fracture toughness**. 2019.

ASTM, I. **Standard test methods for plane-strain fracture toughness and strain energy release rate of plastic materials**. [S.l.]: ASTM Inernational, 2007.

ASTM, I. **Standard Specification for Test Method for Shear Testing of Thin Aluminum Alloy Products. West Conshohocken**. [S.l.]: ASTM Inernational, 2017.

AVALLONE, E. A. *et al.* **Marks' standard handbook for mechanical engineers**. [S.l.]: McGraw-Hill Education, 2007.

BARBERO, E. J. **Introduction to composite materials design**. [S.l.]: CRC press, 2010.

BöGNER-BALZ, H. *et al.* Structural behaviour of fabrics and coatings for architectural fabric structures. In: **Fabric Structures in Architecture**. Woodhead Publishing, 2015, (Woodhead Publishing Series in Textiles). p. 123–157. Available at: <https://www.sciencedirect.com/science/article/pii/B9781782422334000048>. Accessed on: 04 jun. 2023.

CALLISTER, W. D. *et al.* **Materials science and engineering: an introduction**. [S.l.: s.n.], 2007.

CASTRO, D. P. *et al.* Mechanical properties of jute fiber fabric/polyester resin composites produced by resin transfer molding. In: . [S.l.: s.n.], 2021. p. 5.

CHANDEKAR, H. *et al.* A review of jute fiber reinforced polymer composites. **Materials Today: Proceedings**, Elsevier, v. 26, p. 2079–2082, 2020.

CHANDGUDE, S.; SALUNKHE, S. In state of art: Mechanical behavior of natural fiber-based hybrid polymeric composites for application of automobile components. **Polymer Composites**, Wiley Online Library, v. 42, n. 6, p. 2678–2703, 2021.

DANIEL, I. M. *et al.* **Engineering mechanics of composite materials**. [S.l.]: Oxford University Press New York, 2006.

FARUK, O. *et al.* Biocomposites reinforced with natural fibers: 2000–2010. **Progress in Polymer Science**, Elsevier, v. 37, n. 11, p. 1552–1596, 2012. Topical Issue on Polymeric Biomaterials. Available at: <https://www.sciencedirect.com/science/article/pii/S0079670012000391>. Accessed on: 28 jun. 2023.

GANGIL, B. *et al.* Natural and synthetic fibers for hybrid composites. **Hybrid fiber composites: materials, manufacturing, process engineering**, Wiley Online Library, p. 1–15, 2020.

GORIPARTHI, B. K. *et al.* Effect of fiber surface treatments on mechanical and abrasive wear performance of polylactide/jute composites. **Composites Part A: Applied Science and Manufacturing**, v. 43, n. 10, p. 1800–1808, 2012. CompTest 2011. Available at: <https://www.sciencedirect.com/science/article/pii/S1359835X12001649>. Accessed on: 30 jun. 2023.

GRÉDIAC, M. The use of full-field measurement methods in composite material characterization: interest and limitations. **Composites Part A: Applied Science and Manufacturing**, Elsevier, v. 35, n. 7, p. 751–761, 2004. Available at: <https://www.sciencedirect.com/science/article/pii/S1359835X04000260>. Accessed on: 28 jun. 2023.

GUJJALA, R. *et al.* Mechanical properties of woven jute–glass hybrid-reinforced epoxy composite. **Journal of Composite Materials**, SAGE Publications Sage UK: London, England, v. 48, n. 28, p. 3445–3455, 2014.

GÜRDAL, Z. *et al.* **Design and optimization of laminated composite materials**. [S.l.]: John Wiley & Sons, 1999.

HASHIN, Z. Failure criteria for unidirectional fiber composites. 1980.

HASHIN, Z.; ROTEM, A. A fatigue failure criterion for fiber reinforced materials. **Journal of composite materials**, Sage Publications Sage CA: Thousand Oaks, CA, v. 7, n. 4, p. 448–464, 1973.

HE, T. *et al.* Uncertainty analysis in composite material properties characterization using digital image correlation and finite element model updating. **Composite Structures**, v. 184, p. 337–351, 2018. Available at: <https://www.sciencedirect.com/science/article/pii/S0263822317320482>. Accessed on: 28 jun. 2023.

HILL, R. A theory of the yielding and plastic flow of anisotropic metals. **Proceedings of the Royal Society of London. Series A. Mathematical and Physical Sciences**, The Royal Society London, v. 193, n. 1033, p. 281–297, 1948.

HOSSAIN, M. K. *et al.* Mechanical performances of surface modified jute fiber reinforced biopol nanophased green composites. **Composites Part B: Engineering**, v. 42, n. 6, p. 1701–1707, 2011. Available at: <https://www.sciencedirect.com/science/article/pii/S1359836811001077>. Accessed on: 28 jun. 2023.

JOHN, K.; NAIDU, S. V. Tensile properties of unsaturated polyester-based sisal fiber–glass fiber hybrid composites. **Journal of Reinforced Plastics and Composites**, SAGE Publications, v. 23, n. 17, p. 1815–1819, Nov. 2004. Available at: <https://doi.org/10.1177/0731684404041147>. Accessed on: 28 jun. 2023.

JONES, R. M. **Mechanics of composite materials**. [S.l.]: CRC press, 1998.

KHALIL, H. A. *et al.* Exploring biomass based carbon black as filler in epoxy composites: Flexural and thermal properties. **Materials & Design**, Elsevier, v. 31, n. 7, p. 3419–3425, 2010. Available at: <https://www.sciencedirect.com/science/article/pii/S0261306910000580>. Accessed on: 28 jun. 2023.

KISIEL, M.; MOSSETY-LESZCZAK, B. Development in liquid crystalline epoxy resins and composites – a review. **European Polymer Journal**, Elsevier BV, v. 124, Feb. 2020. Accessed on: 28 jun. 2023.

KURAISHI, A. *et al.* Failure criteria in fibre-reinforced-polymer composites. In: **A progressive quadratic failure criterion, part B**. [S.l.]: Elsevier, 2004. p. 903–921.

LAPCZYK, I.; HURTADO, J. A. Progressive damage modeling in fiber-reinforced materials. **Composites Part A: Applied Science and Manufacturing**, Elsevier, v. 38, n. 11, p. 2333–2341, 2007. CompTest 2006. Available at: <https://www.sciencedirect.com/science/article/pii/S1359835X07000218>. Accessed on: 12 jun. 2023.

LEE, C.-S. *et al.* Initial and progressive failure analyses for composite laminates using puck failure criterion and damage-coupled finite element method. **Composite Structures**, Elsevier, v. 121, p. 406–419, 2015.

LEONARD, L. *et al.* Fracture behaviour of glass fibre-reinforced polyester composite. **Proceedings of the Institution of Mechanical Engineers, Part L: Journal of Materials: Design and Applications**, SAGE Publications Sage UK: London, England, v. 223, n. 2, p. 83–89, 2009.

LIU, L. *et al.* Mechanical properties of poly(butylene succinate) (pbs) biocomposites reinforced with surface modified jute fibre. **Composites Part A: Applied Science and Manufacturing**, Elsevier, v. 40, n. 5, p. 669–674, 2009. Available at: <https://www.sciencedirect.com/science/article/pii/S1359835X09000700>. Accessed on: 28 jun. 2023.

MAHLTIG, B.; KYOSEV, Y. **Inorganic and Composite Fibers: Production, Properties, and Applications**. Woodhead Publishing, 2018.

MAJUMDAR, S. N. G. Effect of stacking sequence and hybridization on mechanical properties of jute-glass fiber composites. **International Journal of Performability Engineering**, v. 12, n. 3, p. 229, 2016.

MANALO, A. C. *et al.* Effects of alkali treatment and elevated temperature on the mechanical properties of bamboo fibre–polyester composites. **Composites Part B: Engineering**, Elsevier, v. 80, p. 73–83, 2015. Available at: <https://www.sciencedirect.com/science/article/pii/S1359836815003388>. Accessed on: 01 jun. 2023.

MANSOR, M. *et al.* Natural fiber polymer composites: Utilization in aerospace engineering. In: **Biomass, Biopolymer-Based Materials, and Bioenergy**. Woodhead Publishing, 2019, (Woodhead Publishing Series in Composites Science and Engineering). p. 203–224. Available at: <https://www.sciencedirect.com/science/article/pii/B9780081024263000114>. Accessed on: 28 jun. 2023.

MANUAL, A. S. U. Abaqus 6.11. **http://130.149**, v. 89, n. 2080, p. v6, 2012.

MARICHELVAM, M. *et al.* A novel palm sheath and sugarcane bagasse fiber based hybrid composites for automotive applications: An experimental approach. **Polymer Composites**, Wiley Online Library, v. 42, n. 1, p. 512–521, 2021.

MI, X. *et al.* Toughness and its mechanisms in epoxy resins. **Progress in Materials Science**, Elsevier BV, v. 130, p. 100977, Oct. 2022.

MISHRA, V.; BISWAS, S. Physical and mechanical properties of bi-directional jute fiber epoxy composites. **Procedia Engineering**, v. 51, p. 561–566, 2013. Chemical, Civil and Mechanical Engineering Tracks of 3rd Nirma University International Conference on Engineering (NUiCONE2012). Available at: <https://www.sciencedirect.com/science/article/pii/S1877705813000805>. Accessed on: 28 jun. 2023.

MONTEIRO, S. N. *et al.* Natural-fiber polymer-matrix composites: Cheaper, tougher, and environmentally friendly. **JOM**, Springer Science and Business Media LLC, v. 61, n. 1, p. 17–22, Jan. 2009. Available at: <https://doi.org/10.1007/s11837-009-0004-z>. Accessed on: 28 jun. 2023.

NOPPARUT, A.; AMORNSAKCHAI, T. Influence of pineapple leaf fiber and it's surface treatment on molecular orientation in, and mechanical properties of, injection molded nylon composites. **Polymer Testing**, v. 52, p. 141–149, 2016. Available at: <https://www.sciencedirect.com/science/article/pii/S0142941816302227>. Accessed on: 28 jun. 2023.

PANG, S.-S. *et al.* Modified tsai-wu failure criterion for fiber-reinforced composite laminates. **Polymer composites**, Wiley Online Library, v. 13, n. 4, p. 273–277, 1992.

PINHO, S. T. *et al.* **Failure Models and Criteria for FRP Under-In-Plane or Three-Dimensional Stress States Including Shear Non-Linearity**. 2005.

PRAHARAJ, A. P. *et al.* 2-hydroxyethyl acrylate grafted jute fiber/treated coir pith/vinyl ester hybrid composites. **American Journal of Materials Science and Technology**, v. 4, n. 1, p. 31–46, 2015.

PUCK, A. *et al.* Guidelines for the determination of the parameters in puck's action plane strength criterion. **Composites Science and Technology**, Elsevier, v. 62, n. 3, p. 371–378, 2002.

PUTTEGOWDA, M. *et al.* Potential of natural/synthetic hybrid composites for aerospace applications. In: **Sustainable Composites for Aerospace Applications**. Woodhead Publishing, 2018, (Woodhead Publishing Series in Composites Science and Engineering). p. 315–351. Available at: <https://www.sciencedirect.com/science/article/pii/B9780081021316000219>. Accessed on: 28 jun. 2023.

QIAN, S. *et al.* Effect of hydrothermal pretreatment on the properties of moso bamboo particles reinforced polyvinyl chloride composites. **Composites Part B: Engineering**, Elsevier, v. 82, p. 23–29, 2015. Available at: <https://www.sciencedirect.com/science/article/pii/S1359836815004357>. Accessed on: 28 jun. 2023.

RAFIEE, R. *et al.* Investigating structural failure of a filament-wound composite tube subjected to internal pressure: Experimental and theoretical evaluation. **Polymer Testing**, Elsevier, v. 67, p. 322–330, 2018. Available at: <https://www.sciencedirect.com/science/article/pii/S0142941818300801>. Accessed on: 28 jun. 2023.

RAMASUBBU, R.; MADASAMY, S. Fabrication of automobile component using hybrid natural fiber reinforced polymer composite. **Journal of Natural Fibers**, Taylor & Francis, v. 19, n. 2, p. 736–746, 2022.

RASHID, A. A. *et al.* Utilization of banana fiber-reinforced hybrid composites in the sports industry. **Materials**, MDPI, v. 13, n. 14, p. 3167, 2020.

RAVISHANKAR, B. *et al.* Hybrid composites for automotive applications–a review. **Journal of Reinforced Plastics and Composites**, SAGE Publications Sage UK: London, England, v. 38, n. 18, p. 835–845, 2019.

REDDY, J. N. **Mechanics of laminated composite plates and shells: theory and analysis**. [S.l.]: CRC press, 2003.

REINOSO, J. *et al.* A consistent anisotropic damage model for laminated fiber-reinforced composites using the 3d-version of the puck failure criterion. **International Journal of Solids and Structures**, Elsevier, v. 126, p. 37–53, 2017.

SABA, N. *et al.* Recent advances in epoxy resin, natural fiber-reinforced epoxy composites and their applications. **Journal of Reinforced Plastics and Composites**, Sage Publications Sage UK: London, England, v. 35, n. 6, p. 447–470, 2016.

SAFRI, S. N. A. *et al.* Impact behaviour of hybrid composites for structural applications: A review. **Composites Part B: Engineering**, Elsevier, v. 133, p. 112–121, 2018.

SANJAY, M. R.; YOGESHA, B. Studies on mechanical properties of jute/e-glass fiber reinforced epoxy hybrid composites. **Journal of Minerals and Materials Characterization and Engineering**, Scientific Research Publishing, Inc., v. 04, n. 01, p. 15–25, 2016. Available at: <https://doi.org/10.4236/jmmce.2016.41002>. Accessed on: 28 jun. 2023.

SAWPAN, M. A. *et al.* Flexural properties of hemp fibre reinforced polylactide and unsaturated polyester composites. **Composites Part A: Applied Science and Manufacturing**, Elsevier, v. 43, n. 3, p. 519–526, 2012. Available at: <https://www.sciencedirect.com/science/article/pii/S1359835X11003927>. Accessed on: 28 jun. 2023.

SEVER, K. *et al.* Oxygen plasma treatments of jute fibers in improving the mechanical properties of jute/hdpe composites. **Materials Chemistry and Physics**, Elsevier, v. 129, n. 1, p. 275–280, 2011. Available at: <https://www.sciencedirect.com/science/article/pii/S0254058411003014>. Accessed on: 28 jun. 2023.

SHANMUGAM, D.; THIRUCHITRAMBALAM, M. Static and dynamic mechanical properties of alkali treated unidirectional continuous palmyra palm leaf stalk fiber/jute fiber reinforced hybrid polyester composites. **Materials & Design**, Elsevier, v. 50, p. 533–542, 2013. Available at: <https://www.sciencedirect.com/science/article/pii/S0261306913002483>. Accessed on: 28 aug. 2023.

SHIH, Y.-F. *et al.* Pineapple leaf/recycled disposable chopstick hybrid fiber-reinforced biodegradable composites. **Journal of the Taiwan Institute of Chemical Engineers**, Elsevier, v. 45, n. 4, p. 2039–2046, 2014.

SIENGCHIN, S. Editorial corner–a personal view potential use of'green'composites in automotive applications. **Express Polymer Letters**, Budapest University of Technology and Economics, Faculty of Mechanical . . . , v. 11, n. 8, p. 600–600, 2017.

SMAIL, Y. B. *et al.* Effect of heat treatment on the mechanical properties of jute yarns. **Journal of Composite Materials**, SAGE Publications Sage UK: London, England, 2021.

SONG, H. *et al.* A comprehensive overview of jute fiber reinforced cementitious composites. **Case Studies in Construction Materials**, Elsevier, v. 15, 2021.

SOOD, M.; DWIVEDI, G. Effect of fiber treatment on flexural properties of natural fiber reinforced composites: A review. **Egyptian journal of petroleum**, Elsevier, v. 27, n. 4, p. 775–783, 2018.

TSAI, S. W.; HAHN, H. T. **Introduction to composite materials**. [S.l.]: Routledge, 1980.

TSAI, S. W.; WU, E. M. A general theory of strength for anisotropic materials. **Journal of composite materials**, Sage Publications Sage CA: Thousand Oaks, CA, v. 5, n. 1, p. 58–80, 1971.

XIE, Y. *et al.* Effects of chemical modification of wood particles with glutaraldehyde and 1,3-dimethylol-4,5-dihydroxyethyleneurea on properties of the resulting polypropylene composites. **Composites Science and Technology**, Elsevier, v. 70, n. 13, p. 2003–2011, 2010. ICCM-17: Composites In Biomedical Applications. Available at: <https://www.sciencedirect.com/science/article/pii/S0266353810002939>. Accessed on: 18 may, 2023.

APPENDIX A – TENSILE TESTER CALIBRATION

Figure 44 – Force calibration - Tensile tester.

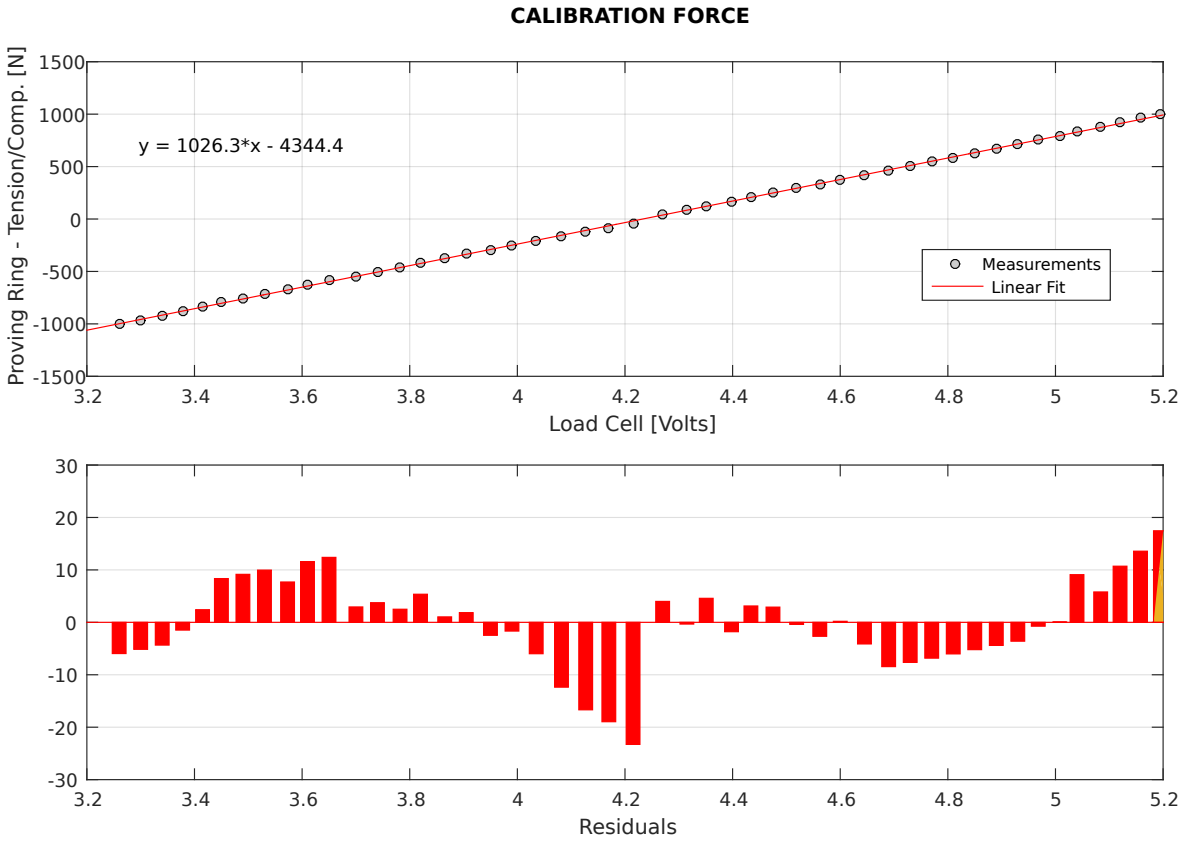

Source: Author.

Figure 45 – Displacement calibration - Tensile tester.

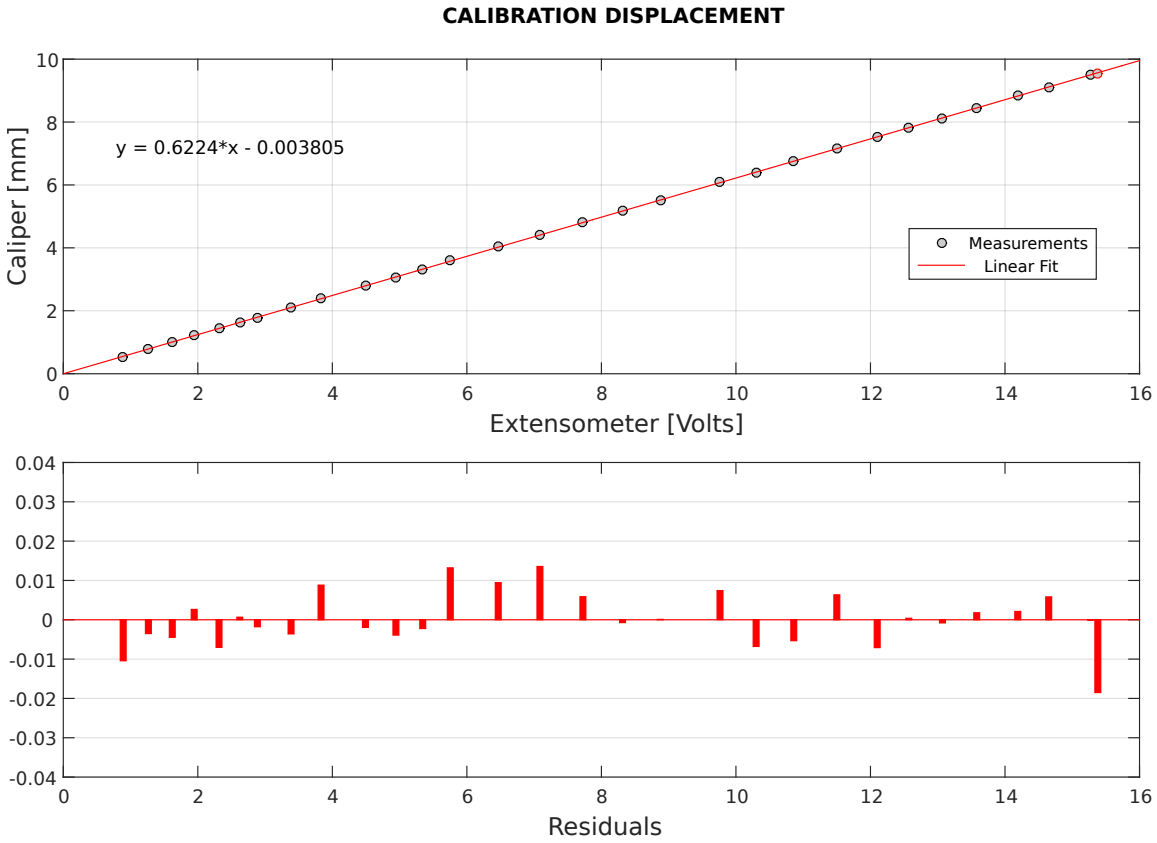

Source: Author.

APPENDIX B – JUTE CHARACTERIZATION

60 specimens with 16 longitudinal fibers were prepared and tested. Figure 46 shows an untreated jute specimen before the tensile test, and Figure 47 shows after.

Figure 46 – Jute specimen before tensile test

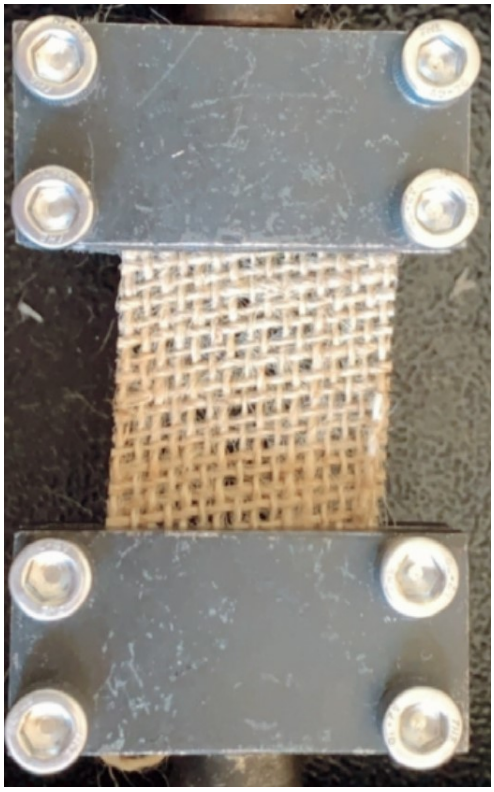

Source: Author.

Characterization tensile test was also performed in treated jute fibers. The main goal of jute treatment is to improve its adhesion with the matrix when jute is a constituent of composite materials. Since numerical analysis is going to be performed using jute properties, treated and untreated fibers were characterized to obtain parameters that later are going to be needed for numerical analysis.

Figures 48 and 49 show, respectively, a treated jute before and after the tensile test. Two visual analyses were made comparing the treated and untreated fibers (presented in Figures 46 and 47. The first is their color. It changes with treatment, treated fibers are darker than untreated ones. The second analysis is their behavior in rupture. Untreated fibers presented a fragile, with no resistance left after the tensile test. Treated fibers, even after their rupture, presented some strength after being tested. Results are presented in Figures 50 and 51. Higher forces were obtained in untreated jute fibers (Figure 50), which is expected because it was heated

Figure 47 – Jute specimen after tensile test

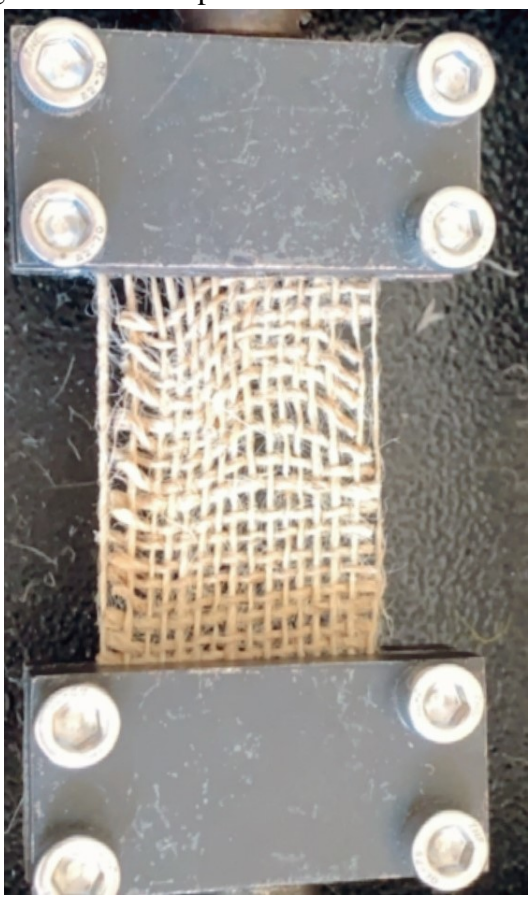

Source: Author.

(SMAIL *et al.*, 2021). Even so, the main goal to perform the treatment is to achieve a better inter-facial bonding between the fiber and the matrix, which will carry into a more resistant composite.

The statistical results for untreated and treated fibers, obtained using Weibull distribution, is presented in Figures 52 and 53, respectively.

Figure 48 – Treated jute specimen before tensile test

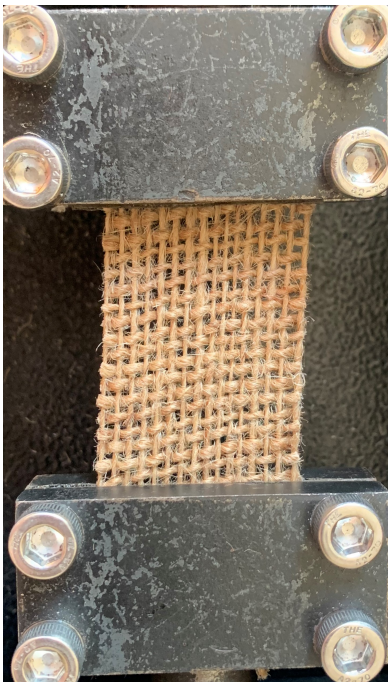

Source: Author.

Figure 49 – Treated jute specimen after tensile test

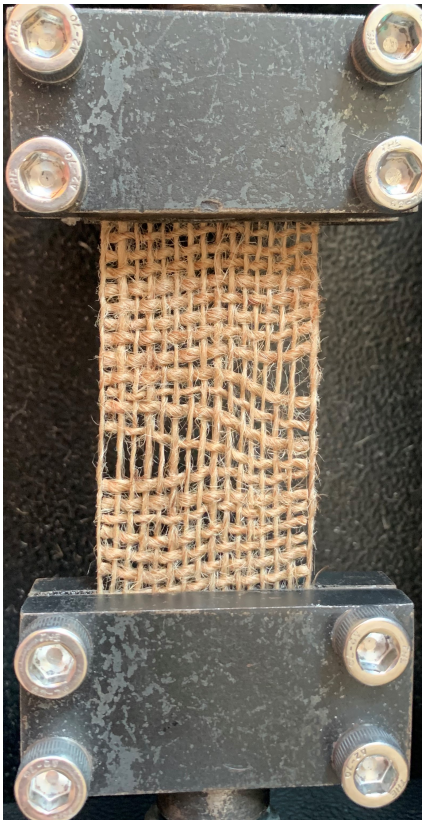

Source: Author.

Figure 50 – Force x displacement results in untreated jute fibers

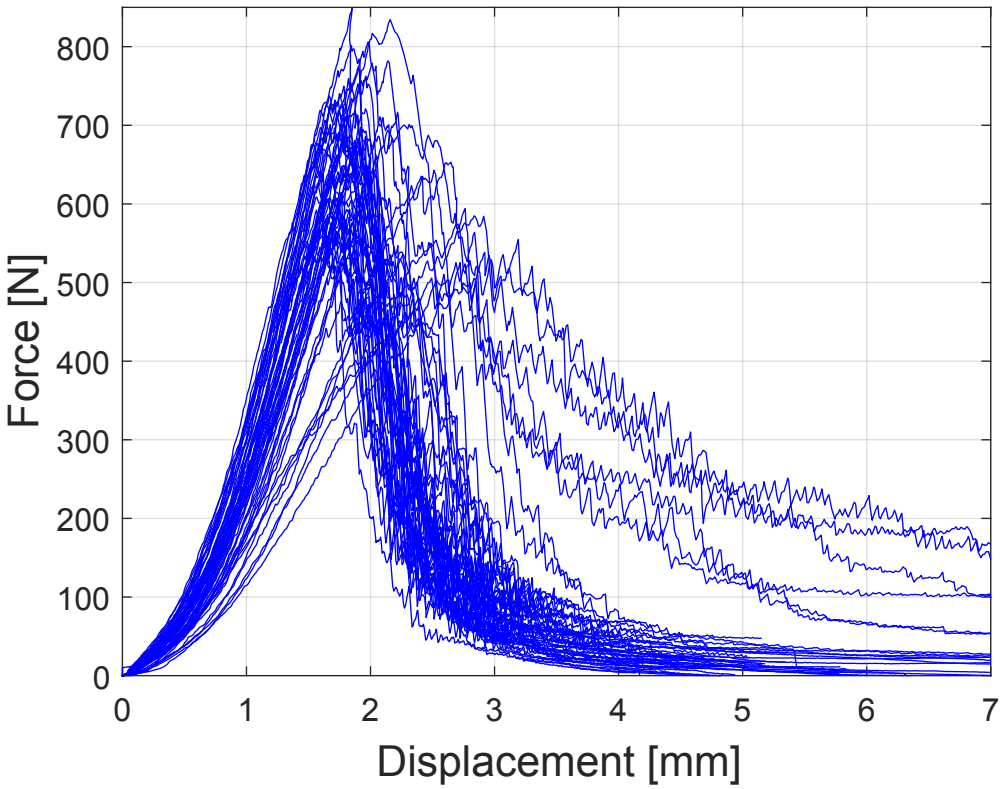

Source: Author.

Figure 51 – Force x displacement results in treated jute fibers

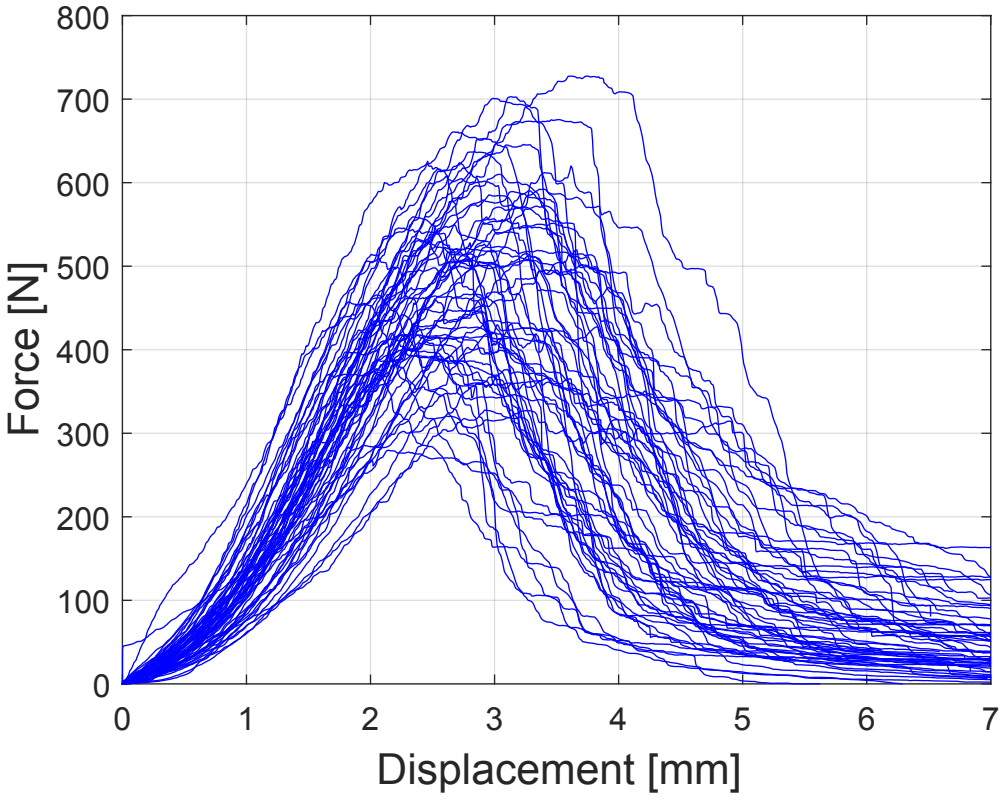

Source: Author.

Figure 52 – Weibull distribution for untreated tensile results.

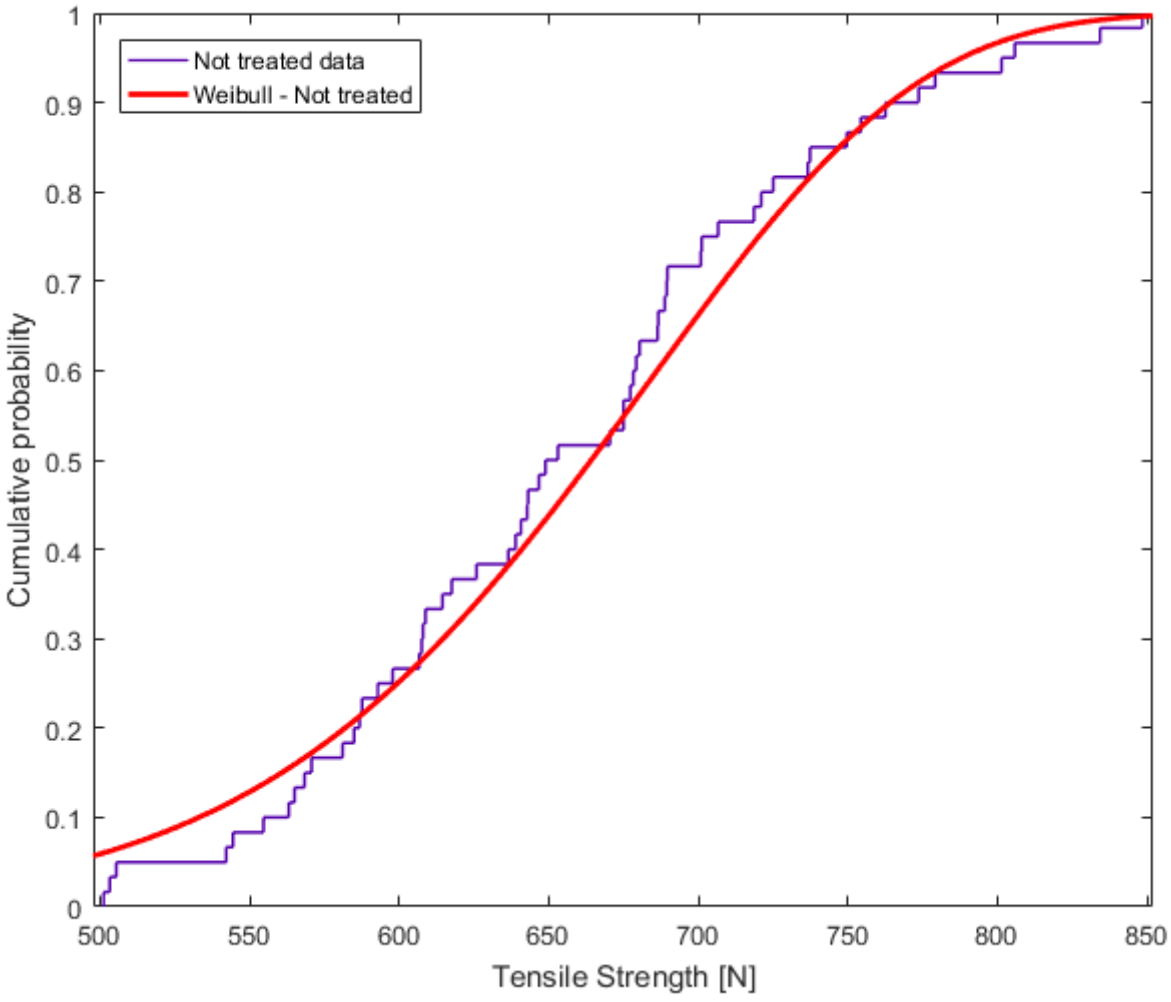

Source: Author.

Figure 53 – Weibull distribution for treated tensile results.

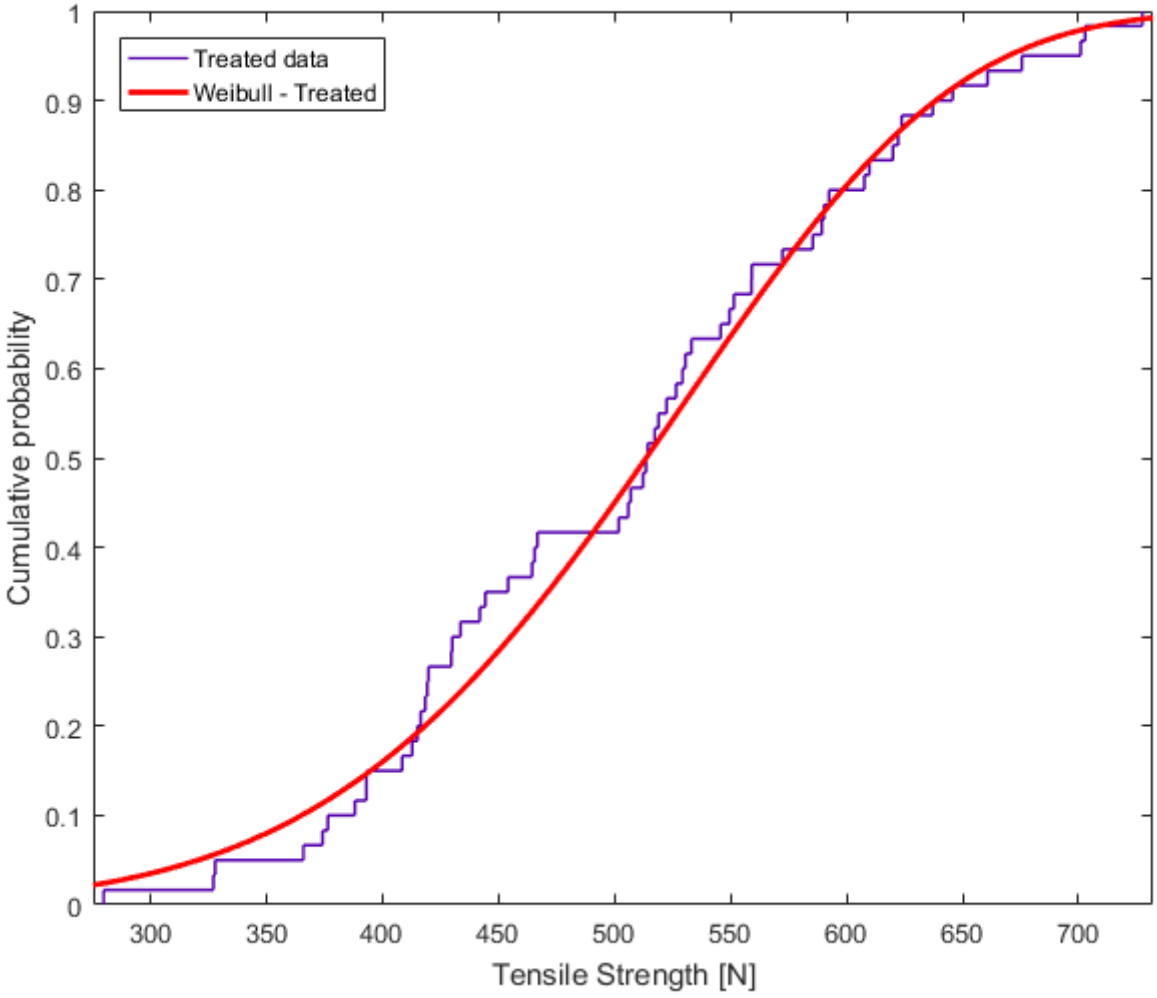

Source: Author.

ANNEX A – GJJJJG AND G8 RESIN PROPERTIES

FORTCOM 3100

Ficha de Informações de Segurança de Produtos Químicos

De acordo com ABNT NBR 14725-4: 2014

Data de emissão: 01/08/2019

Data de revisão: 01/08/2019

Versão: 1.0

SEÇÃO 1: Identificação do Produto e da Empresa

1.1. Identificação do produto

Nome comercial : FORTCOM 3100

Código do produto : FTC 3100

Uso recomendado : Laminação em geral (PRFV)

1.2. Identificação da Empresa

Oswaldo Cruz Química Ind e Com. Ltda.
Rua Mônica Aparecida Moredo 229
CEP: 07177-220 Guarulhos
T (0XX11) 2436-3682 - F (0XX11) 2436-5582
oswaldocruz@ocq.com.br

Número de emergência : AMBIPAR - 0800 707 7022 / 0800 17 2020

SEÇÃO 2: Identificação de perigos

2.1. Classificação da substância ou mistura

Classificação de acordo com GHS BR (ABNT NBR 14725-2)

Líquidos inflamáveis, Categoria 3

Toxicidade aguda (Inalação: poeira,névoa), Categoria 4

Corrosão/Irritação á pele, Categoria 2

Lesões oculares graves/irritação ocular, Categoria 2A

Toxicidade à reprodução, Categoria 2

Toxicidade para órgãos-alvo específicos - Exposição repetida, Categoria 1

2.2. Elementos apropriados de rotulagem

GHS BR rotulagem

Pictogramas de perigo (GHS BR) :

GHS02 GHS07 GHS08

Palavra de advertência (GHS BR) : Perigo

Frases de perigo (GHS BR) : H226 - Líquido e vapores inflamáveis
H315 - Provoca irritação à pele
H319 - Provoca irritação ocular grave
H332 - Nocivo se inalado
H361 - Suspeita-se que prejudique a fertilidade ou o feto
H372 - Provoca danos aos órgãos por exposição repetida ou prolongada

Frases de precaução (GHS BR) : P201 - Obtenha instruções específicas antes da utilização
P202 - Não manuseie o produto antes de ter lido e compreendido todas as precauções de segurança
P210 - Mantenha afastado do calor, faísca, chama aberta, superfícies quentes. - Não fume
P233 - Mantenha o recipiente hermeticamente fechado
P240 - Aterre o vaso contentor e o receptor do produto durante transferências
P241 - Utilize equipamento elétrico/de ventilação/de iluminação à prova de explosão.
P242 - Utilize apenas ferramentas antifaiscantes
P243 - Evite o acúmulo de cargas eletrostáticas
P260 - Não inale poeiras/fumos/gases/névoas/vapores/aerossóis
P261 - Evite inalar poeiras/fumos/gases/névoas/vapores/aerossóis
P264 - Lave mãos, antebraços e rosto cuidadosamente após o manuseio.
P270 - Não coma, beba ou fume durante a utilização deste produto
P271 - Utilize apenas ao ar livre ou em locais bem ventilados
P280 - Use luvas de proteção/roupas de proteção/proteção para os olhos/ proteção facial
P302+P352 - EM CASO DE CONTATO COM A PELE: Lave com água e sabão em abundância
P303+P361+P353 - EM CASO DE CONTATO COM A PELE (ou com o cabelo): Retire imediatamente toda a roupa contaminada. Enxágue a pele com água/tome uma ducha
P304+P340 - EM CASO DE INALAÇÃO: remova a pessoa para local ventilado e a mantenha em repouso numa posição que não dificulte a respiração.
P305+P351+P338 - EM CASO DE CONTATO COM OS OLHOS: Enxágue cuidadosamente com água durante vários minutos. No caso de uso de lentes de contato, remova-as, se for fácil. Continue enxaguando
P308+P313 - EM CASO DE exposição ou suspeita de exposição: Consulte um médico

P312 - Caso sinta indisposição, contate um CENTRO DE INFORMAÇÃO TOXICOLÓGICA/médico/…
P314 - Em caso de mal estar, consulte um médico
P321 - Tratamento específico (veja instrução suplementar de primeiros socorros nesse rótulo)
P332+P313 - Em caso de irritação cutânea: Consulte um médico
P337+P313 - Caso a irritação ocular persista: consulte um médico
P362+P364 - Retire a roupa contaminada e lave-a antes de usá-la novamente
P370+P378 - Em caso de incêndio: Para a extinção utilize outro meio que não seja água para extinguir
P403+P235 - Armazene em local bem ventilado. Mantenha em local fresco.
P405 - Armazene em local fechado à chave
P501 - Descarte o conteúdo/recipiente em ponto de coleta de resíduos especiais ou perigosos de acordo com regulamentação local, regional, nacional e/ou internacional

2.3. Outros perigos que não resultam em uma classificação

Nenhuma informação adicional disponível

SEÇÃO 3: Composição e informações sobre os ingredientes

3.1. Substância

Não aplicável

3.2. Mistura

Nome	Identificação do produto	%
styrene, inhibited	(nº CAS) 100-42-5	<= 65
diethylene glycol	(nº CAS) 111-46-6	<= 3,5

SEÇÃO 4: Medidas de primeiros-socorros

4.1. Descrição das medidas de primeiros socorros

Medidas gerais de primeiros-socorros : EM CASO DE exposição ou suspeita de exposição: Consulte um médico.

Medidas de primeiros-socorros após inalação : Remova a pessoa para local ventilado e a mantenha em repouso numa posição que não dificulte a respiração. Contate imediatamente um CENTRO DE INFORMAÇÃO TOXICOLÓGICA ou um médico.

Medidas de primeiros-socorros após contato com a pele : Após contato com a pele, retirar imediatamente toda a roupa contaminada e lavar com água em abundância. Tenha cuidado, o produto pode permanecer preso debaixo da roupa, calçado ou de um relógio de pulso.

Medidas de primeiros-socorros após contato com os olhos : EM CASO DE CONTATO COM OS OLHOS: Enxágue cuidadosamente com água durante vários minutos. No caso de uso de lentes de contato, remova-as, se for fácil. Continue enxaguando.

Medidas de primeiros-socorros após ingestão : NÃO provoque vômito. Enxaguar a boca com água.

4.2. Sintomas e efeitos mais importantes, agudos ou tardios

Sintomas/efeitos : Provoca danos aos órgãos por exposição repetida ou prolongada. Nocivo se inalado. Pode causar queimaduras severas. Provoca irritação ocular grave.

Sintomas/efeitos em caso de inalação : Pode causar irritação no trato respiratório, espirros, tosse, sensação de queimaduras na garganta com sensação de constrição da laringe e dificuldade de respiração.

Sintomas/efeitos em caso de contato com a pele : Provoca irritação à pele. irritação (coceira, vermelhidão, formação de bolhas).

Sintomas/efeitos em caso de contato com os olhos : Ardência. Vermelhidão. Provoca irritação ocular grave. vermelhidão, coceira, lágrimas.

Sintomas/efeitos em caso de ingestão : Queimaduras ou irritação nos tecidos da boca, garganta e trato gastrointestinal.

Sintomas crônicos : Suspeitas de prejudicar a fertilidade. Suspeito de prejudicar o feto.

4.3. Indicações sobre cuidados médicos urgentes e tratamentos especiais necessários

Notas ao médico : Tratar sintomaticamente

SEÇÃO 5: Medidas de combate a incêndio

5.1. Meios de extinção

Meios de extinção adequados : Pó químico seco, CO2, água pulverizada ou espuma comum.

Meios de extinção inadequados : Não use jato forte de água.

5.2. Perigos específicos decorrentes da substância ou mistura

Perigo de incêndio : Líquido e vapores inflamáveis. Os vapores são mais densos que o ar e podem deslocar-se pelo chão. Possibilidade de ignição à distância. A agitação pode provocar acúmulo de carga eletrostática. Os vapores podem provocar um incêndio/explosão se fontes de ignição estiverem presentes. Em caso de incêndio e/ou explosão não respirar os fumos.

Perigo de explosão : Os vapores podem formar uma mistura explosiva em contato com o ar. A exposição prolongada ao fogo pode causar ruptura e/ou explosão dos recipientes.

Reatividade : O produto não é reativo nas condições normais de utilização, armazenamento e transporte.

5.3. Recomendações para a equipe de combate a incêndio

Medidas preventivas contra incêndios : Manter o recipiente fechado quando não estiver em uso. Este produto não pode ser utilizado em condições de ventilação reduzida.

Instruções de combate a incêndios : Afaste os recipientes da área do fogo, se isso puder ser feito sem risco. Combata o fogo de uma distância segura ou utilize mangueiras com suporte ou canhão motor. Resfrie lateralmente com água os recipientes expostos às chamas, mesmo após o fogo ter sinto extinto. Não entrar na área de incêndio sem equipamento protetor adequado, incluindo proteção respiratória.

Proteção durante o combate a incêndios : Utilize equipamento de respiração do tipo autônomo com pressão positiva e roupa de proteção contra produtos químicos.

Outras informações : Quando exposto a altas temperaturas, pode decompor, liberando gases tóxicos. Em caso de incêndio, gases corrosivos e nocivos são liberados.

SEÇÃO 6: Medidas de controle para derramamento ou vazamento

6.1. Precauções pessoais, equipamento de proteção e procedimentos de emergência

Medidas gerais : Remover qualquer possível fonte de ignição. Impedir a entrada em esgotos, subsolos, fossas ou qualquer outro lugar onde a sua acumulação possa ser perigosa. Evitar o contato com a pele e com os olhos. Contenha o vazamento se puder ser feito com segurança. Notificar as autoridades se o produto entrar nos esgotos ou águas públicas. Absorva o produto derramado a fim de evitar danos materiais.

6.1.1. Para não-socorristas

Equipamento de proteção : Use os equipamentos de proteção pessoal recomendados.

Procedimentos de emergência : Evite chamas e faíscas. Elimine todas as fontes de ignição. Não toque nem caminhe sobre o produto derramado. Abandone a área. Apenas o pessoal qualificado e equipado com equipamento de proteção adequado pode intervir. Notificar o corpo de bombeiros e autoridades ambientais.

6.1.2. Para socorristas

Equipamento de proteção : Utilize equipamento de respiração do tipo autônomo com pressão positiva e roupa de proteção contra produtos químicos. Luvas. Usar óculos de segurança com proteções laterais. Equipamento autônomo de respiração. Roupa de proteção total impermeável, luvas e botas devem ser usadas para evitar qualquer contato com o produto. Roupas à prova de corrosão. Equipar o pessoal da limpeza com proteção adequada.

Procedimentos de emergência : Manter afastado de material combustível. Todo o equipamento utilizado no manuseio do produto deve estar aterrado. Evacuar o pessoal desnecessário. Contenha o vazamento se puder ser feito com segurança.

6.2. Precauções ambientais

Impedir a entrada em esgotos, subsolos, fossas ou qualquer outro lugar onde a sua acumulação possa ser perigosa. Notificar as autoridades se o produto entrar nos esgotos ou águas públicas.

6.3. Métodos e materiais de contenção e limpeza

Para contenção : Evitar a dispersão umedecendo o derramamento com água ou espuma. Contenha qualquer derramamento com barreiras ou materiais absorventes para evitar migração e entrada em esgotos ou córregos. Interromper o vazamento, se possível sem riscos.

Métodos de limpeza : Absorver o líquido restante com areia ou material absorvente inerte e levar para um lugar seguro. Absorver o material derramado com areia ou terra. Limpar superfícies contaminadas com água em abundância. Limpar rapidamente com pá ou aspirador.

SEÇÃO 7: Manuseio e armazenamento

7.1. Precauções para manuseio seguro

Perigos adicionais quando processado : Vapores inflamáveis podem acumular-se no recipiente.

Precauções para manuseio seguro : Fornecer ventilação adequada para minimizar concentrações de poeira e/ou vapor. Mantenha afastado do calor, faísca, chama aberta, superfícies quentes. - Não fume. Manuseie cuidadosamente. Aterre o vaso contentor e o receptor do produto durante transferências. Utilize apenas ferramentas antifaiscantes. Evite o acúmulo de cargas eletrostáticas. Usar equipamento de proteção individual. Obtenha instruções específicas antes da utilização. Tomar todas as medidas técnicas necessárias para evitar ou minimizar o lançamento do produto no local de trabalho. Limitar as quantidades do produto ao mínimo necessário para a manipulação e limitar o número de trabalhadores expostos. Conserve somente no recipiente original. Não manuseie o produto antes de ter lido e compreendido todas as precauções de segurança.

Medidas de higiene : Sempre lave as mãos após manusear o produto. Remova a roupa contaminada. Não coma, beba ou fume durante a utilização deste produto.

7.2. Condições para armazenamento seguro, incluindo incompatibilidades

Medidas técnicas : Assegure uma ventilação adequada, sobretudo em lugares fechados. Armazene em local fechado à chave.

Condições de armazenamento : Mantenha em local fresco. Armazene em local bem ventilado. Mantenha o recipiente hermeticamente fechado. Mantenha em local fresco. Mantenha ao abrigo da luz solar.

Materiais incompatíveis : material combustível.

Materiais para embalagem : Armazenar o produto sempre em recipiente de material igual ao do recipiente original.

SEÇÃO 8: Controle de exposição e proteção individual

8.1. Parâmetros de controle

styrene, inhibited (100-42-5)		
Brasil	Nome local	Estireno (Vinibenzeno)
Brasil	Limite de tolerância NR-15 (ppm)	78 ppm
Brasil	Limite de tolerância NR-15 (mg/mg³)	328 mg/m³
Brasil	Referência regulamentar	Norma Regulamentadora Nº 15 - Actividades e Operaçoes Insalubres
Brasil	Limites de exposição biológicos (NR-7)	1 g/g creatinina Parâmetro: Ácido mandélico - Meio: Urina - Momento de amostragem: Final do último dia de jornada de trabalho (recomenda-se evitar a primeira jornada da semana) - Interpretação: EE (O indicador biológico é capaz de indicar uma exposição ambiental acima do limite de tolerância, mas não possui, isoladamente, significado clínico ou toxicológico próprio, ou seja, não indica doença, nem está associado a um efeito ou disfunção de qualquer sistema biológico) 240 mg/g creatinina Parâmetro: Ácido fenil-glioxílico - Meio: Urina - Momento de amostragem: Final do último dia de jornada de trabalho (recomenda-se evitar a primeira jornada da semana) - Interpretação: EE (O indicador biológico é capaz de indicar uma exposição ambiental acima do limite de tolerância, mas não possui, isoladamente, significado clínico ou toxicológico próprio, ou seja, não indica doença, nem está associado a um efeito ou disfunção de qualquer sistema biológico)
EUA	Nome local	Styrene, monomer
EUA	ACGIH TWA (Média Ponderada no Tempo) (ppm)	20 ppm
EUA	ACGIH STEL (Limites de Exposição a Curto Prazo) (ppm)	40 ppm
EUA	Observação (ACGIH)	TLV® Basis: CNS impair; URT irr; peripheral neuropathy. Notations: A4 (Not classifiable as a Human Carcinogen); BEI
EUA	Referência regulamentar	ACGIH 2019

8.2. Controles de exposição

Controles apropriados de engenharia : Fontes para lavagem dos olhos e chuveiros de segurança para emergência devem estar disponíveis nas imediações de qualquer potencial de exposição.

8.3. Equipamento de proteção individual

Equipamento de proteção individual : Use os equipamentos de proteção pessoal recomendados.

Proteção para as mãos : Luvas de proteção de PVC.

Proteção para os olhos : Usar óculos de segurança herméticos.

Proteção para a pele e o corpo : Usar sapatos de segurança de borracha impermeável.

Proteção respiratória : Recomenda-se o uso de equipamento de proteção respiratória nos casos em que possa ocorrer inalação durante a utilização.

SEÇÃO 9: Propriedades físicas e químicas

9.1. Informações sobre propriedades físico-químicas básicas

Estado físico : Líquido

Cor : Não disponível

Odor : Não disponível

Limiar de odor : Não disponível

pH : Não disponível

Ponto de fusão : -30,6 °C

Ponto de solidificação	:	Não disponível
Ponto de ebulição	:	145,2 °C
Ponto de fulgor	:	31 °C Vaso fechado
Taxa de evaporação relativa (acetato de butila = 1)	:	Não disponível
Inflamabilidade (sólido/gás)	:	Não disponível
Limites de explosão	:	Não disponível
Pressão de vapor	:	Não disponível
Densidade relativa do vapor a 20°C	:	3,6 AR=1
Densidade relativa	:	1,1 - 1,12
Solubilidade	:	inmiscível em água.
Log Kow	:	Não disponível
Temperatura de auto-ignição	:	490 °C
Temperatura de decomposição	:	Não disponível
Viscosidade, cinemática	:	Não disponível
Viscosidade, dinâmica	:	Não disponível

9.2. Outras informações

Não disponível

SEÇÃO 10: Estabilidade e reatividade

Estabilidade química	:	Durante o uso, pode formar misturas de vapor-ar inflamáveis/explosivas
Condições a evitar	:	Mantenha afastado do calor, faísca, chama aberta, superfícies quentes. - Não fume. Evite o contato com superfícies quentes. Temperaturas elevadas. Evite a formação de vapores
Produtos perigosos da decomposição	:	Pode liberar gases tóxicos,Pode decompor-se quando exposto a temperaturas elevadas, liberando gases corrosivos
Materiais incompatíveis	:	Materiais combustíveis
Possibilidade de reações perigosas	:	Os líquidos /vapores podem incendiar-se ou reagirem com outros materiais
Reatividade	:	O produto não é reativo nas condições normais de utilização, armazenamento e transporte

SEÇÃO 11: Informações toxicológicas

11.1. Informações sobre os efeitos toxicológicos

Toxicidade aguda (oral)	:	Não disponível
Toxicidade aguda (dérmica)	:	Não disponível
Toxicidade aguda (inalação)	:	Inalação: poeira, névoa: Nocivo se inalado.

ETA BR (poeira, névoa)	3,411 mg/l/4h
diethylene glycol (111-46-6)	
DL50 oral, rato	19600 mg/kg de peso corporal (OECD 401: Acute Oral Toxicity, Rat, Male, Experimental value, Oral)
DL50 dérmica, coelho	11890 mg/kg (Rabbit, Dermal)
CL50 inalação rato (mg/l)	> 4,6 mg/l air (Other, 4 h, Rat, Weight of evidence, Inhalation (mist))
styrene, inhibited (100-42-5)	
DL50 oral, rato	> 6000 mg/kg de peso corporal (Rat, Male, Weight of evidence, Oral)
DL50 dérmica, rato	> 2000 mg/kg de peso corporal (OECD 402: Acute Dermal Toxicity, 24 h, Rat, Male/female, Experimental value, Dermal)
CL50 inalação rato (mg/l)	11,8 mg/l air (4 h, Rat, Inconclusive, insufficient data, Inhalation (vapours))

Corrosão/irritação à pele	:	Provoca irritação à pele.
Lesões oculares graves/irritação ocular	:	Provoca irritação ocular grave.
Sensibilização respiratória ou à pele	:	Não disponível
Mutagenicidade em células germinativas	:	Não disponível
Carcinogenicidade	:	Não disponível
Toxicidade à reprodução	:	Suspeita-se que prejudique a fertilidade ou o feto .
Toxicidade para órgãos-alvo específicos - Exposição única	:	Não disponível
Toxicidade para órgãos-alvo específicos - Exposição repetida	:	Provoca danos aos órgãos por exposição repetida ou prolongada.
Perigo por aspiração	:	Não disponível

11.2. Sintomas e efeitos mais importantes, agudos ou tardios

Sintomas/efeitos	:	Provoca danos aos órgãos por exposição repetida ou prolongada. Nocivo se inalado. Pode causar queimaduras severas. Provoca irritação ocular grave.
Sintomas/efeitos em caso de inalação	:	Pode causar irritação no trato respiratório, espirros, tosse, sensação de queimaduras na garganta com sensação de constrição da laringe e dificuldade de respiração.
Sintomas/efeitos em caso de contato com a pele	:	Provoca irritação à pele. irritação (coceira, vermelhidão, formação de bolhas).
Sintomas/efeitos em caso de contato com os olhos	:	Ardência. Vermelhidão. Provoca irritação ocular grave. vermelhidão, coceira, lágrimas.
Sintomas/efeitos em caso de ingestão	:	Queimaduras ou irritação nos tecidos da boca, garganta e trato gastrointestinal.
Sintomas crônicos	:	Suspeitas de prejudicar a fertilidade. Suspeito de prejudicar o feto.

SEÇÃO 12: Informações ecológicas

12.1. Toxicidade

Perigoso ao ambiente aquático - Agudo	:	Não disponível
Perigoso ao ambiente aquático - Crônico	:	Não disponível

diethylene glycol (111-46-6)	
CL50 peixes 1	> 5000 ppm (24 h, Carassius auratus)
CE50 Dáfnia 1	> 10000 mg/l (24 h, Daphnia magna)
CL50 peixes 2	75200 mg/l (Other, 96 h, Pimephales promelas, Flow-through system, Experimental value)
CE50 Dáfinia 2	> 10000 mg/l (DIN 38412-11, 24 h, Daphnia magna, Static system, Fresh water, Experimental value)

styrene, inhibited (100-42-5)	
CL50 peixes 1	10 mg/l (OECD 203: Fish, Acute Toxicity Test, 96 h, Pimephales promelas, Flow-through system, Fresh water, Experimental value, GLP)
CE50 Dáfnia 1	4,7 mg/l (OECD 202: Daphnia sp. Acute Immobilisation Test, 48 h, Daphnia magna, Flow-through system, Fresh water, Experimental value, GLP)
CEr50 (algas)	4,9 mg/l (EPA OTS 797.1050, 72 h, Pseudokirchneriella subcapitata, Static system, Fresh water, Experimental value, GLP)

12.2. Persistência e degradabilidade

diethylene glycol (111-46-6)	
Persistência e degradabilidade	Biodegradável no solo. Biodegradável na água.
Demanda bioquímica de oxigênio (DBO)	0,02 g O_2/g substância
Demanda química de oxigênio (DQO)	1,51 g O_2/g substância
DTO - Demanda Teórica de Oxigênio	1,51 g O_2/g substância
DBO (% de ThOD)	0,015

styrene, inhibited (100-42-5)	
Persistência e degradabilidade	Biodegradável no solo. Facilmente biodegradável em água.
Demanda química de oxigênio (DQO)	2,8 g O_2/g substância
DTO - Demanda Teórica de Oxigênio	3,07 g O_2/g substância
DBO (% de ThOD)	0,42 (Literature study)

12.3. Potencial bioacumulativo

diethylene glycol (111-46-6)	
BCF peixes 1	100 (Other, 3 day(s), Leuciscus melanotus, Static system, Fresh water, Experimental value)
Log Pow	-1,98 (Calculated, Other)
Potencial bioacumulativo	Not bioaccumulative.

styrene, inhibited (100-42-5)	
BCF peixes 1	35,5 (Carassius auratus, Literature study)
Log Pow	2,96 (Experimental value, OECD 107: Partition Coefficient (n-octanol/water): Shake Flask Method, 25 °C)
Potencial bioacumulativo	Baixo potencial de bioacumulação (Log Kow < 4).

12.4. Mobilidade no solo

diethylene glycol (111-46-6)	
Tensão superficial	0,0485 N/m
Log Koc	0 (log Koc, SRC PCKOCWIN v1.66, Calculated value)
Ecologia - solo	Highly mobile in soil.

styrene, inhibited (100-42-5)	
Tensão superficial	0,032 N/m (20 °C)
Log Koc	2,55 (log Koc, Estimated value)

styrene, inhibited (100-42-5)	
Ecologia - solo	Baixo potencial de adsorção no solo.

12.5. Outros efeitos adversos

Nenhuma informação adicional disponível

SEÇÃO 13: Considerações sobre destinação final

Métodos de tratamento de resíduos : Deve seguir tratamento especial de acordo com as legislações locais.

Recomendações de despejo de águas residuais : O descarte deve ser realizado de acordo com as legislações oficiais.

Recomendações de disposição de produtos/embalagens : O descarte deve ser realizado de acordo com as legislações oficiais.

Informações adicionais : Vapores inflamáveis podem acumular-se no recipiente. Não reutilizar recipientes vazios.

SEÇÃO 14: Informações sobre transporte

14.1 Regulamentações nacionais e internacionais

Transporte terrestre

Nº ONU(RES 5232) : 1866

Nome apropriado para embarque(RES 5232) : RESINA SOLUÇÃO, inflamável

Classe (RES 5232) : 3 - Líquido inflamável

Número de Risco (Res 5232) : 30 - Líquido inflamável (23ºC ≤ PFg ≤ 60,5ºC), ou líquido ou sólido inflamável em estado fundido com PFg > 60,5ºC, aquecidos a uma temperatura igual ou superior a seu PFg, ou líquido sujeito a auto-aquecimento

Grupo de embalagem(Res 5232) : III - Substâncias que apresentam baixo risco

Provisão especial(Res 5232) : 223

Transporte marítimo

Nº ONU (IMDG) : 1866

Nome apropriado para embarque (IMDG) : RESIN SOLUTION

Classe (IMDG) : 3 - Flammable liquids

Grupo de embalagem (IMDG) : III - substances presenting low danger

EmS-No. (Fogo) : F-E - FIRE SCHEDULE Echo - NON-WATER-REACTIVE FLAMMABLE LIQUIDS

EmS-No. (Derramamento) : S-E - SPILLAGE SCHEDULE Echo - FLAMMABLE LIQUIDS, FLOATING ON WATER

Poluente marinho (IMDG) : Não

Provisão especial (IMDG) : 223,955

Transporte aéreo

Nº ONU (IATA) : 1866

Nome apropriado para embarque (IATA) : Resin solution

Classe (IATA) : 3 - Flammable Liquids

Grupo de embalagem (IATA) : III - Minor Danger

Provisão especial (IATA) : A3

14.2 Outras informações

Nenhuma informação adicional disponível

SEÇÃO 15: Informações sobre regulamentações

Regulamentações locais do Brasil : ANVISA requirements
Federal Police Department
Ministry of Defense
Decreto Federal nº 2.657, de 3 de julho de 1998 – Promulga a Convenção nº 170 da OIT, relativa à Segurança na Utilização de Produtos Químicos no Trabalho, assinada em Genebra, em 25 de junho de 1990.
Norma ABNT NBR 14725.
Portaria nº 229, de 24 de maio de 2011 - Altera a Norma Regulamentadora nº 26
Resolução nº 5232, de 14 de dezembro de 2016 - Aprova as Instruções Complementares ao Regulamento Terrestre do Transporte de Produtos Perigosos, e dá outras providências.

SEÇÃO 16: Outras informações

Outras informações : Esta FISPQ foi elaborada com base nos atuais conhecimentos sobre o manuseio apropriado do produto e sob as condições normais de uso, de acordo com a aplicação especificada na embalagem. Qualquer outra forma de utilização do produto que envolva a sua combinação com outros materiais, além de formas de uso diversas daquelas indicadas, são de responsabilidade do usuário. Adverte-se que o manuseio de qualquer substância química requer o conhecimento prévio de seus perigos pelo usuário. No local de trabalho cabe à empresa usuária do produto promover o treinamento de seus colaboradores quanto aos possíveis riscos advindos da exposição ao produto químico.

Fontes de dados : Classificação de acordo com a Regulamento sobre Classificação, Rotulagem e Embalagem de Substâncias e Misturas (SEA) publicado no Jornal Oficial com o número 28848 a 11 de Dezembro de 2013. REGULAMENTO (CE) No 1272/2008 DO PARLAMENTO EUROPEU E DO CONSELHO de 16 de dezembro de 2008 relativo à classificação, rotulagem e embalagem de substâncias e misturas, que altera e revoga as Diretivas 67/548/CEE e 1999/45/CE, e altera o Regulamento (CE) n.o 1907/2006.

Abreviaturas e acrônimos : CAS - Chemical Abstracts Service
ONU - Organização das Nações Unidas
ADN - Acordo Europeu relativo ao Transporte Internacional de Mercadorias Perigosas por Via Fluvial

ADR - Acordo Europeu relativo ao Transporte Internacional de Mercadorias Perigosas por Estrada

BCF - Fator de bioconcentração

CE50 - Concentração efetiva média

CL50 - Concentração Letal Média

CLP - Regulamento (CE) n.º 1272/2008 relativo à Classificação, Rotulagem e Embalagem

DL50 - Dose Letal Média

DMEL - Nível Derivado de Exposição com Efeitos Mínimos

DNEL - Nível Derivado de Exposição Sem Efeito

DPD - Diretiva referente às Preparações Perigosas 1999/45/CE

DSD - Diretiva refente às Substâncias Perigosas 67/548/CEE

ETA - Estimativa de Toxicidade Aguda

IARC - Agência Internacional de Pesquisa contra o Câncer

IATA - International Air Transport Association

IMDG - International Maritime Dangerous Goods

LOAEL - Nível mínimo com efeitos adversos observáveis

mPmB - Muito Persistente e muito Bioacumulável

NOAEC - Concentração sem efeitos adversos observáveis

NOAEL - Nível sem efeitos adversos observáveis

NOEC - Concentração sem efeitos observáveis

OECD - Organização para a Cooperação e o Desenvolvimento Econômico

PBT - Substância Persistente, Bioacumulável e Tóxica

PNEC - Previsão de Concentração Sem Efeitos

REACH - Regulamento (CE) n.º 1907/2006 relativo ao Registo, Avaliação, Autorização e Restrição de Produtos Químicos

RID - Regulamento relativo ao Transporte Internacional Ferroviário de Mercadorias Perigosas

SDS - Ficha de Informações de Segurança de Produtos Químicos

STP - Estação de tratamento de esgoto

TLM - Limite Médio de Tolerância

FISPQ OCQ

Esta informação está baseada em nosso conhecimento atual e pretende descrever o produto tendo unicamente em vista os requisitos de saúde, segurança e meio ambiente. Não deve, portanto, ser interpretada como garantia de qualquer propriedade específica do produto.